The Tmem63b/Slc19a2 Complex Functions as a Ca^{2+}-Dependent Scramblase

Niu Han

Content

Abstract

Asymmetric phospholipid distribution is maintained by flippases and floppases in an ATP-dependent manner, while scramblases alter this balance to adapt to environmental changes. Two ubiquitous scramblases have been identified: Tmem16f, a Ca^{2+}-dependent scramblase that exposes phosphatidylserine (PS) in platelets for coagulation; and Xkr8, activated by caspase-mediated cleavage for the clearance of apoptotic cells. However, it has been unknown if other scramblase families exist in mammalian cells. Here, I identified another Ca^{2+}-dependent scramblase, Tmem63b, through CRISPR-sgRNA library screening. Tmem63b, a mechanosensitive cation channel, shares structural similarity to the Tmem16 family but differs in amino acid sequence. As Tmem16 family members function as both ion channels and scramblases, Tmem63b was revealed to exhibit phospholipid scramblase activity (PLS) in addition to its ion channel function in this study. Mutations in TMEM63B from patients with developmental and epileptic encephalopathy (DEE) and hematological disorders show constitutive PLS activity without Ca^{2+} ionophore stimulation, and the intensity of PLS activity among TMEM63B mutations correlates with the severity of anemia, linking TMEM63B-mediated PLS activity to hematological disorders in patients. Unlike Tmem16f and Xkr8, which form homodimers for PLS activity, Tmem63b forms a heterodimer with the thiamine transporter Slc19a2 to induce PLS activity. This complex formation is crucial for PLS activity: (1) Tmem63b alanine mutations that disrupt surface interaction between Tmem63b and Slc19a2 inhibit PLS activity; (2) dysfunctional Slc19a2, derived from human patients in thiamine-responsive megaloblastic anemia (THTR1), cannot form a complex with Tmem63b, preventing PLS activity; (3) the level of complex formation correlates with PLS activity among Tmem63b mutations, that is, more complex formation leads to higher PLS activity. Furthermore, Kcnn4, a Ca^{2+}-activated K^+ channel, was identified in the CRISPR-sgRNA library screening result. When Kcnn4 was inhibited with sgRNA or Kcnn4 inhibitors, Tmem63b/Slc19a2-mediated PLS activity was reduced, suggesting that Kcnn4-regulated K^+ efflux induces cell dehydration, thereby changing cell membrane tension and facilitating Tmem63b activation. Collectively, this study demonstrates that Tmem63b and Slc19a2 heterodimer induces PLS activity, indicating that two proteins with different functions exhibit a new function by forming a complex.

Abbreviation

ATP	Adenosine Triphosphate
ABC transporter	ATP-binding cassette transporter
BSG	Basigin
BDKO	Ba/F3 cells deficient in Tmem16f and Xkr8
BN-PAGE	Blue Native-PAGE
Casp3	Caspase-3
CBB	Coomassie brilliant blue
cDNA	Complementary DNA
CHS	Cholesteryl hemisuccinate
DNA	Deoxyribonucleic acid
DEE	Developmental and epileptic encephalopathy
ER	Endoplasmic reticulum
FACS	Fluorescence-activated cell sorting
FBS	Fetal bovine serum
Golgi	Golgi apparatus
HBSS	Hanks' Balanced Salt Solution
HEPES	4-(2-hydroxyethyl)-1-piperazineethanesulfonic acid
HMW	High molecular weight
HX disease	Hereditary xerocytosis disease
IL-3	Interleukin 3
IP	Immunoprecipitation
LMNG	Lauryl Maltose Neopentyl Glycol
LMW	Low molecular weight
MS	Mass Spectrometry
NBD-PC	7-nitrobenz-2-oxa-1,3-diazol-4-yl phosphatidylcholine
NPTN	Neuroplastin
OHCs	Outer hair cells
OSNs	Olfactory sensory neurons
P4-ATPase	Type IV P-type ATPases
PC	Phosphatidylcholine

PE	Phosphatidylethanolamine
PEI	Polyethylenimine
PI	Phosphatidylinositol
PLS	Phospholipid scrambling
PLSCR1	Phospholipids scramblase 1
PMs	Plasma membranes
PS	Phosphatidylserine
RNA	Ribonucleic acid
RT	Room temperature
scRNA-seq	Single cell RNA sequencing
sgRNA	Short guide RNA
SM	Sphinogomyelin
SCRD	Scrambling domain
SDS	Sodium Dodecyl Sulfate
Senicapoc	2,2-Bis (4-fluorophenyl)-2-phenylacetamide
SFO	Subfornical organ
Stim1	Stromal interaction molecule 1
SOCE	Store-operated calcium channel
TM	Transmembrane
TRMA	Thiamine-responsive megaloblastic anemia
TRAM-34	1-[(2-chlorophenyl) diphenylmethyl]-1H-pyrazole

1. Introduction

1.1 Asymmetric distribution of phospholipids

Cell membranes serve as a physical barrier, creating an aqueous environment for organelles while maintaining osmotic balance. Among the three major lipid types in the cell membrane, phospholipids are the most abundant molecules, compared to glycolipids and cholesterol. Phospholipids contain a hydrophilic (polar) head with two hydrophobic (nonpolar) tails, forming the "tail-to-tail" bilayers of the cell membrane. Phospholipids can be divided into different types according to the branch attached to the phosphate group: specifically, 43% of phospholipids are phosphatidylcholine (PC), 21% are phosphatidylethanolamine (PE), 4~7% are phosphatidylserine (PS) and phosphatidylinositol (PI). Additionally, 34% of phospholipids are constituted by sphingomyelin (SM)[1].

As the essential components of the cell membrane, phospholipids play a pivotal role in maintaining its integrity and fluidity. The generation of phospholipids is dynamic, with synthesis and modification in the endoplasmic reticulum (ER) and additional contributions from mitochondria and the Golgi apparatus (golgi)[2]. The generated phospholipids are subsequently transported to other organelles via vesicular transport, assisting with lipid composition and structural integrity. Within the bilayers, phospholipids exhibit several movements: (1) lateral movement for membrane fusion, transport, and receptor signaling; (2) rotational movement enhancing overall fluidity; and (3) transverse movement, catalyzed by specific enzymes, although less frequent, facilitating cell signaling transduction and recognition[3].

Although phospholipids are fluid within the membrane, the arrangement of phospholipids is not random. Freeze-fracture electron microscopy analysis showed that PS is predominantly kept on the cytoplasmic side, along with PE and PI, while PC and SM are mainly located in the outer leaflets (**Fig. 1-1**)[4,5]. Cell membrane fluidity and phospholipids asymmetric distribution are crucial for supporting numerous biological processes, including cell signaling transduction and recognition, membrane fusion, and apoptosis.

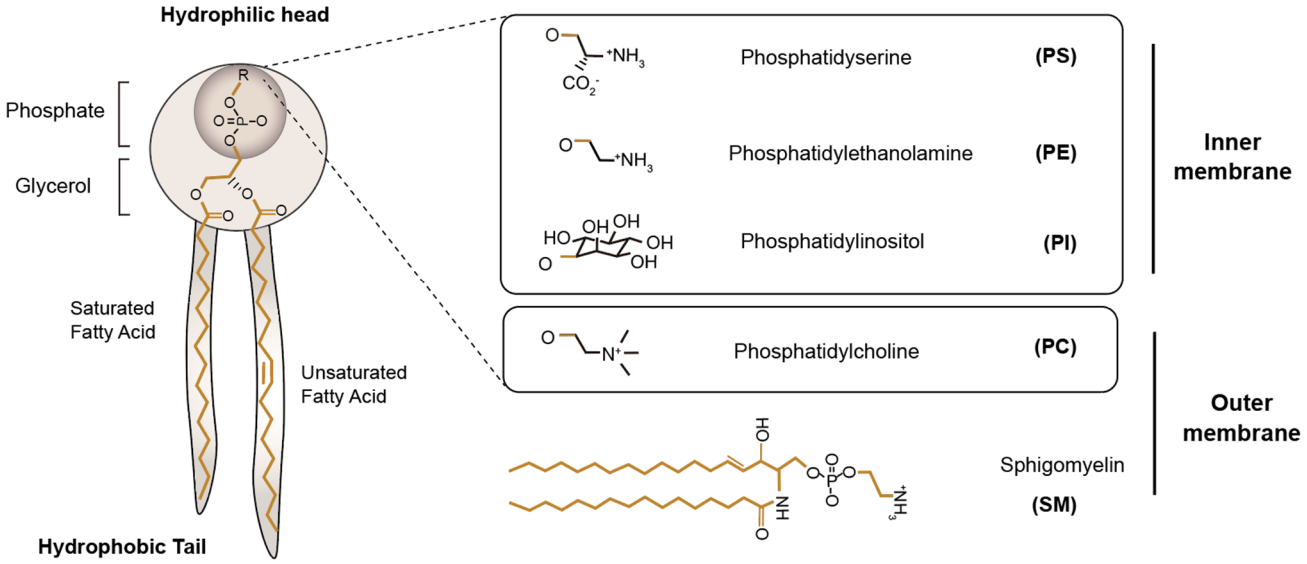

Fig. 1-1: Schematic of phospholipids and their distribution. A phospholipid has a hydrophilic head with two hydrophobic tails (one is saturated and another is unsaturated), divided into different types according to phosphate branches. Phosphatidyserine (PS), phosphatidylethanolamine (PE), and phosphatidylinositol (PI) have inner membrane localization. Phosphatidycholine (PC) and sphigomyelin (SM) have outer membrane localization.

The maintenance of asymmetrical phospholipid distribution relies on designated proteins: flippases, floppases, and scramblases. In humans, flippases are identified as ATP8A2, ATP11A, and ATP11C. ATP11A and ATP11C are members of the P4-ATPase family[6], widely expressed on the plasma membrane. These proteins require the chaperon protein CDC50A for appropriate intracellular localization and presumably flipping activity[7] in transporting anionic phospholipids such as PS and PE from the outer to the inner leaflets. Conversely, floppase refers to a specific type of ATP-binding cassette (ABC) transporter, like ABCB4, which facilitates moving PC from the inner to the outer leaflet[8]. Both flippases and floppases require ATP to establish and maintain asymmetric phospholipid distribution[9]. However, scramblases, which function in an energy-independent manner to scramble phospholipids bidirectionally, disturbs this asymmetry during some certain biological processes, permitting the externalization of PS from inner to outer membrane and the internalization of PC from outer to inner membrane (**Fig. 1-2**)[10,11]. The asymmetric disturbance of the phospholipids, such as exposing PS from the inner to the outer leaflet, has physiological significance as it serves as: (1) an 'eat me' signal for macrophage recruitment in apoptotic cell clearance; (2) a 'fuse me' signal for fusion in osteoclast formation, myotube incorporation, trophoblast generation, and sperm capacitation; and (3) a 'repair me' signal for injury response through vesicle generation that facilitate the release or uptake of viruses or exosomes. Scramblase-mediated rapid asymmetric distribution allows cells to finely tune their responses to environmental changes[12,13].

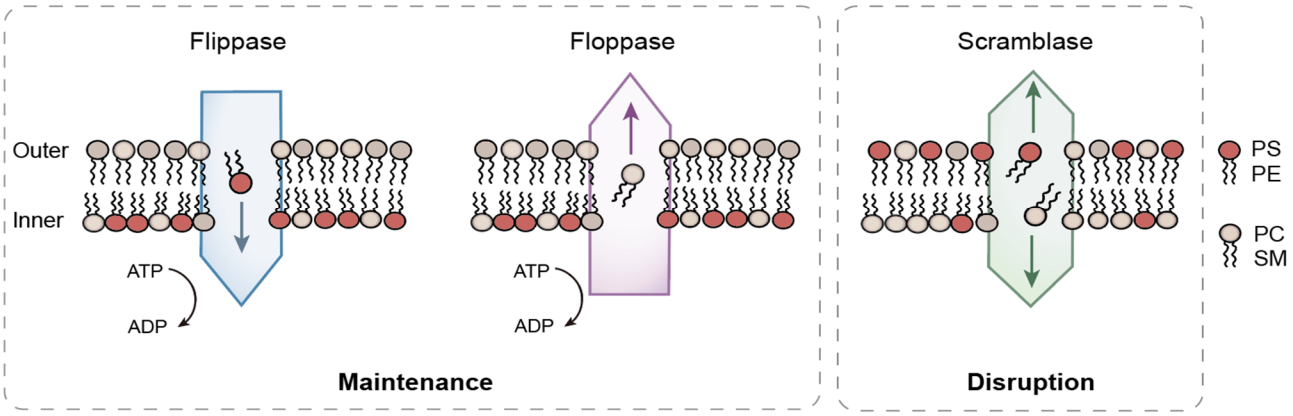

Fig. 1-2: Maintenance and disruption of phospholipid distribution. Asymmetric distribution is maintained by two enzymes, flippase and floppase, in an ATP-dependent manner, flippase is responsible for translocating phospholipids like PS and PE from the outer to inner layer; floppase is in charge of translocating PC and SM from the inner layer to outer layer. The disruption of asymmetric distribution is achieved by scramblase, which bidirectionally scrambles phospholipids in an ATP-independent manner.

1.2 Identified scramblase families

1.2.1 Tmem16 family

In 1996, PLSCR1 (phospholipid scramblase 1) was discovered, which was initially assumed to be a scramblase that revealed PS externalization under Ca^{2+} stimulation[14]. However, its molecular properties and in vivo study did not support PLSCR1's function as a scramblase[15,16]. Later studies employed a cDNA library from cells with high scrambling activity (19 times of PS exposure repeat sorting in mouse cell line Ba/F3 cells under Ca^{2+} ionophore stimulation) to identify bona fide scramblases through a screening method. In high molecular weight (HMW) (>2.5 kb) cDNA library screening, Tmem16f, a plasma membrane (PM) protein containing 10 transmembrane domains, was found to exhibit scrambling activity. The Tmem16f D409G mutant constitutively exposes PS to outer leaflets, confirming that Tmem16f acts as a Ca^{2+}-dependent scramblase[17]. Conversely, loss-of-function mutations in TMEM16F lead to impaired phospholipid scrambling (PLS) activity and have been seen in patients with bleeding disorder (Scott syndrome); in vivo studies have further demonstrated TMEM16F's role in regulating PS exposure during thrombus formation[18], highlighting the physiological significance of TMEM16F-mediated scrambling activity in activated platelets as a scaffold for recruiting coagulation factors (**Fig. 1-3a**)[13,19].

Among the TMEM16 family, TMEM16C, 16D, 16G, and 16J also function as Ca^{2+}-dependent scramblases at the plasma membrane, unlike TMEM16F which has ubiquitous expression, these family members have tissue-specific distribution[19]. TMEM16C is brain-specific; TMEM16D localizes to the

brain, eye, ovary, and uterus; TMEM16G is intestine-specific; and TMEM16J is expressed in the intestine and skin. TMEM16E, 16H, and 16K are intracellular membrane proteins with potential scrambling activity, while TMEM16A and TMEM16B primarily function as Ca^{2+}-activated chloride channels, which were discovered as ion channels prior to the discovering of scramblases among TMEM16 members. TMEM16A is ubiquitously expressed, whereas TMEM16B is specifically expressed in the retina[19].

Tmem16f forms a homodimer to achieve scrambling activity[20]. Each monomer contains two Ca^{2+} binding sites at E624 in TM6, E667, E670 in TM7, and E699, D703 in TM8. Ca^{2+} binding initiates a conformational change in TM6, interrupting contact with TM4 and opening a hydrophilic groove[21] that facilitates charged phospholipid head groups to be inserted while the hydrophobic tails remain in the lipid layer. This is known as the 'credit card' model as shown in **Fig. 1-3b**[22]. Meanwhile, a 15 amino acid scrambling domain (SCRD) encompassing the intracellular regions of TM4 and TM5 is critical for PLS activity; particularly, 9 amino acids are essential for PLS activity in Tmem16f. This SCRD imparts PLS activity onto Tmem16a by replacing the corresponding region with this SCRD region in Tmem16f. Conversely, swapping the Tmem16f SCRD region with Tmem16a greatly reduced PLS activity[23], suggesting that TM4 and TM5 are involved in phospholipid transit. (**Fig. 1-3b**).

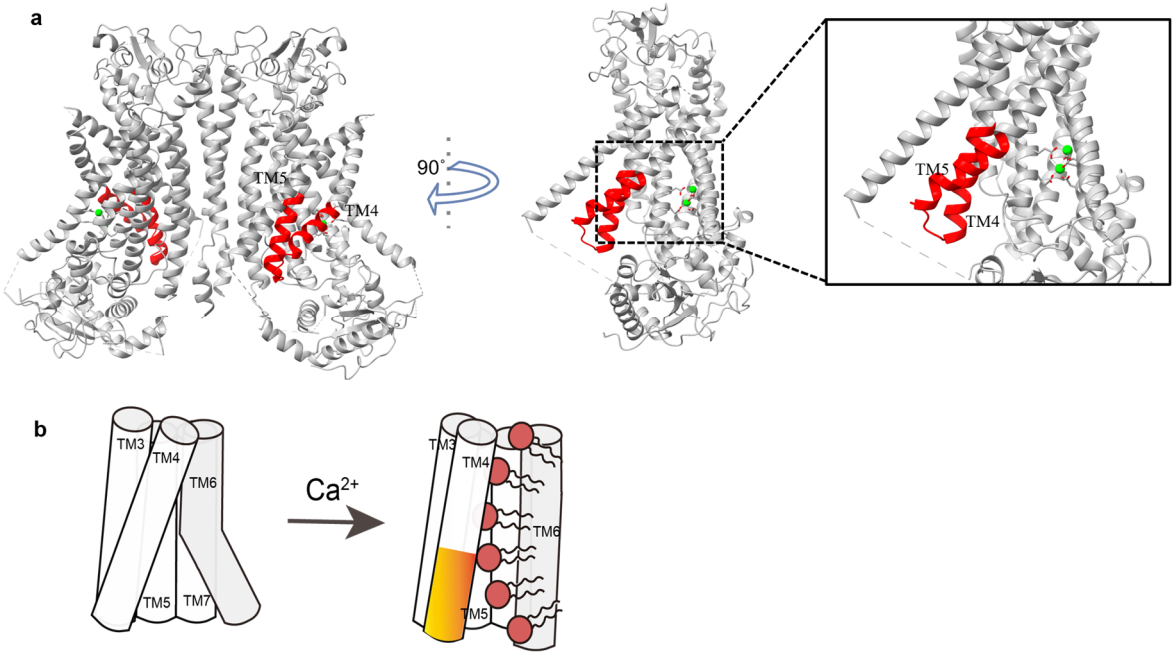

Fig. 1-3: Structure of Tmem16f and a proposed mechanism for its lipid scrambling. a Mouse Tmem16f (PDB: 8b8q) is shown as dimer (left); the red region represents SCRD. Transmembrane helices are numbered. Ca^{2+} (green) binding sites are shown in stick (middle); a closer view of Ca^{2+} binding sites and SCRD is shown on the right. **b** A proposed mechanism of Tmem16f. With no Ca^{2+} binding (left), TM3 to TM7 form a closed lipid-conductive cavity. When binds with Ca^{2+}, TM6 undergoes a conformational change, rendering opened cavity for passing hydrophilic head groups, SCRD labeled by orange is critical for passing phospholipids.

Besides the 'credit card' model, other models are also proposed such as (1) the 'stepping stone' model whereby atomic simulations uncovered two lipid head group interaction sites (extracellular site (*Se*) and intracellular site (*Si*)) flanking the groove[24], *Se* site of TMEM16F serves as "stepping stone" for phospholipids moving by binding to the "stones" via hydrophilic head group[25]; (2) the 'out-of-the groove' model raised by Malvezzi , M. *et al*., where they found fungal afTMEM16 scramblase can flip lipids with head groups larger than the width of the open groove[26]; and (3) the 'membrane distortion' model which pointed out membrane distortion does not require hydrophilic grooves to be opened, but rather distorts and thins the membrane near the groove to facilitate lipid scrambling[27,28]. Each model depicts different aspects of phospholipids scrambling across the cell membrane, integrating atomic simulation with structural analysis to better understand TMEM16F-mediated lipid scrambling.

1.2.2 Xkr family

In contrast to Ca^{2+}-stimulated PS exposure mediated by TMEM16F, thymocytes lacking TMEM16F still exhibit the ability to expose PS in response to apoptotic stimuli, indicating the presence of an alternative scrambling system. Through low molecular weight (LMW) (1-2.5 kb) cDNA library screening, Xkr8, a PM protein carrying 10 transmembrane regions, was identified as an apoptotic-induced scramblase[29]. In Xkr8-deficient cells, PS exposure during apoptosis is impaired, while Ca^{2+}-dependent scrambling activity remains unaffected, suggesting the independent functions of these two scramblases. Studies show that activated Xkr8 mediates PS exposure in senescent neutrophils, thereby regulating neutrophil circulation and homeostasis through apoptosis[29]. The absence of Xkr8 leads to unengulfed apoptotic cell accumulation and lupus-like autoimmune disease due to impaired apoptotic cell clearance, emphasizing its critical role in cell clearance[30,31].

Xkr8 requires basigin (BSG) or neuroplastin (NPTN) for membrane localization[32] and contains a well-conserved caspase-3 recognition site in its C-terminal region for activation[29]. Upon caspase cleavage, activated Xkr8-BSG/NPTN assembles into a heterotetramer that functions as scramblase[33]. This process is accompanied by the inactivation of flippase due to caspase-3 cleavage, resulting in irreversible PS exposure on the outer cell membrane, which serves as an 'eat me' signal for macrophages to engulf the apoptotic cells. In addition to caspase cleavage, Xkr8 can also be activated by phosphorylation at the conserved residues T356, S361, and T375, located downstream of the caspase recognition site. However, the flippase that flips PS to the inner layer is inhibited rather than destroyed by kinase-dependent Xkr8 activation. Consequently, the reversible PS exposure mediated by phosphorylation-activated Xkr8 fails to generate the 'eat me' signal, thus impeding the recruitment of macrophages for engulfment (**Fig. 1-4)**[34].

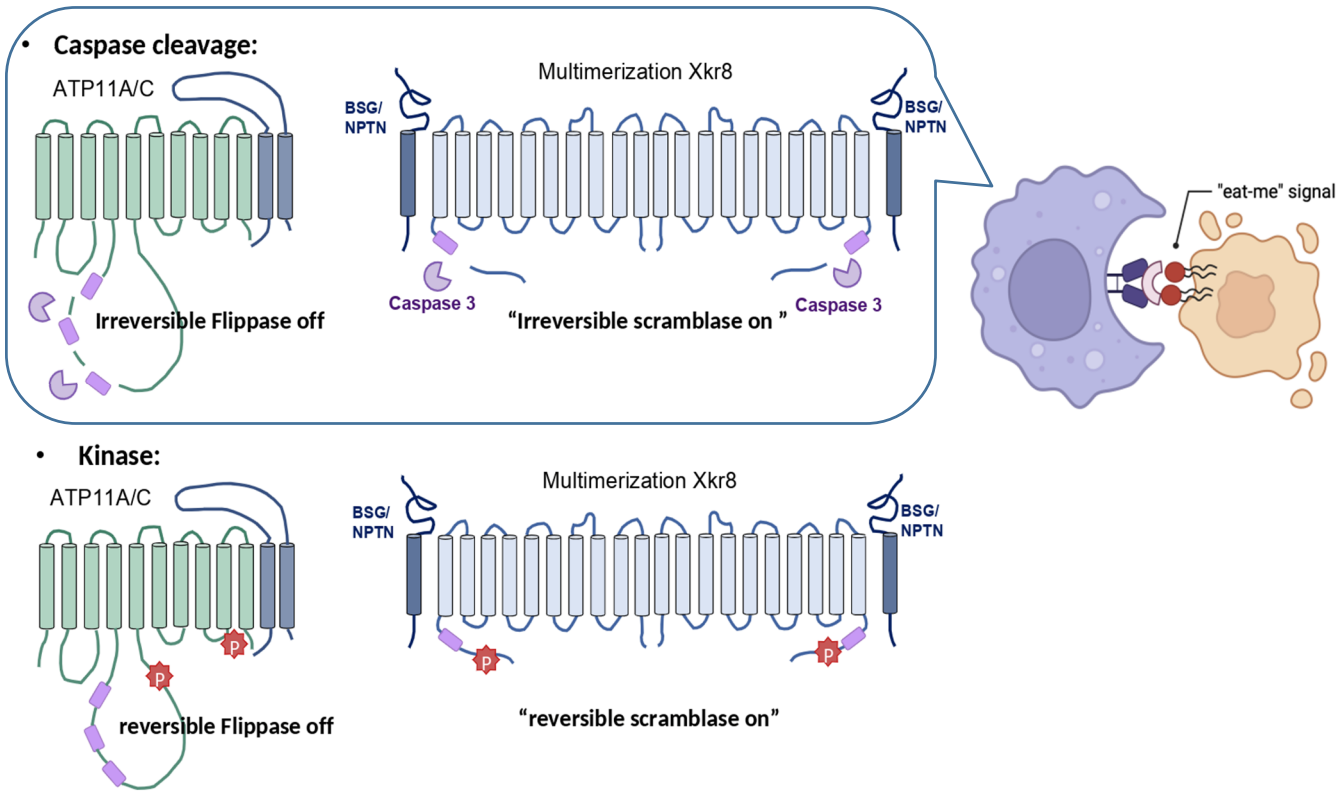

Fig. 1-4: Activation and physiological function of Xkr8. Two ways for activation of Xkr8. (1) Caspase-cleavage activates Xkr8, leading to its multimerization and irreversible PS exposure. This process is accompanied by the cleavage and irreversible inactivation of flippase, resulting in an 'eat-me' signal for macrophages to facilitate engulfment. (2) Phosphorylation activates Xkr8 while inhibiting flippase; however, this activation is reversible and does not function as a clearance signal.

Similarly, among the nine members of the Xkr family, Xkr9 and Xkr4 have specific tissue expression and caspase recognition sites in their C-terminus, enabling them to achieve scrambling activity during apoptosis. In contrast to the ubiquitous expression of Xkr8, Xkr4 is specifically expressed in the brain, and Xkr9 is restricted to the intestines[29,35]. This suggests that Xkr4 and Xkr9 may function as specialized scramblases in different tissues; however, whether they carry out specific functions beyond "clearance" still remains to be determined.

According to the findings of Sakuragi, T. *et al*., a set of hydrophilic residues is required for the stability of Xkr8/BSG, with six charged residues in TM1, TM4, and TM5 being essential for Xkr8 scrambling activity. Two activation models for Xk8 have been proposed: In the first model, phospholipids are initially recruited to the scrambling path via residues R158, Q163, and Q145; after these essential acidic residues create a repulsive force against the negatively charged phospholipid head groups, thereby widening the path for phospholipid passage. The second model resembles the 'credit card' model, as mentioned earlier; caspase cleavage may expand the space between TM1 and TM5, facilitating the insertion of phospholipid head groups into the hydrophilic cleft while leaving the acyl tails embedded in the membrane. In this model, the essential acidic residues are likely to further broaden the path[34].

1.3 Mechanosensitive channel OSCA/TMEM63

1.3.1 Structural similarity between OSCA and TMEM16

Mechanosensitive channels (MSCs) are membrane proteins capable of sensing and responding to mechanical stimuli in their external environment, converting these cues into biochemical signals[36]. They are presented among bacteria, archaea, and eukarya. Mechanical stress can roughly be classified as the following: (1) osmotic pressure, like cell swelling or shrinkage, OSCA/TMEM63 family of ion channels work as both mechanosensors and osmosensors. OSCA mediates stretch-activated currents in response to hyperosmolarity in plants. This process plays a crucial role in regulating water transpiration and root growth, which are essential for maintaining cell volume and viability, resulting in cell swelling or shrinkage[37,38]; (2) Actomyosin- induced cell deformation. TREK/TRAAK are two-pore domain potassium (K2P) channels that contribute to action potential propagation, sensory transduction, and muscle contraction. TREK is highly expressed in the human central nervous system (CNS), and it can be activated by temperature and membrane stretch[39,40]; (3) compressive and tensile stresses. As the first identified mechanically activated (MA) channel in humans, the PIEZO family is activated by touch stimuli that allow the influx of positively charged ions and drive vascular development[41]; (4) fluid shear stress, which acts on cell surfaces and protruding cilia. Primary cilia-localized TRPV4 modulates oscillatory fluid shear-induced calcium signaling and osteogenic gene expression[42]; (5) distortion of specialized structures, such as the stereocilia of auditory hair cells. TMC1, a component of the mechanotransduction complex within inner ear cells, transforms sound into electrical signals and is important for hearing[38,43].

Interestingly, as an ion channel, TMC is structurally similar to the TMEM16 family in that they both form a homodimer in the physiological state, despite having a different primary sequence[44–46]. As previously mentioned, the TMEM16 family includes both scramblase and ion channel members, leaving it unclear whether MA channels have additional functions beyond ion channel conduction. Studies show that inhibiting the mechanoelectrical transduction (MET) channel leads to PS exposure in auditory hair cells in a TMC1-dependent manner, which is a component of the MET channel pore[47]. Mutations in TMC1 in hair cells result in constitutive PS externalization and membrane blebbing, leading to deafness by disrupting membrane homeostasis. On the other hand, *Tmc1*$^{-/-}$ hair cells fail to expose PS, indicating TMC1 might function as Ca^{2+}-inhibited lipid scramblase in addition to forming the MET channel[47].

Based on the ability of TMC1 to externalize PS, there is a possibility that other MA channel proteins, such as OSCA1.2, may also exhibit PLS activity. OSCA1.2 has 11 transmembrane domains; except from one TM helix (TM0), the remaining TM helices generally overlap with Tmem16a, as shown in **Fig. 1-5**. Its homodimer adopts a “butterfly fold” structure similar to Tmem16a. A recent study using liposome and

nanodisc methods uncovered that each subunit of the OSCA1.2 homodimer could open independently under increased membrane tension, forming a "proteo-lipids pore", in which lipids can behave as a wall of the ion permeation pathway[48]. This activated structure is consistent with TMEM16 family subunits that can be activated independently[49,50], allowing both ion conductance and lipid scrambling to occur in the same conformation[51,52].

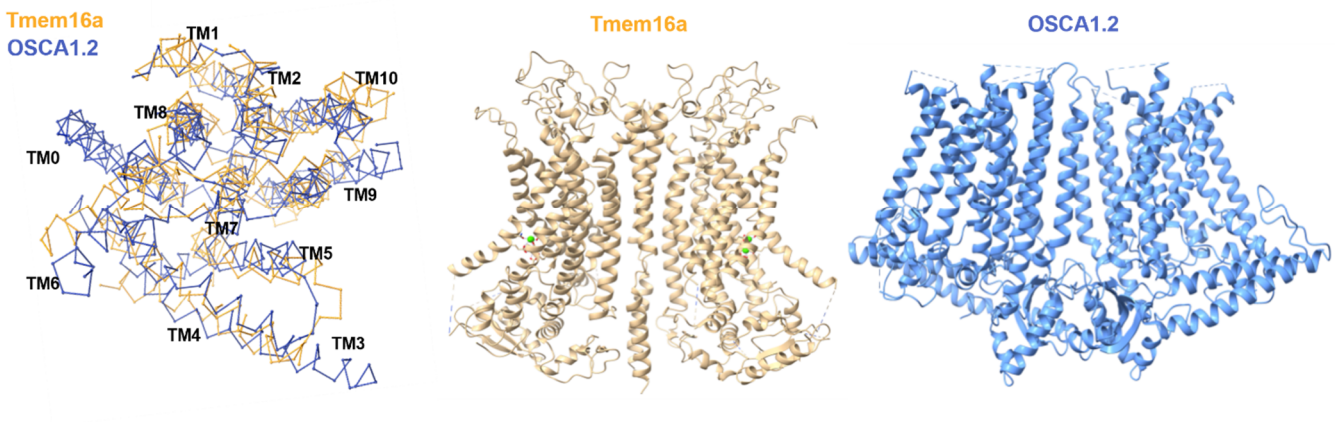

Fig. 1-5: OSCA1.2 structure. Alignment of monomer Arabidopsis thaliana OSCA1.2 (blue, PDB: 6mgv) and monomer mouse Tmem16a (yellow, PDB: 5oyb). OSCA1.2 transmembrane domains are labelled as TM0 ~ TM10 (left). Structures of mouse Tmem16a and OSCA1.2 are presented as homodimers (right).

1.3.2 Physiological functions of TMEM63

In mammals, the OSCA1.2 ortholog is TMEM63B, one of three members of the TMEM63 family, alongside TMEM63A and TMEM63C. TMEM63A has been associated to "infantile-onset transient hypomyelination" disorders, with heterozygous TMEM63A variants causing deficiencies in generating stretch-activated currents[53]. TMEM63C is vital for maintaining the kidney filtration barrier integrity, with variants causing mitochondrial morphology defects[54].

TMEM63B localizes at plasma membranes and contains 11 TM helices with a long intracellular linker for sensing membrane tension between TM2 and TM3. It also shares a similar tertiary structure to the human TMEM16 family, like TMEM16A (**Fig. 1-6a, b**). Unlike OSCA1.2 which forms homodimers in plants, the cryo-EM analysis of the TMEM63 family indicates that TMEM63A, TMEM63C, and TMEM63B exist as monomers[55,56]. On the other hand, unlike OSCA1.2, which is activated under hyperosmotic conditions, TMEM63B mediated ion influx in response to both hypo-osmotic stimuli and hyper-osmotic stimuli[57].

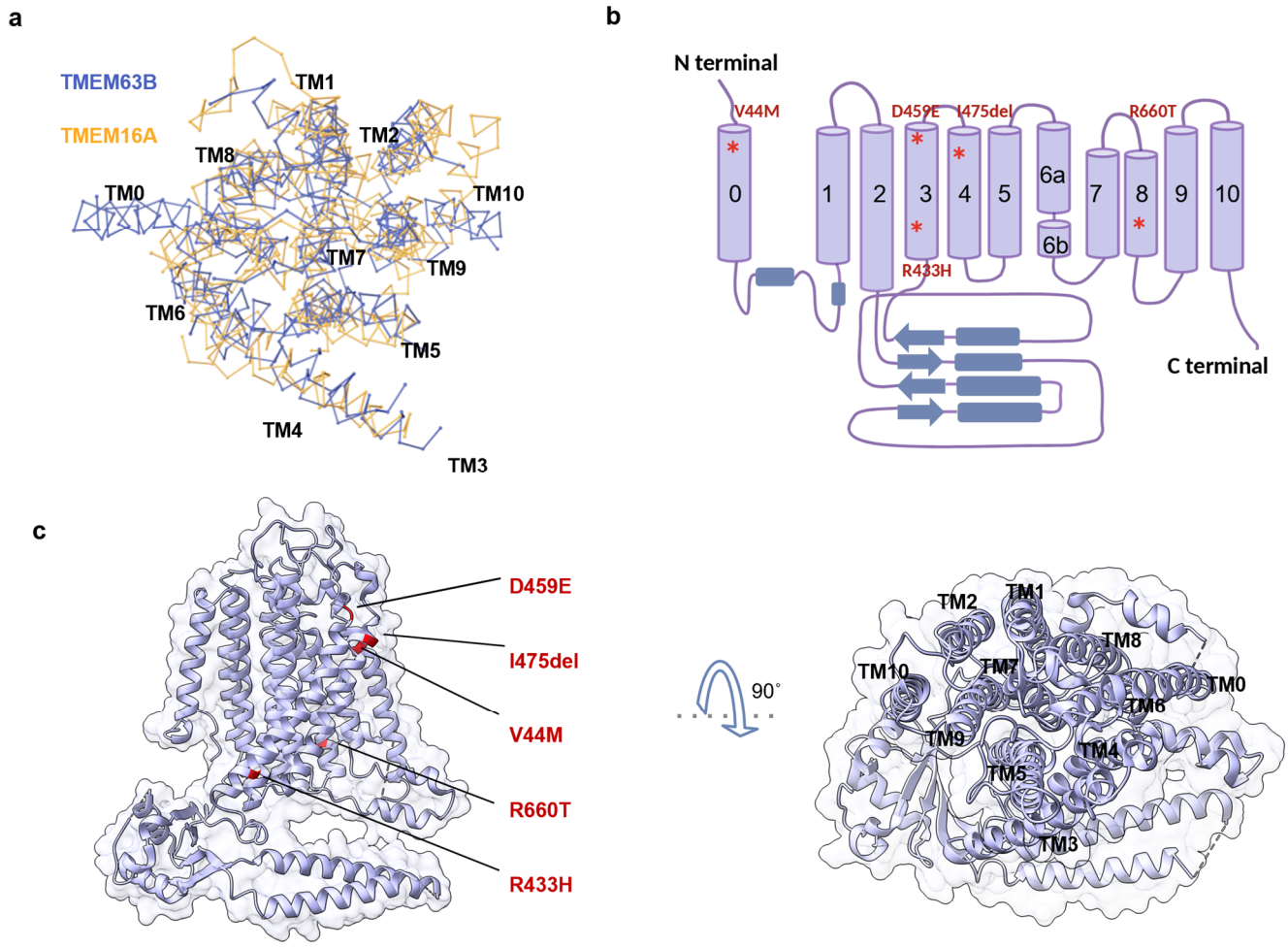

Fig. 1-6: TMEM63B structure. a Alignment of monomer human TMEM63B (blue) and monomer human TMEM16A (yellow). TMEM63B transmembrane domains are labeled as TM0 ~TM10, which overlap with TMEM16A transmembrane domains TM1~TM10. **b** Topology diagram of TMEM63B. Location of the identified disease mutants (V44M, R433H, D459E, I475del, and R660T) on a schematic representation; the position of the mutations is presented as an asterisk. **c** Structure of human TMEM63B protein (PDB: 8ehx). Mutations are colored in bold red.

In animals, TMEM63B plays a variety of roles. In addition to the significance of TMC for hearing, TMEM63B serves as an osmosensor in outer hair cells (OHCs) that is activated by hypotonic stress. Genetic deletion of TMEM63B in OHCs causes progressive hearing loss[58]. On the other hand, TMEM63B enhances cell migration in HEK293T cells and promotes wound healing. Moreover, TMEM63B engages in sensing functions like (1) Humidity sensing, where TMEM63B acts as a humidity sensor to mediate hygrosensation in drosophila olfactory sensory neurons (OSNs)[59]. (2) Thirst sensing, as it functions as an osmosensor in the excitatory subfornical organ (SFO) thirst neurons; deletion of Tmem63b impairs water appetite and hyperosmolarity-induced drinking behavior[60]. (3) Food texture sensing, in which TMEM63B is required for sensing particle size in food in the multidendritic neuron (md-L) of drosophila, while TMC senses the hardness and viscosity of food[61]. These reported TMEM63B functions are primarily associated

with sensory cells or neurons that respond to mechanical inputs, acting as a mechanosensor and osmosensor.

A recent study by Vetro, A. *et al*. identified ten distinct variants of TMEM63B in 16 patients. This is the first time TMEM63B has been associated with clinical pathology in humans[62]. The patients suffered from severe developmental and epileptic encephalopathy (DEE), intellectual disability, severe motor and cortical visual impairment, and progressive neurodegenerative brain changes. Moreover, 12 patients were accompanied with hematological abnormalities such as macrocytosis and hemolysis anemia, with some requiring blood transfusions. Some TMEM63B mutants are listed in **Table 1-1** and their structural localizations are shown in **Fig. 1-6b, c**.

Considering TMEM63B shares structural similarities with TMEM16 and TMC families, TMEM16 has scramblase members and TMC1 can externalize PS; moreover, its ortholog OSCA1.2 possesses a "proteo-lipid" pore. Therefore, TMEM63B is expected to exhibit scrambling activity alongside its ion channel function. However, TMEM63B differs from OSCA1.2 and TMC in that it exists as a monomer, while the latter two form homodimers. This raises questions of whether TMEM63B has a specific mechanism for its activity, as well as how mutations may contribute to neurological diseases and hematological disorders, which needs further study.

Table 1-1: TMEM63B pathological mutations and clinical phenotypes (adapted from Vetro, A. *et al.*[62])

TMEM63B variant	Age at last follow-up/death	Age at seizure onset/type	Seizure types/severity during follow-up	Clinical neurological phenotype	Haematological findings
I475del	16 years	6 months/ infantile spasms	Tonic/daily GTCs/monthly	Global profound DD, generalized hypotonia, microcephaly, visual impairmnt, nystagmus, squint, spastic quadriparesis, dysphagia (PEG 12 years)	Severe hemolytic anemia, transfusion dependent
V44M	17 years	4 months/ infantile spasms	1 year: generalized tonic, focal motor with impaired awareness/daily	Global profound DD, quadriparesis, dysphagia (PEG 12 years)	Severe anemia, occasional transfusions
D459E	3 years	2 weeks/focal	Slow bilateral independent focal, epileptic spasms/daily	Global profound DD, quadriparesis, generalised hypotonia, dysphagia cortical blindness with roving eye movements	Mild macrocytic anaemia
R660T	25 years	11 months/ infantile spasms	Focal with posturing and impaired awareness, recurrent SE/yearly	Global moderate DD, spastic quadriparesis, ASD	Macrocytic anaemia
R433H	10 years	birth/focal	Bilateral independent focal motor with impaired awareness, focal to bilaternal tonic clonic /weekly	Global profound DD, ataxic gait, lower limb hypertonia, nystagmus	Mild abnormalities of RBCt, MCV, MCH

Mutations in the metabolite thiamine transporter are also reported to be responsible for hematologic abnormalities. Thiamine transporters 1 and 2 (THTR1 and THTR2) both contain 12 transmembrane regions and are widely expressed in various tissues. Both THTR1 and THTR2 belong to solute carrier family 19 (Slc19), which primarily facilitates the active transport of B group vitamin such as folic acid

(Slc19a1) and thiamine (Slc19a2 and Slc19a3)[63,64]. Slc19a2 is a highly selective thiamine transporter localized in both PM and intracellular compartments, and dysfunctional mutations in Slc19a2 cause thiamine-responsive megaloblastic anemia (TRMA), as reported by Zhang, S. *et al*., different mutation types such as nonsense, missense and frameshift recurrent mutants in Slc19a2 are listed in **Table 1-2**[65]. Thiamine is an essential component for energy metabolism, amino acid metabolism, and cellular growth, and it participates in multiple metabolic processes[64,66,67]. In addition to Slc19a2, Slc19a3 also facilitates thiamine transport. Hence, thiamine deficiency caused by Slc19a2 mutations can be compensated by Slc19a3 and passive transport. However, Slc19a2 is the only thiamine transporter in the bone marrow, pancreatic beta cells, and a subgroup of cochlear cells. That explains why TRMA mutations in Slc19a2 are typically characterized with a triad of megaloblastic anemia, progressive sensorineural deafness, and nontype 1 diabetes mellitus[68].

Table 1-2: Distribution of mutations on Slc19a2 and the mutation effects (adapted from Zhang, S. *et al*.[65])

Distribution	Mutation	Mutation type	Site of protein be truncated or changed	No. of familits /patients	Area of Origin (NO. of families)
Exon 1	196G > T	nonsense	Extracelluar	7/15	Pakistan (6) / India (1)
Exon 2	241_242insA	nonsense	Transmembrane	10/19	Turkey (3) / Iran (4) / Pakistan (1) / Syria (1) / Italy (1)
Exon 2	428C > T	missense	Transmembrane	4/4	Tunis (1) / Brazil (1) / Saudi Arabia (1) / France (1)
Exon 3	1001G > A	missense	Extracelluar	3/3	Czech Republic (2) / Austria (1)
Exon 4	1147_484delGT	frameshift	Extracelluar	4/4	Turkey(4)
Exon 5	1232delT	frameshift	Cytoplasmic	1/1	China
Exon 6	1370delT	nonsense	Extracelluar	1/2	Italy

1.4 Cation channels involved in scrambling activity and cell apoptosis

1.4.1 Ion homeostasis regulates cell apoptosis

Cellular ionic homeostasis is essential for regulating apoptosis, driving water movement and leading to cell shrinkage. In particular, K^+ homeostasis has been proposed as a significant inducer of apoptosis[69]; apoptotic cells have lower intracellular K^+ levels than healthy cells, and inhibiting K^+ efflux completely eliminates apoptosis. The anti-apoptotic effect of intracellular K^+ is due to its ability to suppress cytochrome C release from mitochondria and prevent Apaf-1 formation[70], thereby inhibiting downstream apoptotic signal transduction[71]. On the other hand, ion regulation in apoptosis takes place not only within

intracellular clues but also in cells lacking nuclei and mitochondria. In erythrocytes, apoptosis occurs in the absence of these key apoptotic-related organelles[72]. Research has shown that ion channels play a critical role in this process, with Ca^{2+} ionophore ionomycin treatment in erythrocytes further activating the Ca^{2+}-sensitive K^+ channel (Gardos channel). This activation leads to K^+ efflux, cell shrinkage, membrane blebbing, and loss of phospholipid asymmetry[72]. PS exposure is blunted at K^+ (~150 mM) or in the presence of the Gardos channel inhibitors, indicating that K^+ depletion is important for erythrocyte apoptosis[73].

1.4.2 Ca^{2+}-activated potassium channel: Kcnn4

Ca^{2+}-activated potassium channels are broadly categorized into three types depending on the channel conductance: small-conductance (SK), intermediate-conductance (IK), and big-conductance (BK) channels. SK channels consist of Kcnn1, 2, and 3, while IK is produced by Kcnn4, and BK channels are most likely generated by Slo (Kcnma1)[74]. IK channels are predominantly expressed in hematopoietic cells and several organs involved in salt and fluid transport, contributing to the K^+ permeability and dehydration, further promote erythrocyte apoptosis[73]. Kcnn4 assembles as tetramers in the plasma membrane of red blood cells (RBCs). Gain-of-function mutations in Kcnn4 increase Ca^{2+} sensitivity and constitutive activation, linking Kcnn4 to hereditary xerocytosis (HX) disease—a rare, autosomal dominant congenital hemolytic anemia (CHA) characterized K^+ and water loss[75,76]. Additionally, HX disease is also caused by mutations in Piezo1[77,78], the mechanosensitive channel related to touch sensation and Ca^{2+} influx, as mentioned before. Many patients have been found to have heterozygous Piezo1 mutations that cause delayed channel inactivation[79]. Studies further show the relevance of Piezo1 in regulating cation permeability in RBCs[80], revealing that mutants Piezo 1 in RBCs have significant Na^+ absorption and pronounced K^+ loss, with this K^+ loss being sensitive to Kcnn4 inhibitors (TRAM-34 and Senicapoc)[79]. The mechanically activated Ca^{2+} influx via Piezo1 then activates Kcnn4, resulting in K^+ loss and dehydration[81]. Taken together, Piezo1 mutations related to HX result in improper activity of enhanced Kcnn4 activity, causing phenotypic variability among patients. Furthermore, Kcnn4 links Piezo1-mediated Ca^{2+} influx to K^+ efflux, facilitating NLRP3 inflammasome activation[82].

1.4.3 Intracellular Ca^{2+} regulators: Stim1/Orai1

In addition to K^+ efflux, Ca^{2+} homeostasis also plays an important role in the regulation of apoptosis[83]. Ca^{2+}, a crucial secondary messenger in various signaling pathways, regulates key cellular activities such as myofilament contraction, hormone secretion, mitotic division, and neurotransmitter release[84–86]. Ca^{2+} homeostasis is strictly controlled by various regulatory mechanisms, including calcium pumps and channels. Increased intracellular Ca^{2+} from ER release and capacitative influx have been proposed to be

apoptogenic[87]. Additionally, intracellular Ca^{2+} inhibits flippase activity and stimulates Ca^{2+}-dependent scramblase like TMEM16F, altering phospholipid asymmetry.

In many non-excitable cells, depletion of Ca^{2+} in ER is sensed by Stromal interaction molecule 1 (Stim1), a single transmembrane protein located in the ER. This triggers a conformational change of Stim1, leading to its oligomerization[88]. Activated Stim1 moves to the ER-PM contact site where it recruits the plasma membrane protein Orai1, the Ca^{2+} release-activated Ca^{2+} (CRAC) channel, to influx Ca^{2+} into the cytosol and finally replenish the Ca^{2+} level in the ER via the sarcoplasmic Ca^{2+}-ATPase (SERCA) pump[88]. In this process, another Ca^{2+}-sensitive protein, E-syt1, is also involved. As part of the synaptotagmins (ESYTs) family, E-syt1 helps tether the ER to the PM in a phosphatidylinositol 4,5-bisphosphate (PIP2)-dependent manner[89]. Live-cell super-resolution microscopy has shown that during Stim1 activation for ER Ca^{2+} replenishment, E-syt1 contributes to the formation of new ER-PM contacts into ring structures, facilitating rapid replenishment of ER Ca^{2+} stores (**Fig. 1-7**)[85,89] catalyzing phospholipid shutting, and mediating sustained receptor-induced Ca^{2+} signaling. This process is somewhat related to the scrambling ability of some anoctamins[85,90]. When the concentration of Ca^{2+} reaches a certain threshold, the store-operated calcium channel (SOCE) (include Stim1 and Orai1) will be inactivated by the SARAF (TMEM66) protein through its association with Stim1[91].

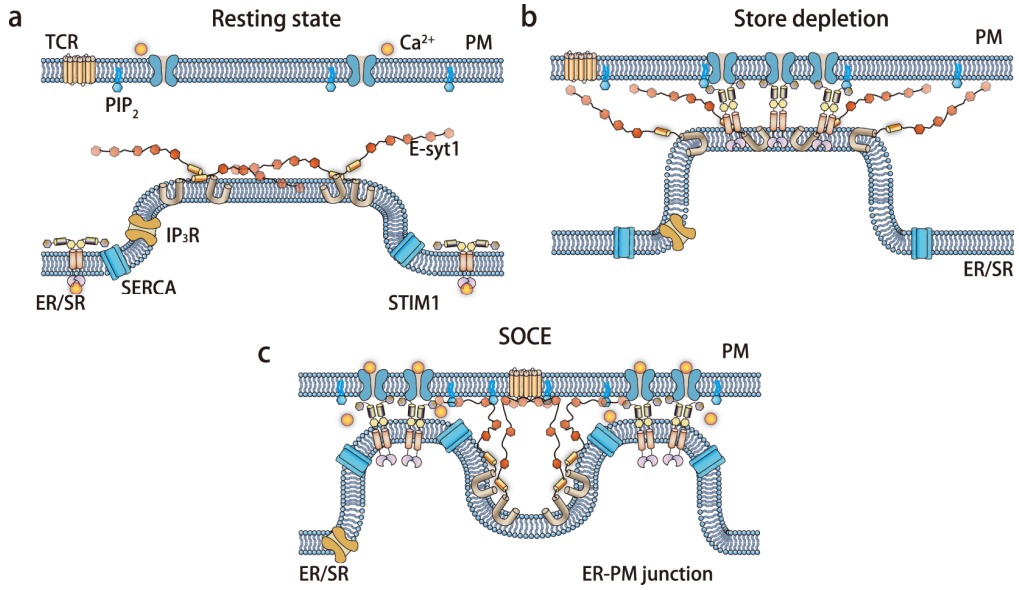

Fig. 1-7: Stim1/Orai1 collaborates with E-syt1 to regulate ER-PM contact site and replenish Ca^{2+}. a Resting state. **b** ER Ca^{2+} store depletion. Activated Stim1 multimer gates with Orai1 to influx Ca^{2+} in the cytosol. **c** Store replenishment. Initial Ca^{2+} influx mediated by Stim1/Orai1 prompts Esyt-1 to reshape the ER-PM contact site to facilitate Ca^{2+} replenish. This image comes from Kang, F. *et al.*[89]

Mutations in Stim1/Orai1 are associated with various disease phenotypes. Loss-of-function mutations in Stim1/Orai1 cause severe combined immunodeficiency (SCID), autoimmune hemolytic anemia,

thrombocytopenia, muscular hypotonia, and disturbed enamel dentition[92]. Gain-of-function mutations lead to constitutive activation of the CRAC channel, associated with an overlapping spectrum of diseases[93].

1.5 Lipid transportation protein: SNARE protein

Cell membrane fusion is promoted by lipid movement via SNARE proteins, which bring two membrane lipid bilayers into close proximity, inducing membrane fusion[94]. SNARE proteins contain three highly conserved families: Vamps (vesicle-associated membrane proteins), syntaxins (STXs), and SNAPs (synaptosome-associated proteins)[95]. They assist in transporting proteins between cell compartments and forming transport vesicles, such as lysosomes or endosomes, which deliver proteins to their destination[96]. Additionally, SNARE proteins can regulate lipid transport between cellular compartments.

1.6 Project aim and summary

Based on identified scramblases in the TMEM16 family and the XKR family, TMEM16F and XKR8 are both plasma membrane proteins. Among hundreds to thousands of plasma proteins, it is highly possible that other plasma membrane proteins function as scramblases, with different physiological implications. In this study, my aim was to discover a novel scramblase, understand its mechanism, and explore its physiological function.

To identify potential scramblase(s), I conducted an unbiased sgRNA library screening in TMEM16F- and XKR8-deficient cells. Through the knockout and overexpression of the candidate gene, I confirmed that Tmem63b is the new PLS activity factor. Then Tmem63b mutations found in patients with DEE and hematological disorders can exhibit constitutive PLS activity, and the PLS activity level correlates with hematological severity. Given that TMEM63B is specifically expressed in the erythrocytes within bone marrow through scRNA-seq analysis, I hypothesize that Tmem63b functions as an RBC scramblase, regulating PS exposure on the RBC membrane to trigger phagocytosis-induced anemia.

To explore the mechanism of the Tmem63b-mediated PLS activity pathway, sgRNA library screening was performed in Tmem63b-expressing cells, and co-factors Kcnn4 and Slc19a2 were revealed to be integrated in the Tmem63b-PLS pathway. Kcnn4 inhibitor treatment and extracellular K^+ incubation assay indicated that activated Kcnn4 assists Tmem63b to achieve PLS activity. On the other hand, BN-PAGE and IP-MS assays suggested that Slc19a2 forms a complex with Tmem63b, which is essential for PLS activity. Based on the AlphaFold2 prediction of the Tmem63b/Slc19a2 complex, substituting surface interaction residues in Tmem63b with alanine results in a loss of binding with Slc19a2 and inhibition of PLS activity, indicating that Tmem63b/Slc19a2 complex, along with Kcnn4 activation, initiates PLS activity.

2. Materials and Methods

2.1 List of plasmids and reagents

REAGENT or RESOURCE	SOURCE	IDENTIFIER
Genes		
mTmem63a	NCBI	no. NM_001417552.1
mTmem63b	NCBI	no. NM_001413622.1
mTmem63c	NCBI	no. NM_001361704.1
mCsnk2b	NCBI	no. NM_ 001303445.1
mSlc19a2	NCBI	no. NM_054087.3
mKcnn4	NCBI	no. NM_001163510.2
mStim1	NCBI	no. NM_001374058.1
mOrai1	NCBI	no. NM_175423.3
Antibodies		
Anti-AnnexinV-Cy5	Biovision	5K04L0130
Anti-Kcnn4	Proteintech	2371-1-AP
Anti-DDDDK	MBL	PM020
Anti-HA.11 Epitope Tag	Biolegend	16B12
Goat anti-rabbit immunoglobulins/HRP	DAKO	Cat# P0488
Anti GFP HRP	MBL	598-7
Chemicals		
NBD-PC	Avanti Polar Lipids	810132P
BSA Fatty-acid free	Sigma-aldrich	A6003
A23187	Sigma	C7522
Fluo4-AM	Dojindo	WH620
PEG 1500	Roche	783641
DAPI	Dojindo	D523

Propidium iodide (PI)	Dojindo	25535-16-4
Puromycin	InvivoGen	58-58-2
Fatty acid (FA)-free BSA	Sigma	A6003
BAPTA-AM	Dojindo	EQ042
Cholesteryl hemisuccinate (CHS)	Sigma	C6512
Lauryl Maltose Neopentyl Glycol (LMNG)	Anatrace	NG310
TRAM-34	Selleck	S1160
Senicapoc	Selleck	E0501
Poly-L-lysin	Sigma	P2636
Reagent		
Gel /PCR Extraction kit	FastGene	FG-91302
Miniprep kit	FastGene	FG-90502
Midiprep kit	Roche	75028900
RNeasy kit	Qiagen	74104
High-capicity RNA-to-DNA kit	Thermo fisher scientific	4387406
TB Green Premix Ex Taq™ II (Tli RNaseH Plus)	TAKARA	RR820S
Experimental Models: Cell Lines		
293T cells	Pear. *et al*., 1993	Nagata. S lab, Osaka Univ.
BDKO cells (Ba/F3 cells deficient in Xkr8 and TMEM16F)	This paper	N/A
Stim1$^{-/-}$ BDKO cells	This paper	N/A
Tmem63b$^{-/-}$ BDKO cells	This paper	N/A
Stim1$^{-/-}$ *Tmem63b*$^{-/-}$ BDKO cells	This paper	N/A
Recombinant DNA		
Plenti-CAG HIV-Gag-Pol	Riken	RDB04394
Plenti-CMV VSVG-RSV-REV	Riken	RDB04393
GeCKO v2 Mouse CRISPR Knockout Pooled Library	Addgene	#1000000052 #1000000053

pMX-neo-DsRED	This paper	N/A
PMX-puro-GFP	This paper	N/A
Plenti-*sgTmem63b*-Puro	This paper	N/A
Plenti-*sgStim1*-Puro	This paper	N/A
Plenti-*sgEsyt1*-Puro	This paper	N/A
Plenti-*sgOrai1*-Puro	This paper	N/A
Plenti-*sgSnap23*-Puro	This paper	N/A
Plenti-*sgStx4*-Puro	This paper	N/A
Plenti-*sgCsnk2b*-Puro	This paper	N/A
Plenti-*sgKcnn4*-Puro	This paper	N/A
Plenti-*sgSlc19a2*-Puro	This paper	N/A
Plenti-mTmem63a-tagRFP	This paper	N/A
Plenti-mTmem63b-tagRFP	This paper	N/A
Plenti-mTmem63c-tagRFP	This paper	N/A
Plenti-mTmem63a-GFP	This paper	N/A
Plenti-mTmem63b-GFP	This paper	N/A
Plenti-mTmem63c-GFP	This paper	N/A
Plenti-mTmem63b I475del-GFP	This paper	N/A
Plenti-mTmem63b V44M-GFP	This paper	N/A
Plenti-mTmem63b D459E-GFP	This paper	N/A
Plenti-mTmem63b R660T-GFP	This paper	N/A
Plenti-mTmem63b R433H-GFP	This paper	N/A
Plenti-mSlc19a2-tagRFP	This paper	N/A
Plenti-mSlc19a2-S143F-tagRFP	This paper	N/A
Plenti-mKcnn4-tagRFP	This paper	N/A
Plenti-mKcnn4-H358N-tagRFP	This paper	N/A
Plenti-Tmem63b-GFP-Flag	This paper	N/A

Plenti-Kcnn4-HA-tagRFP	This paper	N/A
Plenti-Slc19a2-HA-tagRFP	This paper	N/A
Plenti-mStim1-tagRFP	This paper	N/A
Plenti-mOrai1-tagRFP	This paper	N/A
Plenti-Orai1-R91W-GFP	This paper	N/A
Plenti-mCsnk2b-GFP	This paper	N/A
Plenti-Tmem63b-Ala (F213A / F217A / M711A / F712A / I719A)-GFP	This paper	N/A

Software and Algorithms		
ImageJ	Schneider, C. A. *et al*., 2012[97]	https://imagej.nih.gov/ij/
GraphPad PRISM 10	GraphPad	https://www.graphpad.com
Illustrator V 28.1	Adobe Illustration	https://www.adobe.com/products/illustrator.html
FastQC	Babraham Bioinformatics	https://www.bioinformatics.babraham.ac.uk/projects/fastqc/
Cutadapt	Martin, M. 2011[98]	http://code.google.com/p/cutadapt/
MAGeCK	Li, W. *et al.* 2014[99]	https://sourceforge.net/projects/mageck/
GuideV.1.0.0	Noguchi, Y. *et al.* 2024[100]	https://github.com/SuzukiLab-icems/guide-caller/tree/main/v1.0.0
FlowJo	FlowJo. LLC	https://www.flowjo.com/
Chimera X-1.5	UCSF chimera program	https://www.rbvi.ucsf.edu/chimerax/
CRISPRdirect	CRISPRdirect	https://crispr.dbcls.jp/
Other		
GFP conjugated beads	Protech	SVP-15-5

2.2 Cell culture

HEK293T cells were cultured in the High Glucose DMEM (WAKO) with supplements of 10% Fetal Bovine Serum (FBS) (Gibco) and 1% Penicillin-Streptomycin solution (Nacalai). Mouse interleukin 3(IL-3)-dependent pro-B cell line Ba/F3 cells with Xkr8 and Tmem16F (BDKO cells) deficiency were maintained in RPMI1640 (WAKO) containing 10% FBS (Gibco), 1% Penicillin-Streptomycin solution, 45 units/ml IL-3 (as prepared before[17]), and 55 μM beta-mercaptoethanol (Gibco). Cells were maintained in a culture incubator set at 37˚C, supplied with 5% CO_2 at 90-95% humidity.

2.3 Construction of plasmids

Plasmid construction included utilizing a lentivirus vector (plenti)[19] that was digested by restriction enzymes to combine with amplified target genes using the In-Fushion system from Takara. In particular, target genes like mTmem63a, mTmem63b, mTmem63c, mSlc19a2, mKcnn4, mStim1, mOrai1, and mCsnk2b were obtained from BDKO cDNA through PCR and fused with GFP or tagRFP at the C-terminus. In some cases, amplified DNA was fused with FLAG, HA, FLAG-GFP, or HA-tagRFP. Plasmids were confirmed by sequencing.

The mutant plasmids were generated by using the primers targeting desired mutation sites to achieve specific amino acid substitutions and each gene was amplified by PCR, followed by inserting them into plenti vectors and confirming with sequencing. Tmem63b variants (V44M, R433H, D459E, I475del, and R660T) were generated by replacing valine with methionine at 44, replacing arginine with histidine at 433, replacing aspartic acid with glutamic acid at 459, deleting isoleucine at I475 and replacing arginine with threonine at 660, respectively. The Tmem63b alanine mutant (F213A, L217A, M711A, F712A, and I719A) was generated by substituting phenylalanine at 213, Leucine at 217, methionine at 711, phenylalanine at 712, and isoleucine at 719 with alanine. An Slc19a2 mutant (S143F) was generated by replacing serine with phenylalanine at 143. A Kcnn4 mutant (H358N) was generated by replacing histidine with asparagine at 358. An Orai1 mutant (R91W) was generated with substitution of arginine with tryptophan at 91.

In the construction of rescue plasmids (Tmem63b, Kcnn4, Slc19a2, Stim1, and Orai1), silence mutations were introduced into the sgRNA target regions to prevent the exogenous expressing genes being targeted.

2.4 Establishment of KO cell lines

The sgRNAs were designed using CRISPRdirect and selected for their highly specificity with low off-target hits, as shown below: mTmem63b (5’-CGGAGGTGAGACGCTCATAC-3’), mStim1 (5’-CATCGTCATCCATCAGCTTA-3’), mSlc19a2 (5’-AGGGCAGATCCTCGTCTCCG-3’), mKcnn4 (5’-

TGCGGTAGGACGCGTTGAGC-3'), mCsnk2b (5'-CCAGAGCGACTTGATCGAAC-3'), mE-syt1 (5'-CTTTAGCCATTACGAATCAT-3'), mOrai1 (5'-CCTCAACGAGCACTCGATGC-3'), mSnap23 (5'-GATTACAAATGGTCAGCCTC-3'), and mStx4a (5'-GCTGTTTGATCTCCTCTCGC-3'). All sgRNAs have the same overhangs at 5', with the sequence —GACCG was attached to oligo1 and AAAC was attached to oligo2— to generate the cohesive ends for BsmBI enzyme cutting site ligation. After phosphorylating and annealing each pair of oligos, the BsmBI digested lentiGuide-puro[100] backbone was used for cloning. Subsequently, reconstructed lentiGuide-puro plasmids were introduced into Cas9-expressing BDKO cells, and puromycin was added into the medium to select the resistant cells for two days, then the medium was changed into the fresh medium for culturing. KO cell lines were obtained from one single cell and confirmed by sequencing the genomic DNA region that sgRNA targeted.

2.5 Lentiviral production

Lentiviruses were generated by transfecting HEK293T cells with reconstructed plenti-vectors or lentiGuide-puro plasmids together with two virus envelope plasmids (pCAG HIV-Gag-Pol and pCMV VSVG-RSV-REV) at specific weight ratios (2:1:1). Then, the plasmid mixture was combined with polyethylenimine (PEI) solution and applied to HEK293T cells for 48h transfection. Virus-containing medium was collected through a 0.22 μM filter and concentrated 20 times via centrifugation (6,000 g, 16 hr, 4 ˚C). The concentrated virus was then suspended in 500μl medium containing 10 μg/ml polybrene and incubated with cells for 6 hr, after which the medium was changed to the fresh medium for further culturing.

2.6 NBD-PC uptake assay

In the NBD-PC uptake assay, 1×10^6 cells were obtained and washed with chilled HBSS buffer containing 1 mM $MgCl_2$ and 1 mM $CaCl_2$ (washing buffer). The cells were then suspended in 500 μl of washing buffer and incubated on ice for 7 min, followed by the addition of an equal volume of lipid buffer containing 1 μM NBD-PC. After 3 min on ice incubation, 3.0 μM A23187 was added for stimulation, and the reaction was stopped by adding an equal volume of 5 mg/ml fatty acid-free BSA with 1μM DAPI in solution on ice for 5 min. Then cells were applied to flow cytometry for analysis, DAPI-negative cells were selected under the 405 nm laser, and the NBD-PC uptake level was analyzed using the 488 nm laser.

In the larger-scale NBD-PC uptake system for revival screening, the assay began with 4×10^7 cells. The washing buffer and lipid buffer were both expanded to 10 ml, followed by stimulation with 3.0 μM A23187 and incubation with 20 ml BSA to stop reaction. Finally, cells were centrifuged and resuspended within 5 ml of reaction solution, then analyzed using flow cytometry for screening.

2.7 PS exposure assay

1×10^6 cells were collected and washed with PBS, resuspended in 1 ml Annexin buffer containing 10 mM HEPES-NaOH (pH 7.4), 140 mM NaCl, 2.5 mM $CaCl_2$ with 1μl AnnexinV-Cy5 and 1 μg/ml Propidium iodide (PI), followed by stimulation with 3.0 μM A23187. Then cells were applied to flow cytometry for analysis; PI-negative cells were selected under 561 nm laser, and PS exposure level was analyzed by the 633 nm laser. For room temperature setup, PS exposure was usually recorded for 720 sec. For the 4˚C condition, PS exposure was recorded every 10 min on ice, and all the buffers were used in chilled conditions.

In a larger-scale PS exposure system for revival screening, the assay was performed with 4×10^7 cells. Cells were washed with 10 ml PBS, stimulated with 3.0 μM A23187 in Annexin V buffer containing Annexin V-Cy5 and 1 ug/ml PI, concentrated and resuspended with 5 ml reaction solution, and then analyzed by flow cytometry for screening.

In some cases, 140 mM NaCl was substituted with different concentrations of KCl (0 mM, 0.5 mM, 5.0 mM, 50 mM, and 140 mM) in Annexin V buffer to observe the effect of extracellular K^+ on PS exposure.

In drug treatment experiments, Kcnn4 inhibitors (TRAM-34 and Senicapoc) were applied to cells in Annexin V buffer for 4 min incubation before 3.0 μM A23187 stimulation. TRAM-34 was typically used at 10 μM, and Senicapoc was generally used at 0.5 μM[79]. During the concentration-dependent manner experiments, cells were incubated with senicapoc ranging from 0.25 μM to 5 μM.

2.8 Establishment of high PLS cells

High PLS cells were generated by 19 times repeating sorting. 4×10^7 Cas9-expressing BDKO cells were obtained and washed by chilled NBD-PC washing buffer, an equal volume of lipid buffer was added and stimulated by 0.5 μM A23187 in 10˚C water bath for 8 min, after which the reaction was stopped by adding BSA, DAPI-containing solution. Finally, cells were centrifuged and resuspended within 5 ml of reaction solution then sorted by flow cytometry for high PLS activity selection. Sorted cells were cultured with medium containing 0.5 mM EGTA. The next day, the medium was changed to the fresh medium, and the cells were cultured for the next sorting round. After repeating the process for 19 times, BDKO cells exhibiting sensitive PLS activity were acquired, and the established cell line was named hPC19.

2.9 Cell fusion

8×10^6 hPC19-DsRED cells and WR19 *Tmem16f*$^{-/-}$-GFP cells were obtained, washed by PBS twice, and removed from PBS completely. Then, the tube was tapped softly and incubated in a 37˚C water bath. Pre-

warmed 400μl PEG 1500 (Roche #783641) was added over a period of 1 min while stirring. After another 1 min of stirring, pre-warmed 400μl serum-free RPMI was added over a period of 1min, followed by adding another 400 μl RPMI and 3.2 ml serum-free RPMI for 1 min and 3 min, respectively. Then cells were centrifuged and resuspended in 10 ml RPMI contained with 10% FBS and 1% IL-3. The next day, EGFP and DsRED-positive cells were sorted by flow cytometry, and were cultured in 1μg/ml puromycin and 1mg/ml geneticin (G418, ThermoFisher) for drug selection.

2.10 Revival sgRNA library screening

For revival screening, hPC19 cells were utilized for introducing a lentiviral sgRNA library (GeCKO v2 Mouse CRISPR Knockout Pooled Library[100]). After 2 days of puromycin selection, resistant cells were washed in the fresh medium and cultured for an additional day, then applied to NBD-PC screening by using 4×10^7 cells. Approximately 1% of NBD-PC uptake negative cells were sorted during each time sorting, followed by gDNA extraction and amplification of the enriched sgRNA region using the primers as shown: sgRNA FW: GTTTTAAAATGGACTATCATATGC and RV: TATCCATCTTTGCACCCGGGC. The PCR products were combined with SmaI and NdeI (NEB) digested lentiGuide-puro plasmid by using the NEBuilder® HiFi DNA Assembly (NEB) system at 52˚C for 1 hr, then subjected to mixing with MegaX DH10B T1R ElectrocompTM Cells (Invitrogen) for electroporation. After shaking culture at 32˚C in 5 ml SOC medium for 2 hr, the mixture was then spread on LB agar plates for overnight incubation. The colony number representing the variety of the newly generated library was expected to be 1×10^6, and this new sgRNA library was prepared for next-time screening[101]. After 3 repetitions of this process, the enriched sgRNAs in the PC uptake-negative population were ready for next-generation sequencing (NGS).

Similar processes were performed in Tmem63b-expressing BDKO cells for PS exposure screening.

2.11 Next generation sequencing

The enriched sgRNA library was first amplified with the primers sgRNA Fw/Rv mentioned above, then applied to another amplification using primers attached to the adapter region and barcode sequence:

Sequencing Fw: AATGATACGGCGACCACCGAGATCTACACTCTTTCCCTACACGACGCTCTTCCGATCTATCGACTCTTGTGGAAAGGACGAAACACCG

Sequencing Rv: CAAGCAGAAGACGGCATACGAGATTCTACTATTCTTTCCCCTGCACTGT

After two PCR cycles, the amplified DNA fragments were sent to Macrogen for the Illumina HiSeq2500 analysis and certificated by QC quality check.

2.12 sgRNA data processing

The raw sgRNA sequence data was examined using guide-caller v1.0.0[100], which employs a common analysis framework including FastQC, Cutadapt[98], and MAGeCK[99]. More precisely, the 20 bp sgRNA sequences were trimmed from 51 bp by using dual-round trimming in Cutadapt, with the parameters "-u 30" for the initial trim and "-u -1" for the following trim. Subsequently, the trimmed reads were aligned to a modified annotation using MAGeCK, displaying total read counts and mapped targets.

2.13 Fluo4-AM Assay

1×10^6 cells were collected and washed with PBS buffer, then incubated with culture medium containing 1 μM Fluo4-AM at 37˚C for 30 min[102]. After completing Fluo4-AM permeation, cells were washed, resuspended in 1 ml Annexin buffer, and analyzed using flow cytometry. Initially, 100 sec were recorded for the resting state, followed by another 100 sec recording after 3.0 μM A23187 stimulation. Intracellular Ca^{2+} level was detected by the 488 nm laser.

2.14 BAPTA-AM Assay

1×10^6 cells were collected and washed by PBS buffer, then incubated with culture medium containing 1 μM BAPTA-AM at 37˚C for 30 min[17]. After completing BAPTA-AM permeation, cells were washed, resuspended in chilled 1 ml Annexin buffer, and either treated with 3.0 μM A23187 or not based on the cells condition. PS exposure was analyzed using flow cytometry by the 633 nm laser.

2.15 Identification of TMEM63B-expressing cell type

Jardine, L. *et al.*[103]conducted single-cell analysis of emergent hemopoiesis in the human fetal bone marrow (10 ×) from 12-19 post-conception weeks. Database E-MTAB-9389 was analyzed by normalization and scaling processes with broad categories (https://github.com/haniffalab/FCA_bone_marrow/blob/master/fig1_fbm_disomic_and_trisomy21/fig1a_suppfig1b_fbm_overall_dr_plots_SW.ipynb). TMEM63B-expressing cell types were identified following 'fig1b_fbm_scaled_gex_updated_dr_ 20210104.h5ad.' and depicted as UMAP.

2.16 Cell lysate preparation

1×10^6 cells were counted and washed with cold PBS, then resuspended in solubilization buffer containing 25 mM Tris-HCl (pH 8.0), 140 mM NaCl, 1% Lauryl Maltose Neopentyl Glycol (LMNG) / 0.1% Cholesteryl hemisuccinate (CHS), 10% (vol/vol) Glycerol, 1 mM p-APMSF, EDTA-free protease inhibitor cocktail (Nacalai), 100 mM 6-aminocaprotic acid, 1 mM NaF, 2 mM DTT, then rotated at 4°C for

1 hr. After finishing solubilization, samples were centrifuged at 20,000 g, 4˚C for 20 min to remove insoluble materials and protein quantification was measured by Bradford assay.

2.17 Membrane fraction preparation

Membrane fractions were obtained using Dounce homogenizer with 2×10^7 cells in a hypotonic buffer containing 25 mM Tris-HCl (pH 8.0), 10 mM $MgCl_2$, 20 mM KCl, 250 mM sucrose, 1 mM p-APMSF, protease inhibitor cocktail (Nacalai), 1 mM NaF, and 2 mM DTT. Then isotonic buffer (25 mM Tris-HCl (pH 8.0), 200 mM NaCl, 10 mM $MgCl_2$, 20 mM KCl, 250 mM sucrose, 1 mM p-APMSF, protease inhibitor cocktail (Nacalai), 1 mM NaF, and 2 mM DTT) was added into solution for osmotic balance. After removing nuclei and mitochondria, the supernatant was transferred into an ultracentrifugation tube for centrifugation at 100,000 g at 4 ˚C for 1 hr. The pellet was subsequently solubilized in solubilization buffer as described before, containing 1% LMNG and 0.1% CHS, and rotated at 4˚C for 2 hr, followed by centrifugation and concentration determination.

2.18 BN-PAGE analysis

In the Blue Native PAGE assay, cell lysate was loaded to Blue Native (BN)-PAGE Novex Bis-Tris gel (Life Technologies), and electrophoresis was performed in 1 × NativePAGE™ Dark Blue Cathode buffer (containing 0.02% CBB G-250) at 150 V, 4 ˚C for 35 min, then the running buffer was replaced with 1 × NativePAGE™ Light Blue Cathode buffer containing 0.002% CBB G-250, and ran another 120 min. After finishing electrophoresis, the gel was incubated with SDS running buffer at room temperature for 20 min, followed by Immobilon-P PVDF membrane transfer setup at 100 mA for 1 hr, followed by western blotting. For gel-shift assay, cell lysate sample was firstly adjusted to 0.5 mg/ml, and 2 µl antibody (anti-DDDDK or anti-HA) was added into 30 µl protein for 1 hr at 4˚C before loading to the gel.

2.19 Western Blotting

After transferring proteins to the PVDF membrane, blocking was performed using 5% skim milk in TBS-T buffer, followed by overnight incubation with primary antibody, such as anti-GFP-HRP or anti-Kcnn4, at 4˚C while shaking. The next day, the membrane was washed in TBS-T buffer 4 times for 5 min each, then incubated with secondary antibody (goat anti-rabbit) at room temperature for 1 hr, or it was prepared directly for chemiluminescent signal detection according to the antibody's requirement. Both signals were detected by using Immobilon Western chemiluminescent HRP substrate (Millipore) and visualized by the FUSION chemiluminescence imaging system (Vilber). For loading amount quantification, the membrane was stained with CBB staining buffer and washed with destaining buffer to visualize the protein amounts.

2.20 Real-time PCR

1×10^6 cells were used for RNA extraction by using the RNeasy kit, then extracted RNA was conversed into cDNA according to High-Capacity RNA-to-cDNA Kit instruction. Primers ~ 20bp targeted the genes of interest with medium GC content and compatible Tm value were designed by Primer-BLAST and listed as below: Kcnn4 FW: 5'-GCAAGATTGTCTGCCTGTGC-3'; Kncc4 RV: 5'-TCTCCGCCTTGTTGAACTCC-3'. Slc19a2 FW: 5'-ATGAGCCTCCGGTGGAAGAA-3'; Slc19a2 RV: 5'-GGGCGGGAGGAATAACACAT-3'. Beta-actin gene was utilized as endogenous control to normalize amplification level, the sequences of control primers were shown as follows: Actin FW: 5'-GGCTGTATTCCCCTCCATCG-3'; Actin RV: 5'-CCAGTTGGTAATGCCATGT-3'.

Then, cDNA from target cells was mixed with primers and TB Green Premix Ex TaqTM II (Tli RNaseH Plus) and processed using the Thermal Cycler Dice Real Time System Lite. Comparative quantification algorithms were adopted to calculate the fold change of the target gene relative to the endogenous control gene. ΔCt was determined to assess the expression difference of the target gene between parental cells with sgRNA-expressing cells, followed by adjustments made for the normalizer gene (Actin) from both samples. Subsequently, the ΔΔCt value was incorporated to determine the fold difference in expression between the calibrator sample and the normalizer sample.

2.21 Immunoprecipitation

A total of 2×10^6 cells were collected and washed twice with PBS; subsequently, 0.1% formaldehyde was added, and cells were incubated at room temperature for 10 min. Following this, the cells were treated with 1M glycine-NaOH for 4 min, centrifuged and washed by PBS, then resuspended in 500 µl solubilization buffer, which consisted of 25 mM Tris-HCl (pH 8.0), 140 mM NaCl, 1% Lauryl Maltose Neopentyl Glycol (LMNG) / 0.1% Cholesteryl hemisuccinate (CHS), 10% (vol/vol) Glycerol, 1 mM p-APMSF, EDTA-free protease inhibitor cocktail (Nacalai), 100 mM 6-aminocaprotic acid, 1 mM NaF and 2 mM DTT. Additionally, 1/500 benesonase was added to the solution, and the mixture was rotated at 4 ˚C for 1 hr. The supernatant was collected after centrifugation (20,000 g, 20 min, 4 °C) and incubated with GFP-Trap magnetic agarose beads, which had already been equilibrated with solubilization buffer twice prior to being added, then rotated at 4 °C for 3 hr. After the incubation, the precipitated beads were separated using a magnetic rack and washed three times by washing buffer composed of 25 mM Tris-HCl (pH 8.0), 100 mM 6-aminocaprotic acid, 140 mM NaCl, 0.01% LMNG, and 0.001% CHS. The beads were washed two additional times with 50 mM ammonium bicarbonate. Finally, samples were flash frozen in liquid nitrogen and stored at -80˚C for further use[102].

2.22 Mass spectrometry

The separation of proteins bound to GFP-beads is inclusive of digestion with trypsin/Lys-C mix (Promega) at 37˚C for 16 hr, reduction, alkylation, acidification, and desalting using GL-Tip SDB (GL Sciences). The sample was concentrated by a SpeedVac concentrator and dissolved in 0.1% trifluoroacetic acid with 3% acetonitrile (ACN) solution. Then, the generated peptides were subjected to EASY-nLC 1200 UHPLC with 75 μm inner diameter × 150 mm C18 reversed-phase column (Nikkyo Technos), using a linear 4–32% acetonitrile (ACN) gradient over 0–100 min, followed by a 10-min increase to 80% ACN. The liquid chromatography was connected with Orbitrap Fusion mass spectrometer detection via a nanoelectrospray ion source (Thermo Fisher Scientific). The mass spectrometer was operated in a data-dependent acquisition mode with a maximum duty cycle of 3 sec. MS1 spectra were recorded at a resolution of 120,000 FWHM from 375 to 1,500 *m/z*. HCD MS/MS spectra were acquired in the linear ion trap with the automatic gain control (AGC) target set to 4×10^5, injection time of 100 ms with a max, and precursors with intensity higher than 1×10^4 were selected for fragmentation with an isolation window of 1.6 *m/z* and a normalized collision energy of 30. Dynamic exclusion was set to 20 sec.

The raw data were directly analyzed by comparing with the SwissProt database restricted to *Mus musculus* using Proteome Discoverer version 2.5 (Thermo Fisher Scientific) with the Sequest HT search engine. The search parameters included trypsin as the enzyme with accepting up to two missed cleavages in the peptide chain, a precursor mass tolerance of 10 parts per million (ppm), a fragment mass tolerance of 0.6 Da, carbamidomethylation of cysteine as a fixed modification, and acetylation of the protein N-terminus and oxidation of methionine as variable modifications. The false discovery rate (FDR) was set to 1% of the identified peptides using the percolator node. The analysis employed label-free quantification using the precursor ions quantifier node, and normalization was performed to account for the variations in samples and ensure the total sum of abundance values for each sample over all peptides remained consistent, facilitating accurate comparisons between different samples.

2.23 Prediction of Tmem63b/Slc19a2 heterodimer

Prediction of the complex structure of Tmem63b/Slc19a2 was conducted using AlphaFold2 (v 2.3.2)[104] on the AlphaFold ColabFold v1.5.5 via the Supercomputer System at Kyoto University's Institute for Chemical Research. The default settings included msa_method=mmseqs2_uniref_env, pair_mode=unpaired_paired, model_type=auto, num_recycles=3, recycle_early_stop_tolerance=auto, and AMber relaxation. As a result, 5 trained models were generated, with parameters: model 1 (pLDDT=72.3 pTM=0.612 ipTM=0.355); model 2 (pLDDT=69.9 pTM=0.575 ipTM=0.331), model 3 (pLDDT=70.3 pTM=0.535 ipTM=0.157); model 4 (pLDDT=70.9 pTM=0.535 ipTM=0.161); model 5

(pLDDT=69.1 pTM=0.528 ipTM=0.161). Referring to the OSCA1.2 homodimer structure, the Tmem63b/Slc19a2 heterodimer structure also has a high score for prediction accuracy. Interface interaction analysis to identify potential contact sites with distance labeling between two proteins was performed using ChimeraX software.

3. Results

3.1 A novel Ca^{2+}-dependent scramblase

In the mouse pro-B cell line Ba/F3, scrambling activity can be assessed by using an NBD-conjugated PC uptake assay. Tmem16f and Xkr8 induced scrambling activity was observed under low concentration (0.5μM) of Ca^{2+} ionophore (A23187) stimulation, resulting in over 80% PC uptake in the population in 10 min compared to 0 min treatment (**Fig. 3-1a, upper left**). At a higher concentration (3.0 μM) of A23187 treatment, up to 88% of cells exhibited positive PC uptake (**Fig. 3-1a, upper right**). When the PC uptake assay was performed using Ba/F3 Double Knock Out (BDKO) cells deficient in Tmem16f and Xkr8, there was a significant decrease of PC uptake under 0.5 μM A23187 stimulation (**Fig. 3-1a, bottom left**), indicating that the scrambling activity primarily originates from the known scramblases, particularly Tmem16f, the Ca^{2+}-activated scramblase. However, when I utilized 3.0 μM A23187 to treat BDKO cells, approximately 80% of cells showed PC uptake positive (**Fig. 3-1a, bottom right**), suggesting the existence of additional Ca^{2+}-activated scramblase(s) beyond Tmem16f and Xkr8 in the Ba/F3 cell line.

In order to enrich the expression of new scramblase(s) in BDKO cells, 19 cycles of NBD-PC uptake sorting were conducted to establish scrambling activity sensitive cells. This was established by Suzuki, J. *et al*. In particular, BDKO cells were stimulated with 0.5 μM A23187 and applied to the NBD-PC assay, 0.5% PC-positive cells were acquired and expanded for further selection. After repeating this process 19 times (**Fig. 3-1b**), the cell line enriched with putative scramblase(s) was renamed as high PC-uptake 19 times sorting (hPC19) cells.

To verify hPC19 cells exhibit sensitive scrambling activity, the NBD-PC assay was conducted under 0.5 μM A23187 treatment, revealing that over 75% of the cells in the population showed scrambling activity (**Fig. 3-1c, left**), and this population increased to 97% with treatment at 3.0 μM A23187 (**Fig. 3-1c, right**). Since scramblases permit bidirectional phospholipids transportation, in addition to uptake PC, I wondered whether hPC19 cells were capable of externalizing PS. Accordingly, PS exposure assay was performed by utilizing Annexin V/PI system, with Annexin V-specific binding to exposed PS on the cell membrane thereby confirming scrambling activity. Compared to BDKO cells, which elicited PS exposure over 4 min under 3.0 μM A23187 treatment, hPC19 cells elicited PS exposure within 100 sec (**Fig. 3-1d**), suggesting that the hPC19 cells contain scramblase candidates and exhibit scrambling activity even under the lower concentration of Ca^{2+} ionophore stimulation.

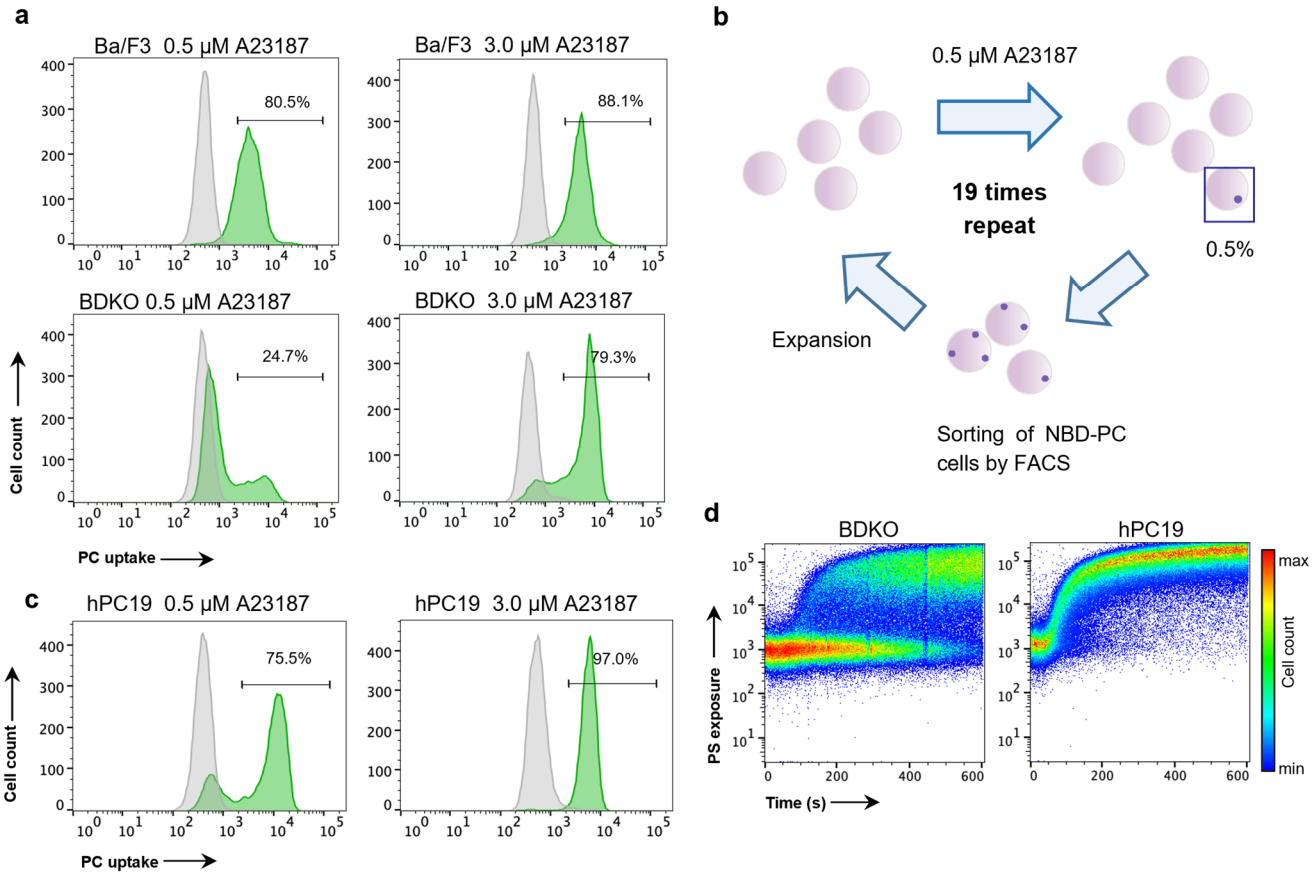

Fig. 3-1: Ca^{2+}-dependent scramblase. a NBD-PC assay performed in Ba/F3 cells and those defective in Tmem16f and Xkr8 BDKO cells under treatment of 0.5 μM or 3.0 μM A23187. Bar, PC uptake positive region; number, population in the region. **b** Schematic of hPC19 cells establishment. BDKO cells were used for a 19-time NBD-PC assay repeat, stimulated by 0.5 μM A23187, and 0.5% PC uptake positive cells were sorted for expansion. **c** PC uptake assay in hPC19 cells, 0.5 μM and 3.0 μM A23187 were used. Bar, PC uptake positive region; number, population in the region. **d** PS exposure assay performed in BDKO cells and hPC19 cells. Annexin V/PI were added to reaction buffer and PI-negative region was analyzed, a period of 10 min was recorded.

3.2 Strategy for identification of the novel Ca^{2+}-dependent scramblase

3.2.1 Optimizing screening method for identification of scramblase candidate

On the other hand, PLS activity can also be detected upon Ca^{2+} ionophore stimulation in the WR19L cell (mouse T-cell). Knocking out Tmem16f in WR19L cells abolished PLS activity even with 3.0 μM A23187 treatment (**Fig. 3-2a**), unlike hPC19 cells which elicited rapid PS exposure within 4 min (**Fig. 3-2b**). To identify the candidate scramblase(s), I planned to use a cDNA library from hPC19 cells and introduce it into WR19L *Tmem16f*$^{-/-}$ cells for screening. Before starting the cDNA library screening, a cell fusion experiment was conducted using hPC19 cells and WR19L *Tmem16f*$^{-/-}$ cells to ensure that the candidate scramblase(s) in hPC19 cells also elicit PLS activity in WR19L cells. PMX-neo-DsRED was used for

hPC19 cells to express DsRED, followed by selection with 1 mg/ml geneticin. PMX-puro-EGFP was used for WR19L *Tmem16f*$^{-/-}$ to express GFP, followed by selection with 1 ug/ml puromycin. The fusion step was performed using PEG 1500, resulting in fused cells exhibiting both DsRED and EGFP signals and were cultured in media containing both geneticin and puromycin. However, the fused cells did not show PLS activity upon 3.0 µM Ca^{2+} ionophore stimulation (**Fig. 3-2c**), similar to WR19L *Tmem16f*$^{-/-}$. This indicates that WR19L *Tmem16f*$^{-/-}$ cells are predominant in the regulation of PLS activity over hPC19 cells in fused cells, either due to the absence of activators or the presence of scramblase inhibitors.

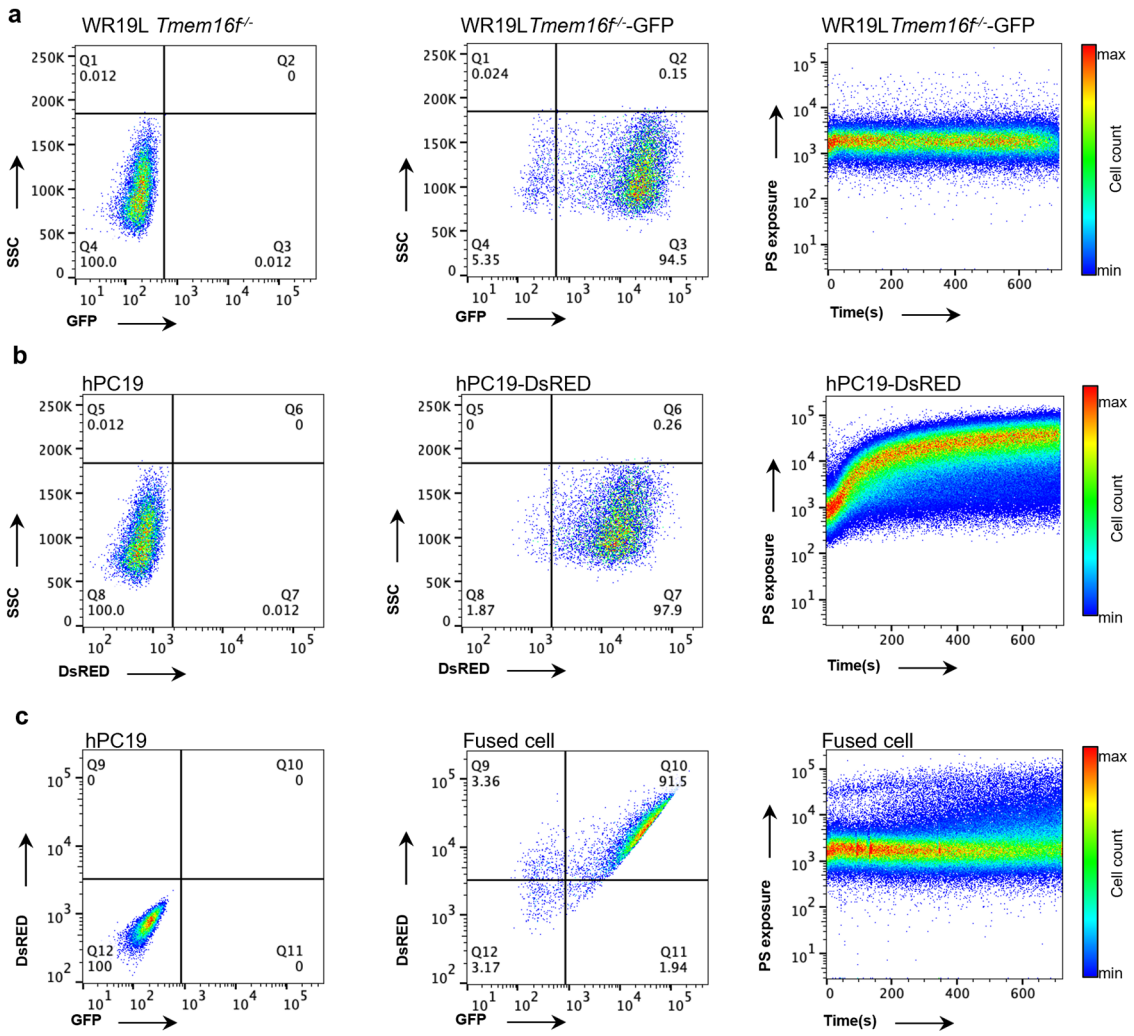

Fig. 3-2: PLS activity in fusion cell. a WR19L *Tmem16f*$^{-/-}$-GFP cells show more than 90 % GFP positive signal compared to WR19L *Tmem16f*$^{-/-}$, PS exposure assay was performed under 3.0 µM A23187 treatment, Annexin V/PI were added into reaction buffer, and PI negative region was analyzed. **b** middle lane, hPC19 cells and DsRED expressing hPC19 cell, over 90% DsRED positive signal was detected, followed by PS exposure assay. **c** WR19L *Tmem16f*$^{-/-}$-GFP cells and hPC19-DsRED fused cell show double GFP and DsRED positive signal, PS exposure assay was performed in the Annexin V/PI containing reaction buffer, treated with 3.0 µM A23187 and PI negative region was analyzed.

3.2.2 Revival sgRNA library screening

Considering cDNA library screening was not appropriate for identifying the new scramblase(s), I intended to perform CRISPR-sgRNA revival screening on hPC19 cells. Following Maruoka, M. *et al*., who established this method in 2021[105], revival screening prevents sgRNAs loss due to sorting procedures and proliferation issues. As shown in **Fig. 3-3a**, Cas9-expressing hPC19 cells infected with GeCKO v2 Mouse CRISPR Knockout Pooled library were treated with 3.0 μM A23187 for 10 min during the NBD-PC assay. Approximately 1% of the PC uptake-negative population was sorted and applied to genomic DNA (gDNA) extraction. Primers with the recognition sequence for the restriction enzyme BsmBI were used to amplify sgRNA regions from the gDNA, which were then inserted into digested plenti-guide-puro vector. Reconstituted sgRNA library plasmids were generated using the In-Fusion system and subjected to a new round of infection (**Fig. 3-3a**). After repeating this process three times, the PC uptake-negative population was increased from 1.1% (sgPC0, original library sorting) to 22.6% (sgPC3, third-generated library sorting), representing an enrichment of genes contributing to Ca^{2+}-dependent scrambling activity through this unbiased screening method (**Fig. 3-3b**). Considering that additional rounds of repeat potentially enrich bias candidates because of PCR amplification, sgPC3 was selected as the optimal time point. Next, gDNA from sgPC3-sorted cells was extracted and amplified with the previously mentioned primers, followed by an additional PCR reaction to add adapter sequences at both ends. Finally, the PCR products after the two amplifications were sent to Macrogen for next-generation sequencing (NGS). The analyzed results were ranked by total reads, excluding genes with less than two mapped targets, which represented non-effective sgRNAs (**Fig. 3-3c**).

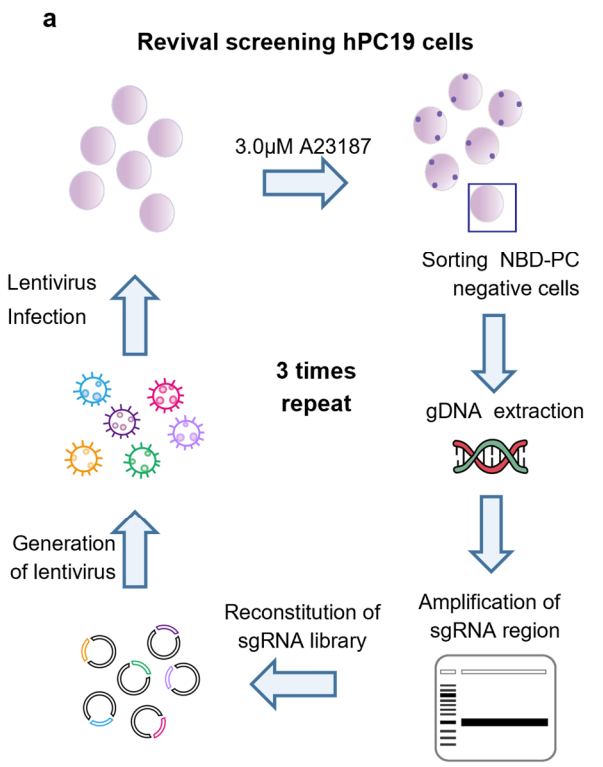

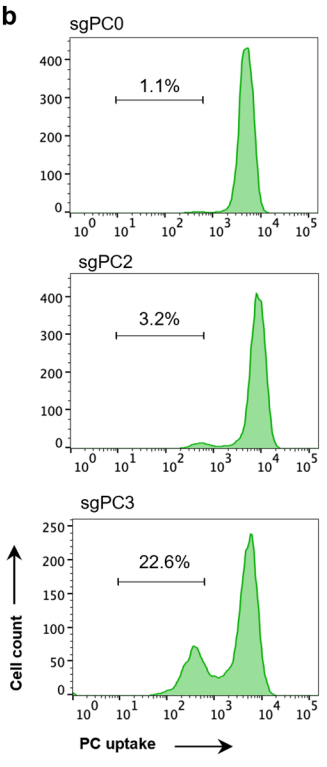

c

Gene	Total read	Mapped target
Stim1	**437962**	**6**
Mcu	170354	6
Scd2	82254	4
Scap	65095	5
Stim2	62478	6
Smdt1	38248	5
Gbf1	29631	5
Esyt1	22395	5
Snap23	3713	4
Kcnn4	2351	5
Tmem63b	**1934**	**3**
Slc19a2	1219	3

Fig. 3-3: NBD-PC Revival screening of hPC19 cells. a Schematic of revival screening. Cas9-expressing hPC19 cells were infected with GeCKO v2 Mouse knockout library, then NBD-PC assay was performed on hPC19 cells under 3.0 μM A23187 treatment for 10 min. 1% NBD-PC negative cells were sorted, followed by gDNA extraction and sgRNA region amplification, then the amplified region was inserted into plenti-guide vector to reconstruct a new sgRNA library. The next round of sorting began with the infection of a newly generated sgRNA library on hPC19 cells and repeat this process was repeated three times. **b** Revival screening NBD-PC result. sgPC0 represents original library sorting; sgPC3, third-time sorting. Bar, PC uptake negative region; number, population in the bar. **c** NGS sequencing. The result was obtained by Illumina HiSeq2500 sequencing; candidates were ranked by total reads among effective genes (mapped target more than three among six). Red-labeled genes were further analyzed as candidates.

3.3 Tmem63b is the Ca^{2+}-dependent scramblase

3.3.1 Two scramblase candidates mediate scrambling activity

From the result, the top candidate, Stim1, has the highest reads with 6 mapped targets. To investigate whether Stim1 is the Ca^{2+}-dependent scramblase, a sgRNA targeting Stim1 was designed using CRISPRdirect, followed by annealing and ligation to generate the plenti-*sgStim1*-puro plasmid, which was then introduced into Cas9-expressing BDKO cells. After two days of puromycin selection and limiting dilution, a single colony was obtained. Sanger sequencing verified the knockout efficiency (**Fig. 3-4a**). Then PS exposure assay was performed with BDKO *Stim1*$^{-/-}$ cells, which revealed delayed PS exposure compared to BDKO parental cells under Ca^{2+} ionophore stimulation. And the delayed scrambling activity

was restored by introducing exogenous Stim1(**Fig. 3-4c**). Since Stim1/Oria1 are the major components of SOCE that maintain Ca^{2+} homeostasis and replenish Ca^{2+} between the ER and PM. I questioned can Ca^{2+} influx induced by ionophore A23187 be independent of Stim1-regulated Ca^{2+} homeostasis? To examine changes in Ca^{2+} influx before and after A23187 treatment, I performed a Fluo4-AM assay on BDKO and BDKO *Stim1*$^{-/-}$ cells. The results indicated that knocking out Stim1 in BDKO cells did not prevent Ca^{2+} influx following A23187 stimulation (**Fig. 3-4d**). This suggests that Stim1-mediated scrambling activity was activated by A23817 stimulation, possibly through ER Ca^{2+} release.

However, Stim1 is not the scramblase, as it specifically localizes in ER membranes and indirectly mediates scrambling activity. Instead, Stim1 might act as a co-factor involved in the scrambling activity at ER-PM contact sites. Given that Stim1 ranked highest among the NGS results but is not a scramblase itself, I supposed that more than one scramblase pathway exists in hPC19 cells, and the total reads of sgRNA served as a partial indicator for candidate selection. Then I checked the NGS result again, and found that Tmem63b is included. Given the hints mentioned earlier between Tmem63b and scrambling activity, it is highly possible that Tmem63b is the target candidate. To demonstrate that Tmem63b possesses scrambling activity, I conducted the PS exposure assay in both BDKO *Tmem63b*$^{-/-}$ cells (validated by sequencing as shown in **Fig. 3-4b**) and BDKO *Tmem63b*$^{-/-}$ cells restored with exogenous Tmem63b. PS exposure decreased greatly with Tmem63b deletion but increased drastically with Tmem63b overexpression (**Fig. 3-4b**). Based on these findings, I concluded that Tmem63b is the Ca^{2+}-dependent scrambling activity inducing factor.

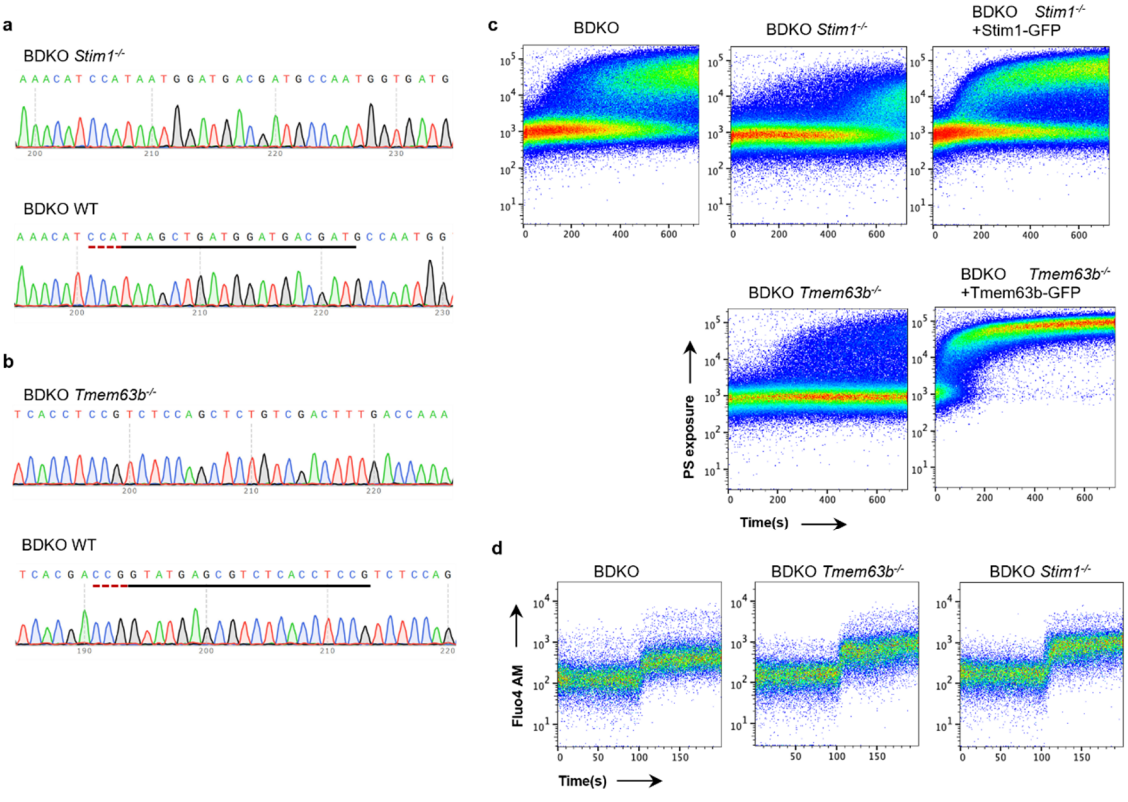

Fig. 3-4: Candidates for Ca^{2+}-dependent scramblase. a, b Sequences of BDKO *Stim1*$^{-/-}$ cells and BDKO *Tmem63b*$^{-/-}$ cells. Around 400 bp sgRNA target region was amplified using gDNA extracted from both BDKO cells and knockout cells; sequences were confirmed by Sanger-sequencing. Black, sgRNA sequence; red, PAM site. **c** PS exposure assay. Cells were incubated in Annexin V/PI containing reaction buffer, treated with 3.0 μM A23187; in some cases, the GFP positive signal was gated and the PI negative region was analyzed. **d** Fluo4-AM assay. Intracellular Ca^{2+} was initially recorded around 100 sec, then 3.0 μM A23187 was added and recorded for another 100 sec.

3.3.2 Tmem63b and Stim1 can independently induce scrambling activity

Since both Stim1 and Tmem63b can induce scrambling activity, I questioned whether they work independently or cooperatively in PLS activity. Hence, BDKO *Stim1*$^{-/-}$ *Tmem63b*$^{-/-}$ cells were established, and either Stim1 or Tmem63b was restored. From the PS exposure assay result, double knockout of these two proteins almost completely inhibited scrambling activity, while individual expression of Stim1 or Tmem63b could elicit PS exposure. However, Tmem63b-restoring cells exhibited more pronounced PS exposure than those cells restored with Stim1 (**Fig. 3-5a**), similar to **Fig 3-4**. On the other hand, an NBD-PC uptake assay was also performed to confirm the scrambling activity of Tmem63b and Stim1. As shown in **Fig. 3-5b**, both Tmem63- and Stim1-restoring cells exhibited NBD-PC uptake, indicating the existence of two scramblase pathways that bidirectionally scramble phospholipids in an independent manner.

Moreover, activated Stim1 binds with Orai1 at the ER-PM contact site to regulate Ca^{2+} homeostasis; Orai1 is likely involved in Stim1-mediated scrambling activity[88]. To prove that, I introduced *sgOrai1, sgOrai1* + Orai1 WT, and *sgOrai1* + Orai1 R91W (Orai1 loss-of-function mutation)[94] into Stim1-restoring *Stim1*$^{-/-}$ *Tmem63b*$^{-/-}$ BDKO cells, respectively. The results showed that Orai1 is required for Stim1-mediated scrambling activity, as *sgOrai1* introduction inhibited the PS exposure elicited by Stim1, while Orai1 WT rescued this inhibition, and dysfunctional Orai1 (R91W) could not (**Fig. 3-5c**). This Indicates Stim1 and Orai1 work together for the PLS pathway.

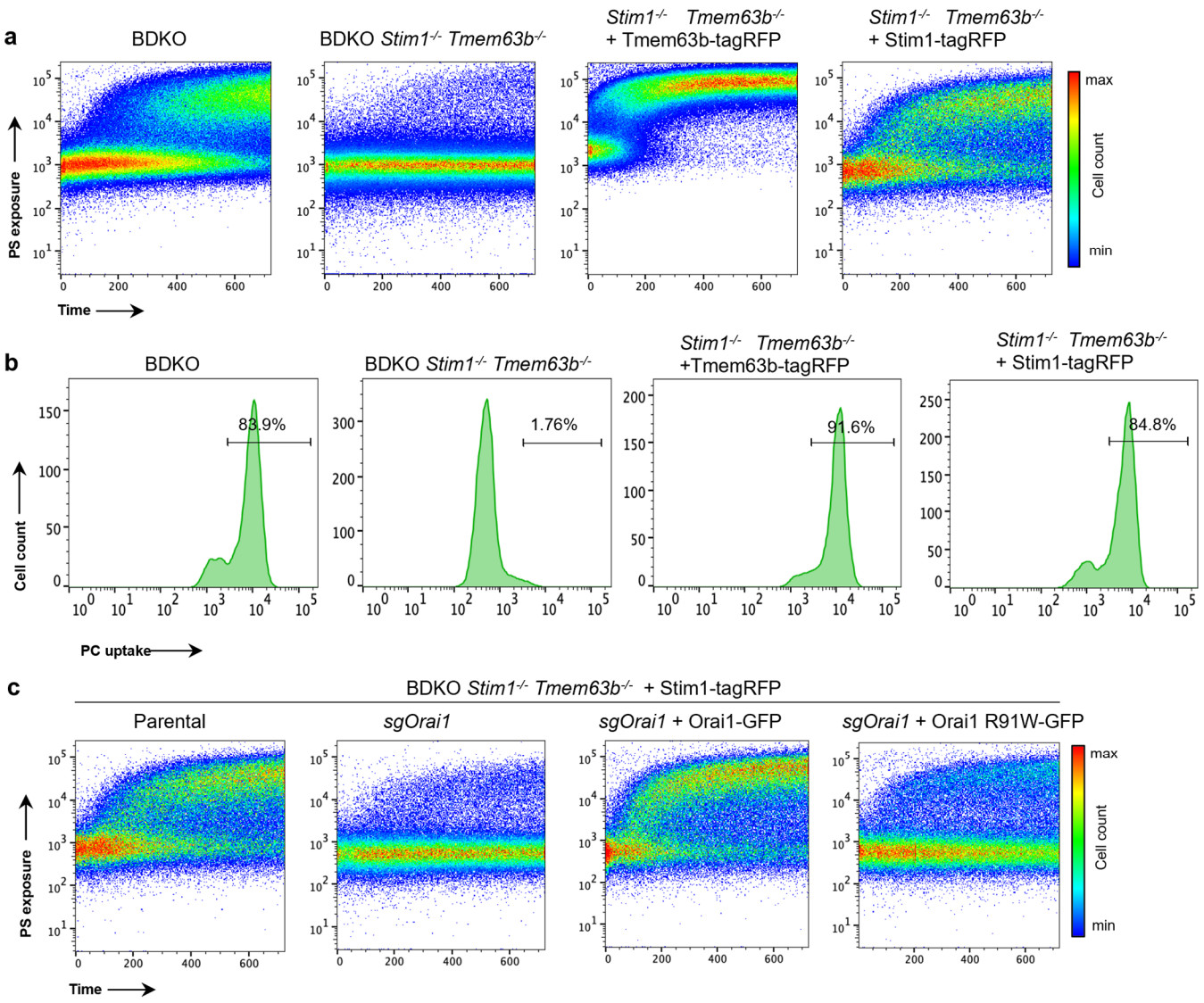

Fig. 3-5: Two different scrambling activity induced factors. a PS exposure assay. PS exposure assay was performed in BDKO parental cells (same as **Fig 3-4c**), *Stim1*$^{-/-}$ *Tmem63b*$^{-/-}$ BDKO cells, and *Stim1*$^{-/-}$ *Tmem63b*$^{-/-}$ cells restored with Tmem63b-tagRFP or Stim1-tagRFP. Cells were incubated in the Annexin V/PI containing buffer and stimulated with 3.0 μM A23187; tagRFP positive regions were collected and analyzed. **b** PC uptake assay. A PC uptake assay was performed in cells from (**a**). Cells were resuspended with lipid buffer, followed by incubation with NBD-PC and stimulation with 3.0 μM A23187 for 10 min. tagRFP-positive cells were collected, and the DAPI-negative region was analyzed. Bar, PC uptake positive region; number, cell population in the bar. **c** PS exposure assay. PS exposure assay was performed in *Stim1*$^{-/-}$ *Tmem63b*$^{-/-}$ cells restored with Stim1-tagRFP (same as **a**) and those introduced with *sgOrai1*, *sgOria1*+ Orai1 WT GFP, and *sgOrai1* + Orai1 R91W GFP. Cells were incubated in the Annexin V/PI containing buffer and stimulated with 3.0 μM A23187; tagRFP and/or GFP positive cells were collected, and PI negative region was analyzed.

3.3.3 Scrambling activity is not affected by lipid transportation proteins

Certain SNARE proteins like Snap23 and Stx4a were also enriched in the revival screening result. Given that SNARE proteins might be involved in the regulation of lipid distribution, they may potentially

contribute to or even elicit the scrambling activity. Next, I designed sgRNAs targeting SNARE proteins and introduced them into Stim1- or Tmem63b-restoring cells to see whether these SNARE proteins affected the Stim1/Orai1-PLS pathway or the Tmem63b-PLS pathway (**Fig. 3-6a, b**). In PS exposure assay, neither Stim1/Orai1- nor Tmem63b-elicited scrambling activity was inhibited after *sgSnap23* or *sgStx4* introduction, indicating that SNARE proteins were not involved in either scrambling pathway. Additionally, the effect of *sgOrai1* was also tested in Tmem63b-restoring cells; however, it did not inhibit Tmem63b-mediated scrambling activity, indicating Orai1 is specific to Stim1 but not Tmem63b for scrambling activity.

Moreover, lipid transfer protein E-syt1, which cooperates with Stim1/Orai1 in forming EM-PM contact sites during Ca^{2+} replenishment[90], was also identified in the revival screening result. To assess whether E-syt1 effected two scrambling pathways, scrambling activity was confirmed by introducing *sgE-syt1* into Stim1- or Tmem63b-restoring cells. No significant difference was observed in PS exposure between *sgE-syt1*-expressing or non-expressing cells, indicating that E-syt1 is not involved in both Stim1/Orai1 and Tmem63b-mediated PLS pathways (**Fig. 3-6a, b**).

On the other hand, the differences between Stim1/Orai1- and Tmem63b-mediated scrambling activity were more obvious when performing PS exposure at 4˚C. Low temperature inhibits ATPase flippase and floppase from transporting phospholipids, and slows down the reaction speed and phospholipids fluidity, rendering scrambling activity more sensitive and specific to the effects of a scramblase. As a result, PS exposure was detectable in Tmem63b-expressing BDKO cells for 40 min after A23187 stimulation, but not in BDKO or Stim1-expressing BDKO cells (**Fig. 3-6c**). Given that Tmem16f also elicits PS exposure at 4˚C, it is convincing that Tmem63b acts as the scramblase, whereas Stim1/Orai1 indirectly regulates scrambling activity by an unknown endoplasma-plasma-scramblase (epSCR) (**Fig. 3-6d**).

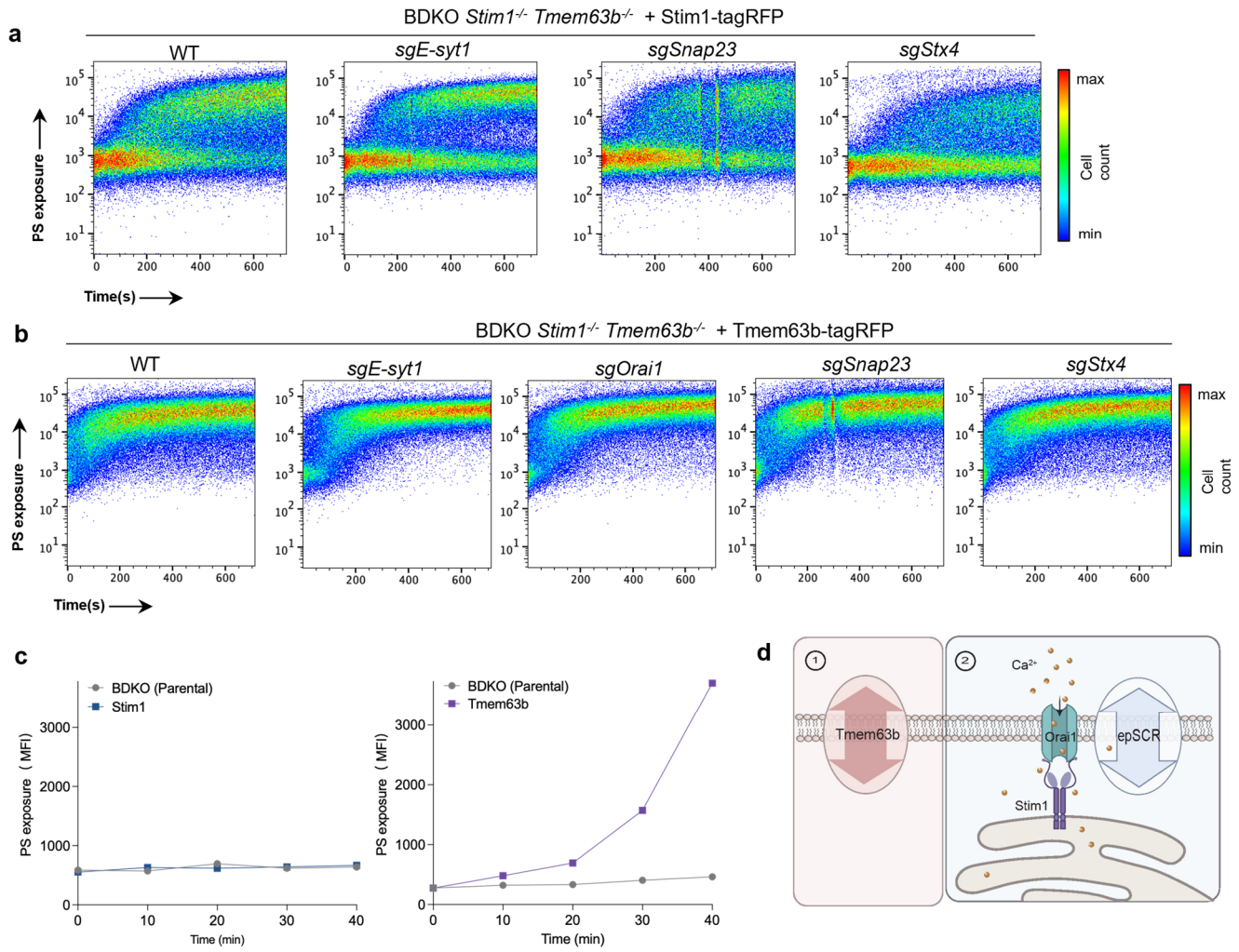

Fig. 3-6: The effect of lipid-related transportation SNARE proteins and E-syt1 on scrambling activity. a PS exposure assay in Stim1-restoring cells (same as **Fig. 3-5a**) and those with *sgSnap23, sgStx4,* or *sgE-syt1* introduced, after two days of puromycin treatment, then cultured in the fresh medium for further analysis. Cells were incubated in the Annexin V/PI containing buffer and stimulated with 3.0 μM A23187; tagRFP-positive regions were collected and analyzed. **b** PS exposure assay was performed in Tmem63b-restoring cells and those with *sgE-syt1*, *sgOrai*, *sgSnap23, or sgStx4* introduced. **c** 4˚C PS exposure assay. Using chilled Annexin V/PI buffer for reaction and after 3.0 μM A23187 treatment, put the cells were put on ice and PS exposure was recorded every 10 min for 40 min. GFP-positive regions were collected, and PI-negative regions were analyzed. **d** Two PLS pathways: one is Stim1/Orai1 incorporated in unknown epSCR PLS pathway; another one is Ca^{2+}-dependent Tmem63b PLS pathway.

3.3.4 Tmem63 family members Tmem63a and Tmem63c are not scramblases

I then investigated whether the other two members of Tmem63 family, Tmem63a and Tmem63c, also exhibit scrambling activity or not. To do this, I introduced Tmem63a-GFP and Tmem63c-GFP into BDKO cells and performed the PS exposure assay on these cells. From the result, only Tmem63b induced the PS exposure in less than 100 sec after A23187 stimulation, whereas Tmem63a or Tmem63c did not (**Fig. 3-7a**), suggesting that Tmem63b is the only scrambling activity inducing factor among Tmem63 family.

Considering the SCRD region between TM4 and TM5 in Tmem16f, which is essential for eliciting scrambling activity, I wondered whether such region also exists in Tmem63b for scrambling activity. Next, I performed chimera construction by swapping TM4 and TM5 of Tmem63b with those of Tmem63a and Tmem63c; accordingly, swapping TM4 and TM5 of Tmem63a or Tmem63c with Tmem63b—the swapped sequence is shown in **Fig. 3-7b**. After confirming by sanger-sequencing, a PS exposure assay was performed among these chimeras: Tmem63a+b represents Tmem63b "SCRD" region that was introduced into Tmem63a; Tmem63b+a represents Tmem63b "SCRD" region that was replaced by Tmem63a; Tmem63c+b represents Tmem63b "SCRD" region that was introduced into Tmem63c; and Tmem63b+c represents Tmem63b "SCRD" that was replaced by Tmem63c. The result indicated that, while introducing the Tmem63b "SCRD" region did not confer PLS activity to Tmem63a and Tmem63c, replacing this region in Tmem63b impaired scrambling activity drastically (**Fig. 3-7c**), representing this region is important for Tmem63b to exhibit PLS activity. However, it differs from the canonical SCRD region found in Tmem16f.

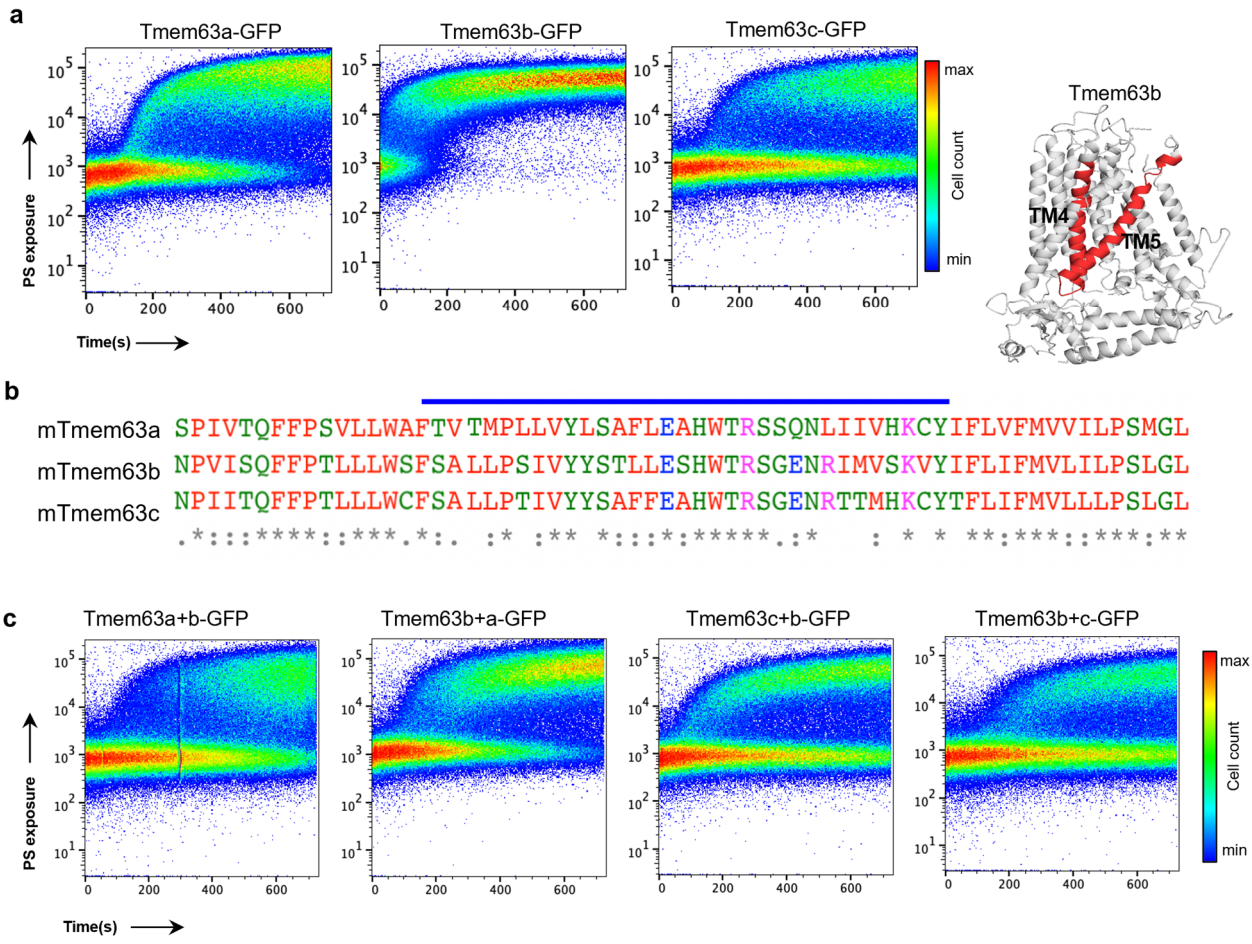

Fig. 3-7: Tmem63 family members scrambling activity. a PS exposure assay. Tmem63a/b/c-GFP-expressing BDKO cells were incubated in the Annexin V/PI-containing reaction buffer and stimulated with 3.0 μM A23187. GFP-positive cells were collected, and the PI-negative region was analyzed. **b** Sequence alignment of "SCRD" region among Tmem63 family by using Clustal Omega. Uncharged acids were labeled as green; negatively charged acids were labeled as blue; and hydrophobic acids were labeled as red. The asterisk shows positions where amino acids were conserved; the colon indicates similar amino acids; the blue underline was the swapping region among these proteins. Upper right, Tmem63b structure with red labeled TM4 and TM5. **c** PS exposure assay. PS exposure assay was performed among chimeras under Annexin V/PI buffer with 3.0 μM A23187 treatment, GFP positive signal was collected and PI negative region was analyzed.

3.4 Tmem63b physiological function

3.4.1 Disease mutations in Tmem63b induce constitutive scrambling activity

Tmem63b functions as an osmosensor and is responsible for hearing in mice or thirst in drosophila; and has mechanosensor functions in sensing food texture and humidity in drosophila. As a scrambling activity-inducing factor, it would be interesting to explore the physiological function that Tmem63b-mediated scrambling activity induces. Given the mutations of TMEM63B found in patients with DEE and hematological disorders, I questioned whether Tmem63b mutations induce abnormal PLS activity that correlates with diseases. Five mutations—I475del, V44M, D459E, R433H, and R660T—were selected. As shown in **Fig. 3-8a**, the sequences of Tmem63b across species—human, mouse, chicken, frog, and fish were aligned, and these five residues were completely conserved in humans, mice, and chickens, suggesting these residues were important for Tmem63b's physiological function. From the structural picture, these five residues are positioned in different transmembrane regions: V44M is in TM0, R433H and D459E are present in TM3, I475del is in TM4, and R660T is found in TM8 (**Fig. 3-8b**).

I introduced these Tmem63b mutations into BDKO cells for scrambling activity analysis. Considering that Tmem63b WT elicits PS exposure within 1min under A23187 stimulation at RT (**Fig. 3-8a**), I found it is difficult to examine the differences in scrambling activity among these variants at RT. To overcome this limitation and slow down the reaction speed, the PS exposure assay reaction temperature was reduced from RT to 4˚C, as shown in **Fig. 3-6c**, with recording taken over 40 min. The results show that the mutations I475del, V44M, D459E, and R660T can induce PS exposure within 10 min after A23187 stimulation, compared to parental Tmem63b requires 40 min to exhibit the activity. Furthermore, these mutations retained the ability to induce scrambling activity without A23187 stimulation, indicating that these Tmem63b mutations are gain-of-function mutations with constitutive scrambling activity; however, one mutant, R433H, could not (**Fig. 3-8c, d**). Interestingly, the level of PS exposure elicited by Tmem63b variants correlates with the severity of hematological disorders. Patients with high PLS-inducing mutants

like I475del and V44M suffer severe anemia and are transfusion-dependent, while those with moderate PLS-inducing mutants such as D459E and R660T develop intermediate levels of anemia. In contrast, patient carries the no PLS activity mutant R433H does not display anemia but rather present with abnormal RBCs (**Table 1-1**).

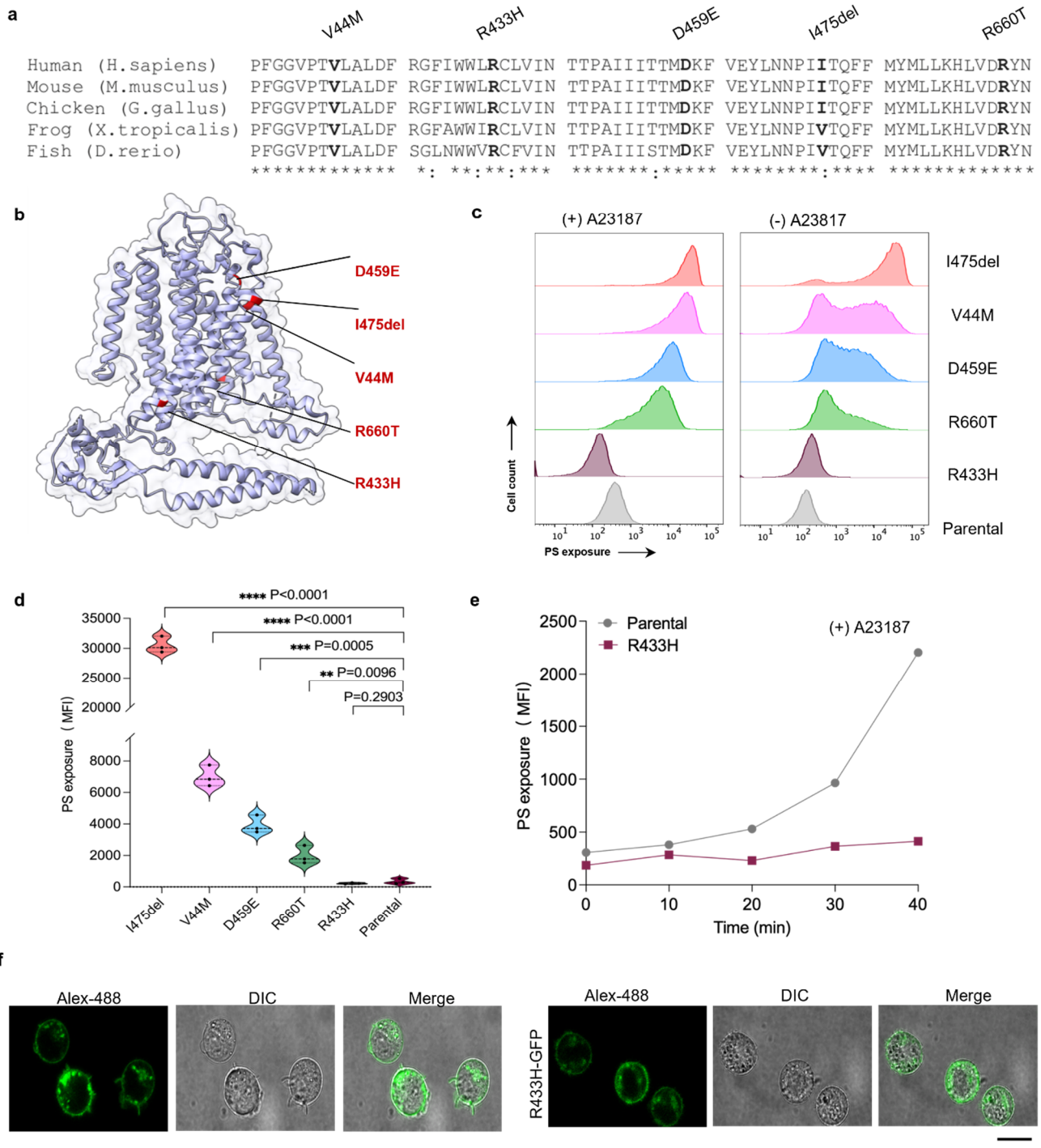

Fig. 3-8: Tmem63 mutation-mediated PLS activity: a Sequence alignment of Tmem63b among different species. Bold labeling represents the five mutations picked; asterisk shows positions where amino acids were conserved; the colon indicates similar amino acids. **b** Structure of human TMEM63B protein (PDB: 8ehx). Mutations are colored in bold red. **c** 4˚C PS exposure assay. Tmem63 mutant-GFP-expressing BDKO Cells were incubated in the chilled Annexin V/PI containing reaction buffer, left, with 3.0 μM A23187 at 10 min; right, without 3.0 μM A23187 treatment at 10 min. GFP-positive cells were collected, and the PI-negative region was analyzed. **d** Statistical analysis of 4˚C PS exposure assay among Tmem63b mutations without A23187 treatment used a two-tailed Student's t-test and is presented as mean ± SEM; a P-value of less than 0.05 was considered statistically significant. * represents P value less than 0.05, *** represents P value less than 0.001, **** represents P value less than 0.0001. **e** 4˚C PS exposure assay. Tmem63b WT and Tmem63b R433H were incubated in the Annexin V/PI-containing reaction buffer with A23187 treatment for 40 min. GFP-positive cells were collected, and the PI-negative region was analyzed. **f** Localization of Tmem63b R433H. Tmem63b R433H-GFP-expressing BDKO cells were observed by confocal microscopy; left, Tmem63b WT-GFP-expressing cells; right, Tmem63b R433H-GFP-expressing cells. Bar, 10 μm.

Tmem63b mutants elicited PS exposure in 10 min, however, Tmem63b WT requires 40 min (**Fig. 3-6c**). Therefore, it is necessary to clarify whether the R433H mutant could expose PS for 40 min, like Tmem63b WT. As shown in **Fig. 3-8e**, no PS exposure was detected in the R433H mutant, even after extending the reaction time to 40 min with A23187 stimulation, compared to the obvious PS exposure in Tmem63b WT. Considering the scrambling activity loss might be caused by protein membrane mislocalization, hence, I compared the expression of R433H and Tmem63b WT by using confocal microscopy. The R433H mutant was localized at the plasma membrane as per normal, congruent with Tmem63b WT (**Fig. 3-8f**), indicating that the lack of scrambling activity of R433H was due to a loss-of-function rather than a localization issue.

Overall, Tmem63b mutations can induce continuous PS exposure without Ca^{2+} ionophore stimulation, with the extent of PS exposure correlating with anemia severity. This suggests that Tmem63b-induced PLS activity is associated with hematological disorders.

3.4.2 Tmem63b associates with hematology disorders with specific cell type expression

In order to further prove Tmem63b is associated with hematological disorders, Tmem63b-expressing cell types were analyzed by single-cell RNA-seq (scRNA-seq) of the human fetal bone marrow samples. The public database (E-MTAB-9389) was reanalyzed by using the code provided by Jardine, L. *et al*.[103] More detailed cell type annotations, including basophil (Baso); eosinophil (eo); megakaryocyte (MK); netrophil; monocyte; and early/mid/late stage of erythrocyte, were grouped and separated. From the results, TMEM63B showed specific expression in erythrocytes during early, mid, and late erythroid stages, particularly in the mid and late stages, which occur prior to nuclear extrusion during erythrocyte development; however, TMEM63A and TMEM63C did not show erythrocyte expression (**Fig. 3-9**),

suggesting TMEM63B functions as a specific scramblase within the TMEM63 family in erythrocytes. This specific cellular expression may link TMEM63B scrambling activity to hematological disorders.

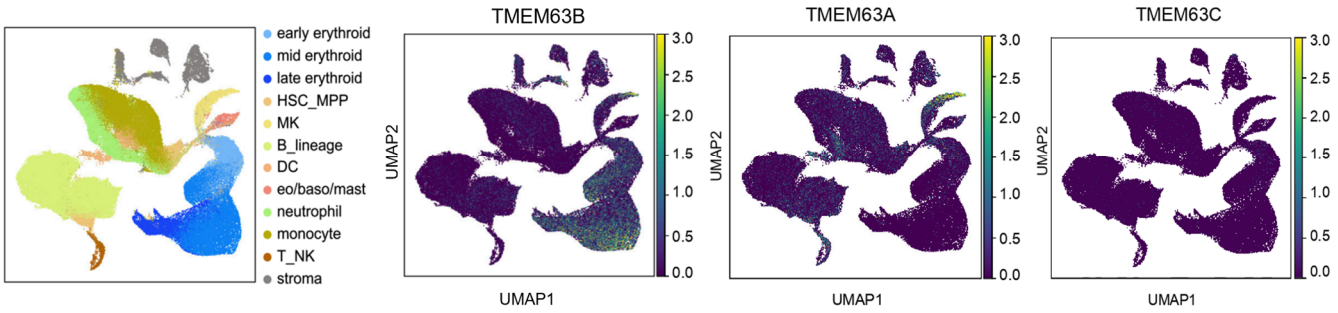

Fig. 3-9: scRNAseq analysis of TMEM63 family members. scRNA-seq analysis using human fetal bone marrow. Cell type annotation in bone marrow was classified using different colors: blue represents erythroid; light blue represents early stage of erythoid; moderate blue represents mid stage of erythroid; dark blue represents late stage of erythroid; Baso, basophil; eo, eosinophil; MK, megakaryocyte; neturophil; and monocyte. Cell types expressing TMEM63A, TMEM63B, and TMEM63C were analyzed; the color bar from purple to yellow represents the strength of expression.

3.4.3 Intracellular Ca^{2+} is not required for Tmem63b mutants-induced scrambling activity

Since Tmem63b is a mechanosensitive cation channel that permeates cations, including Ca^{2+}, whether intracellular Ca^{2+} affects Tmem63b-induced scrambling activity is interesting to know. Notably, Ca^{2+}-activated Tmem16f scrambling activity can be inhibited by BAPTA-AM treatment, which also inhibits continuous scrambling activity in the Tmem16f gain-of-function mutant, representative of BAPTA-AM's function as a chelator of intracellular Ca^{2+}. Hence, I treated Tmem63b mutant-expressing cells with BAPTA-AM prior to the PS exposure assay. As Tmem63b mutations exhibit constitutive PS exposure without Ca^{2+} ionophore stimulation, it is unlikely that BAPTA-AM treatment impedes scrambling activity. Consistent with the results, Tmem63b mutant-mediated PLS activity did not have significant change with or without BAPTA-AM treatment (**Fig. 3-10a, b**), which is different from the Tmem16f mutant result, suggesting that Tmem63b-PLS activity is not intrinsically Ca^{2+}-dependent. However, BAPTA-AM treatment inhibited Tmem63b WT elicited PS exposure, as Tmem63b WT induced scrambling activity requires Ca^{2+} ionophore stimulation, indicating that the connection between Ca^{2+} and Tmem63b (WT)-mediated scrambling activity is still missing.

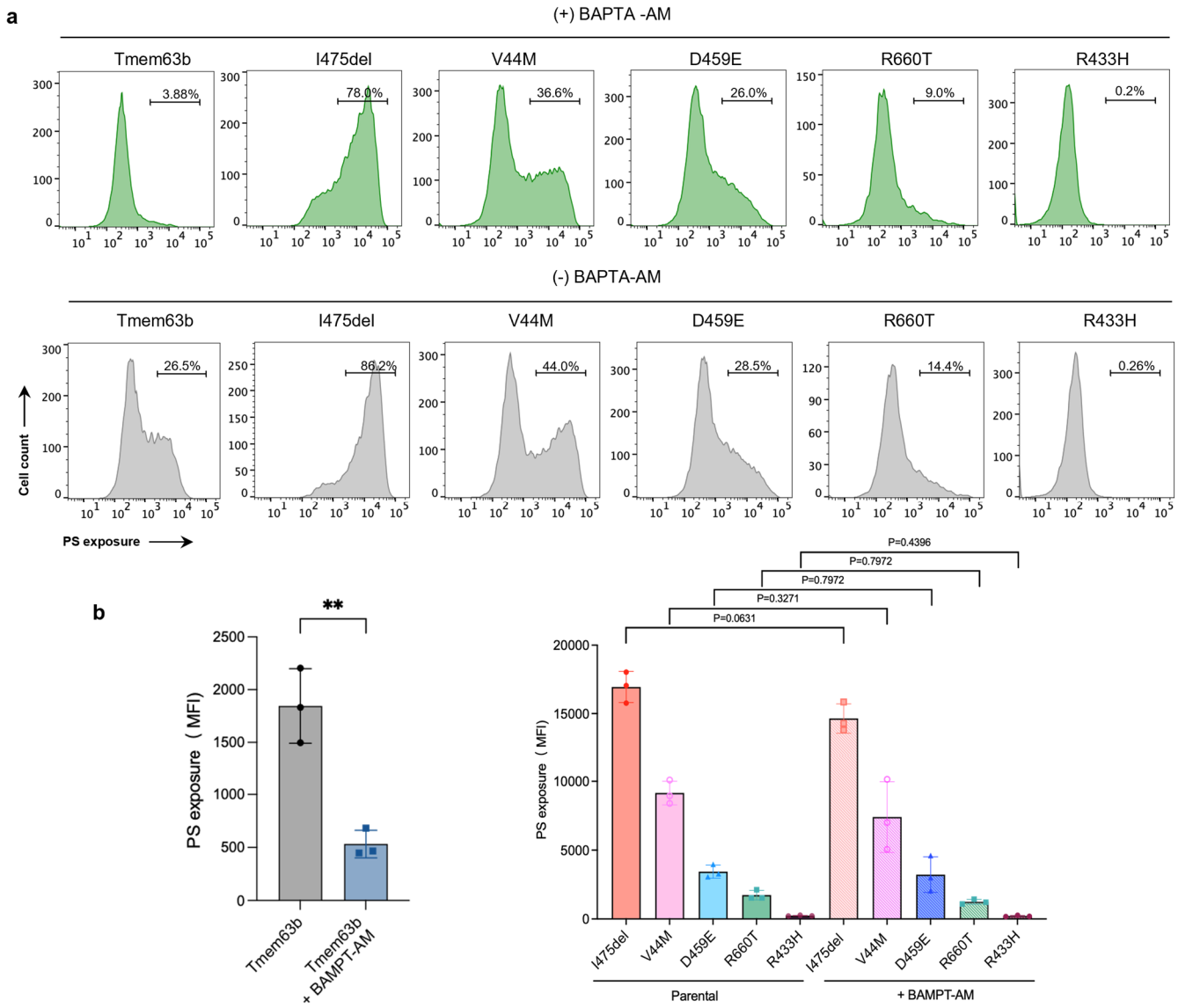

Fig. 3-10: BAPTA-AM assay in Tmem63b-expressing cells. a 4 ˚C PS exposure assay. In both Tmem63 WT- and Tmem63b mutant-expressing cells, the samples were treated with 1 μM BAPTA-AM at 37˚C for 30 min, then PS exposure assay was performed as early described. PS exposure of mutant cells was recorded at 10 min, while Tmem63b WT cells were acquired at 40 min. Grey, no BAPTA-AM treated; green, with BAPTA-AM treated; bar, PS exposure region; number, cell population in the bar. **b** Statistical analysis of **a** used a two-tailed Student's t-test and is presented as mean ± SEM; a P-value of less than 0.05 was considered statistically significant. * represents P value less than 0.05, *** represents P value less than 0.001, **** represents P value less than 0.0001.

3.5 Mechanism of Tmem63b-PLS pathway

3.5.1 Factors involved in Tmem63b-PLS pathway

In order to explore the factor(s) linked to Ca^{2+} with Tmem63b (WT)-PLS activity. I used Tmem63b-expressing cells to perform the revival sgRNA library screening again. The strategy was similar to **Fig. 3-**

3a; instead of PC uptake assay, the PS exposure assay was performed at 4 ˚C using chilled Annexin/V PI reaction buffer, contrasted to the previous 40 min recording, the reaction time was extended to 1 hr after A23187 stimulation to ensure the reaction was fully completed. As a result, the population of PS exposure-negative cells increased from 7.76% in the initial sorting to 16.3% in the third sorting (**Fig. 3-11a**), suggesting the sgRNAs targeting genes involved in the Tmem63b-PLS pathway were enriched. The enriched sgRNAs were sequenced using NGS. Consistent with early NGS sequencing result analysis, mapped targets with fewer than two reads were excluded, and candidates were ranked based on their total reads.

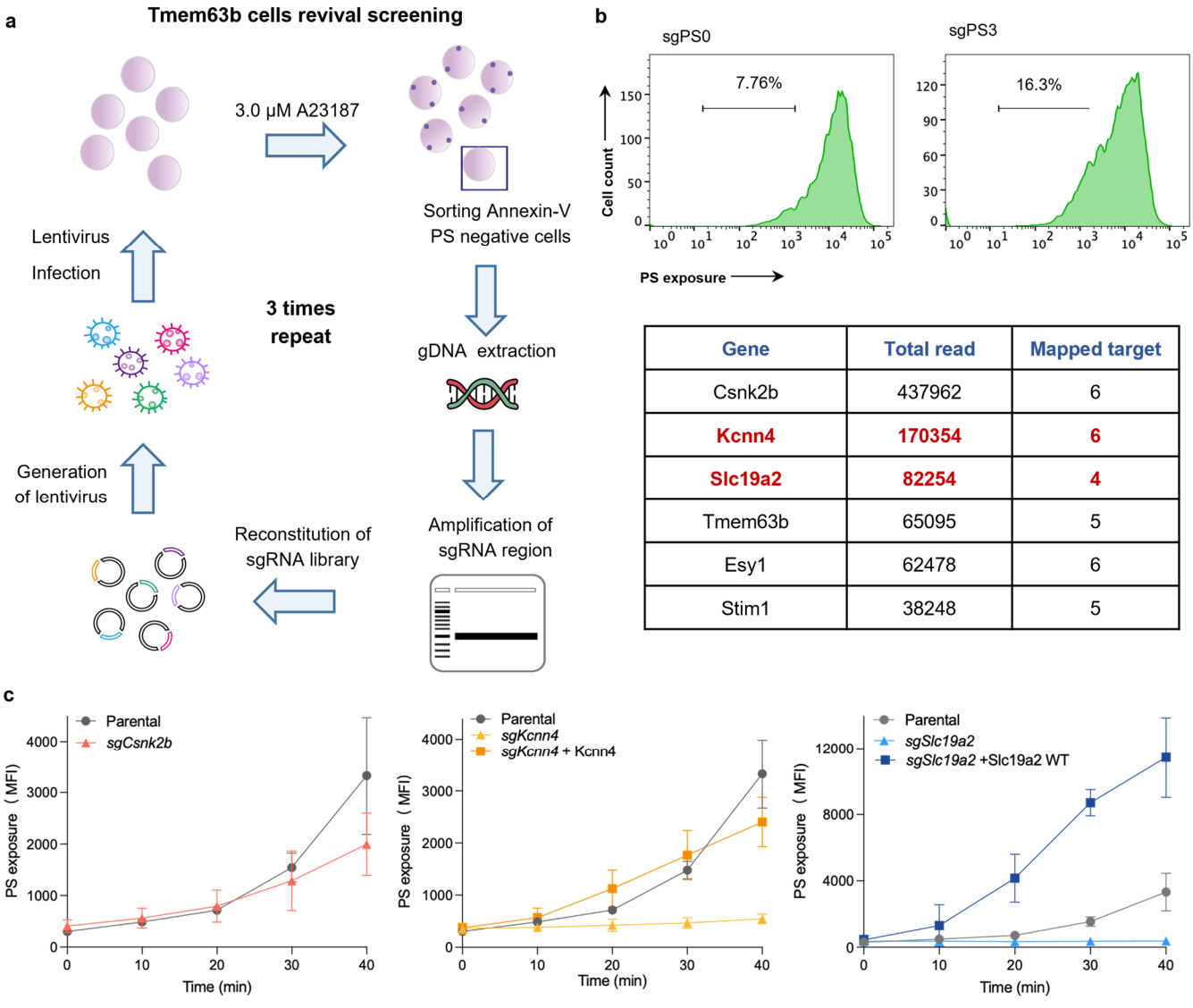

Gene	Total read	Mapped target
Csnk2b	437962	6
Kcnn4	**170354**	**6**
Slc19a2	**82254**	**4**
Tmem63b	65095	5
Esy1	62478	6
Stim1	38248	5

Fig. 3-11: Identification of factors involved in Tmem63b-PLS pathway. a sgRNA revival screening. GeCKO v2 Mouse knockout library was infected into Cas9-expressing BDKO cells which were overexpressing with Tmem63b, then PS exposure assay was performed at 4˚C under incubation in Annexin/V after 3.0 μM A23187 stimulation for 1 hr, and 1% PS exposure negative cells were sorted. Then gDNA was extracted from the sorted cells and amplified for reconstitution of new sgRNA library. The new sgRNA library was introduced into Tmem63b-expressing cells again. **b** Upper, sgPS0 represents original library sorting; sgPS3, third time sorting. Bar, PS exposure region; number, cell population in the bar. Bottom, NGS sequencing. result was performed by Illumina HiSeq2500 sequencing, with candidates ranked by total reads among effective genes (mapped target more than three among six). Red-labeled genes were further analyzed as candidates. **c** 4˚C PS exposure. Tmem63b-expressing cells and those introduced with *sgCsnk2b*, *sgKcnn4* and restored with Kcnn4, *sgSlc19a2* and restored with Slc19a2, cells were incubated in the Annexin V/PI containing reaction buffer with A23187 treatment for 40 min, recorded every 10 min, three times repeated and the mean and standard error of the mean (SEM) were calculated.

The top three genes were Csnk2b, Kcnn4, and Slc19a2; Tmem63b was enriched more than Stim1, compared to hPC19 cell screening result, suggesting that Tmem63b and Stim1 were distinct PLS-inducing pathways. This time, the results were specific to Tmem63b-PLS pathway (**Fig. 3-11b**). Casein Kinase 2 beta (Csnk2b) is a serine/threonine kinase which is involved in the phosphorylation of various substrates. Given that phosphorylation also activates Xkr8, it is possible that Csnk2b regulates the phosphorylation of Tmem63b to exhibit scrambling activity. To investigate the role of Csnk2b in the Tmem63b-related scrambling activity, *sgCsnk2b* was introduced into Tmem63b-expressing cells; however, *sgCsnk2b* introduction did not significantly reduce scrambling activity elicited by Tmem63b (**Fig. 3-11c**), suggesting Csnk2b is not involved in the Tmem63b-PLS pathway. Similarly, *sgKcnn4* and *sgSlc19a2* were also introduced into Tmem63b-expressing cells, respectively. As shown in **Fig. 3-11c**, both *sgKcnn4* and *sgslc19a2* introduction suppressed Tmem63b-induced PS exposure. Introducing Kcnn4 into *sgKcnn4*-expressing cells rescued the suppressed PS exposure to the normal level comparable to Tmem63b WT, while introducing Slc19a2 into *sgSlc19a2*-expressing cells not only rescued but also greatly enhanced Tmem63b-induced PS exposure. These results suggested both Kcnn4 and Slc19a2 were implicated in the Tmem63b-induced PLS pathway, potentially affecting Tmem63b-PLS activity from different aspects. The fact that expressing Slc19a2 enhanced Tmem63b scrambling activity suggests that it may play a more direct regulatory role. The next step is to understand how these two factors affect Tmem63b-PLS activity.

3.5.2 Kcnn4 regulates Tmem63b scrambling activity through K^+ efflux

3.5.2.1 Extracellular K^+ slows down Tmem63b-PLS activity

Kcnn4 plays an important role in regulating intracellular ion metabolism associated with phospholipid asymmetry distribution and water loss during erythrocyte apoptosis. As a Ca^{2+}-activated K^+ channel, it is

possible that Kcnn4 contributes to Tmem63b-mediated scrambling activity by regulating K^+ efflux in a Ca^{2+}-activated manner. This also provided insight into how Ca^{2+} relates to Tmem63b-PLS activation. To demonstrate that K^+ efflux acts in the Tmem63b PLS pathway, I replaced 140 mM Na^+ with varying concentrations of K^+ in Annexin V/PI buffer as the following combinations: 0.5 mM K^+/139.5 mM Na^+, 5 mM K^+/135 mM Na^+, 50 mM K^+/90 mM Na^+, and 140mM K^+/0 mM Na^+, then conducted the PS exposure assay using these buffers. After A23187 stimulation for 40 min at 4˚C, Tmem63b-PLS activity was showed to be extracellular K^+ concentration dependent (**Fig. 3-12a**). This suggests that increasing extracellular K^+ concentration slows down K^+ efflux, resulting in decreased Tmem63b-related PLS activity.

Notably, Tmem63b-induced PLS activity is almost suppressed at 5 mM extracellular K^+ incubation, which is the physiological concentration of K^+ required to maintain normal cellular function and electrophysiological properties. Following this, I questioned whether Kcnn4 is functionally present in BDKO cells. To check the expression of Kcnn4, firstly, protein expression was measured through BN-PAGE assay. To detect endogenous protein expression, membrane fractions from BDKO parental cells, as well as Kcnn4-expressing and *sgKcnn4*-expressing cells, were prepared and solubilized using LMNG/CHS detergent; the exact methods were described in the 'Materials and Methods' section. To avoid strong detection signals caused by protein overexpression, the loading amount of the Kcnn4-expressing sample was decreased to one-fifth relative to other samples. From the result, Kcnn4 bands were detected in BDKO cells sample, confirming their presence in BDKO cell line; *sgKcnn4* introduction resulted in a half decrease in protein expression, suggesting effective downregulation of the Kcnn4 gene; in contrast, Kcnn4-expressing cells increased protein expression by 30-fold (**Fig. 3-12b**). On the other hand, qRT-PCR was used to confirm Kcnn4 gene expression levels among BDKO cells, Kcnn4-expressing BDKO cells, and *sgKcnn4*-expressing BDKO cells; beta-actin gene was utilized as endogenous control to normalize amplification levels. As a result, *sgKcnn4*-introducing cells reduced gene expression by half, while Kcnn4-expressing cells increased gene expression around 25-fold (**Fig. 3-12c**).

Given that Kcnn4 exists and functions in BDKO cells, it is still unclear why Tmem63b-PLS activity was almost inhibited in 5 mM extracellular physiological K^+ condition. I recognized that the PS exposure assay was set up at 4˚C to easily detect differences in PLS activity; however, lower temperature slows down the reaction rates, membrane fluidity, inhibition of flippase/floppase activity together with ATP1a1-mediated K^+ influx, creating a sensitive environment for PLS activity responding to K^+ incubation. To demonstrate Kcnn4 functionality at physiological ion condition and temperature in Tmem63b-PLS activity, I performed the PS exposure assay at RT with various K^+ concentrations. This time, a mild decrease tendency in PLS activity was shown in a K^+-dependent manner; particularly in 0.5 mM K^+ and 5.0 mM K^+ conditions while PLS activity was exhibited the same as the 0 mM K^+ condition, representing that

Kcnn4 was functional for Tmem63b-induced PLS activity at 5 mM physiological condition (**Fig. 3-12e**). However, when extracellular K^+ was increased to more than 50 mM K^+ (and 140 mM), the PS exposure was greatly inhibited. The restriction of PS exposure at 50 mM and 140 mM K^+ was more pronounced compared to 0.5 mM or 5.0 mM K^+ at RT (**Fig. 3-12d**), based on the proportion of PS exposed cells in initiation (time < 100 sec) and termination (time > 620 sec) stages. On the other hand, the inhibition effect of extracellular K^+ was consistent at the endogenous Tmem63b level; *Stim1*$^{-/-}$ BDKO cells were utilized to demonstrate endogenous Tmem63b-related PLS activity. According to *Stim1*$^{-/-}$ BDKO cells showed delayed scrambling activity under A23187 stimulation (around 10 min started to expose PS) (**Fig. 3-4c**); hence, to compare differences in PLS activity under varying K^+ conditions induced by endogenous Tmem63b, the recording of PS exposure during the assay began from 10 min after A23187 stimulation. Consequently, a similar tendency to Tmem63b-expressing was shown; at 0.5 mM and 5 mM K^+, Kcnn4 remained effective, and endogenous Tmem63b elicited PS exposure, however at 50 mM K^+ and 140 mM K^+, PS exposure was almost inhibited.

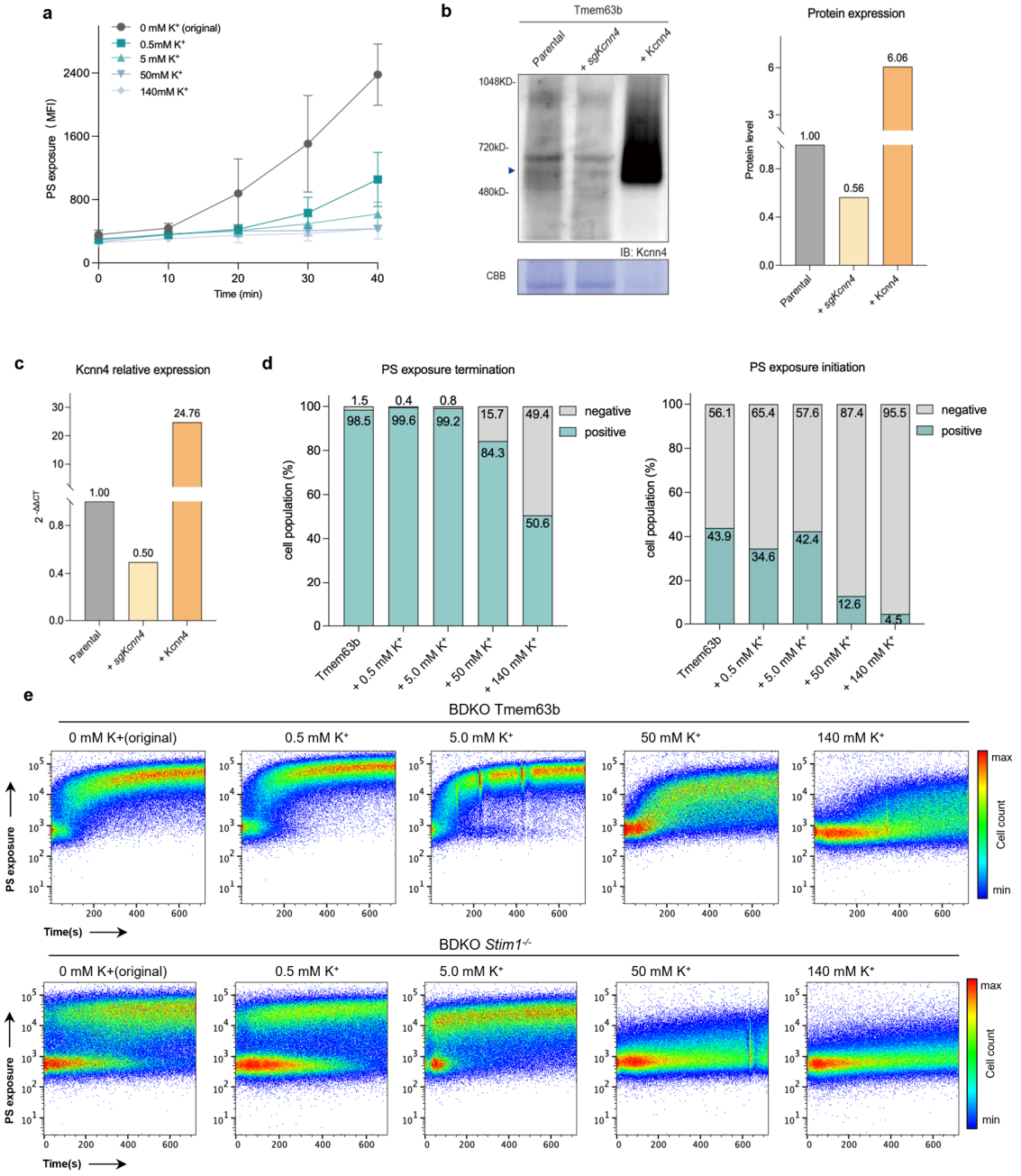

Fig. 3-12: Kcnn4 regulates K^+ efflux to effect Tmem63b-related PLS activity. a 4 ˚C PS exposure assay. Tmem63b-GFP-expressing cells were stimulated with 3.0 µM A23187 in different series of Na^+/K^+ Annexin V/PI buffer; GFP-positive cells were acquired, and the PI-negative region was analyzed. Three repeats with the mean and standard error of the mean (SEM) were calculated. **b** Kcnn4 expression. The BN-PAGE assay was performed using Tmem63b-expressing cells that were introduced with *sgKcnn4* or Kcnn4. The blue arrow shows Kcnn4 protein. CBB staining was used as the loading standard, and the relative expression was calculated by normalizing parental Tmem63b-expressing cells. **c** PS exposure assay. PS exposure assay in (**a**) was performed at RT. **d** Initiation and termination of PS exposure assay. The definition of PS exposure initiation and termination is the cell population of PS exposure within beginning 100 sec (0 sec~100 sec) and last 100 sec (620 sec~720 sec) stages; blue represents cells showing PS exposure positive signal, gray represents cells showing PS negative signal. Number, the population of the cells. **e** PS exposure assay. *Stim1*$^{-/-}$ BDKO cells were stimulated with A23187 in series Na^+/K^+ in Annexin V/PI buffer as described before; recording started after 10 min A23187 treatment.

On the other hand, Tmem63b mutations exhibit scrambling activity in a Ca^{2+}-independent manner (**Fig. 3-8c, 3-10a**); so I questioned whether Tmem63b mutations bypass Kcnn4's requirement for scrambling activity. I introduced Kcnn4 and *sgKcnn4* into Tmem63b mutant cells. The result showed that Kcnn4 had no major impact on Tmem63b mutants-induced PLS activity (**Fig. 3-13b**). Additionally, PS exposure assay under extracellular K^+ incubation was also conducted among Tmem63b mutants. I used 140 mM K^+ in Annexin V/PI buffer to slow down K^+ efflux to the maximum extent and testing the PLS activity without A23187 stimulation. Similar to the introduction of *sgkcnn4*, incubating in 140 mM K^+ yielded no significant difference in PLS activity compared to normal 140 mM Na^+ incubation, indicating that Tmem63b mutants skip the requirement of Kcnn4 (**Fig. 3-13a, c**). These results suggest Kcnn4 probably serves as a linker between Ca^{2+} stimulation and Tmem63b-PLS activation. In other words, Tmem63b WT requires Ca^{2+} stimulation along with Kcnn4 activated K^+ efflux, while Tmem63b mutants that bypass Ca^{2+} stimulation also do not require Kcnn4 to efflux K^+, which is consistent with BAMPTA-AM results and the extracellular K^+ incubation assay.

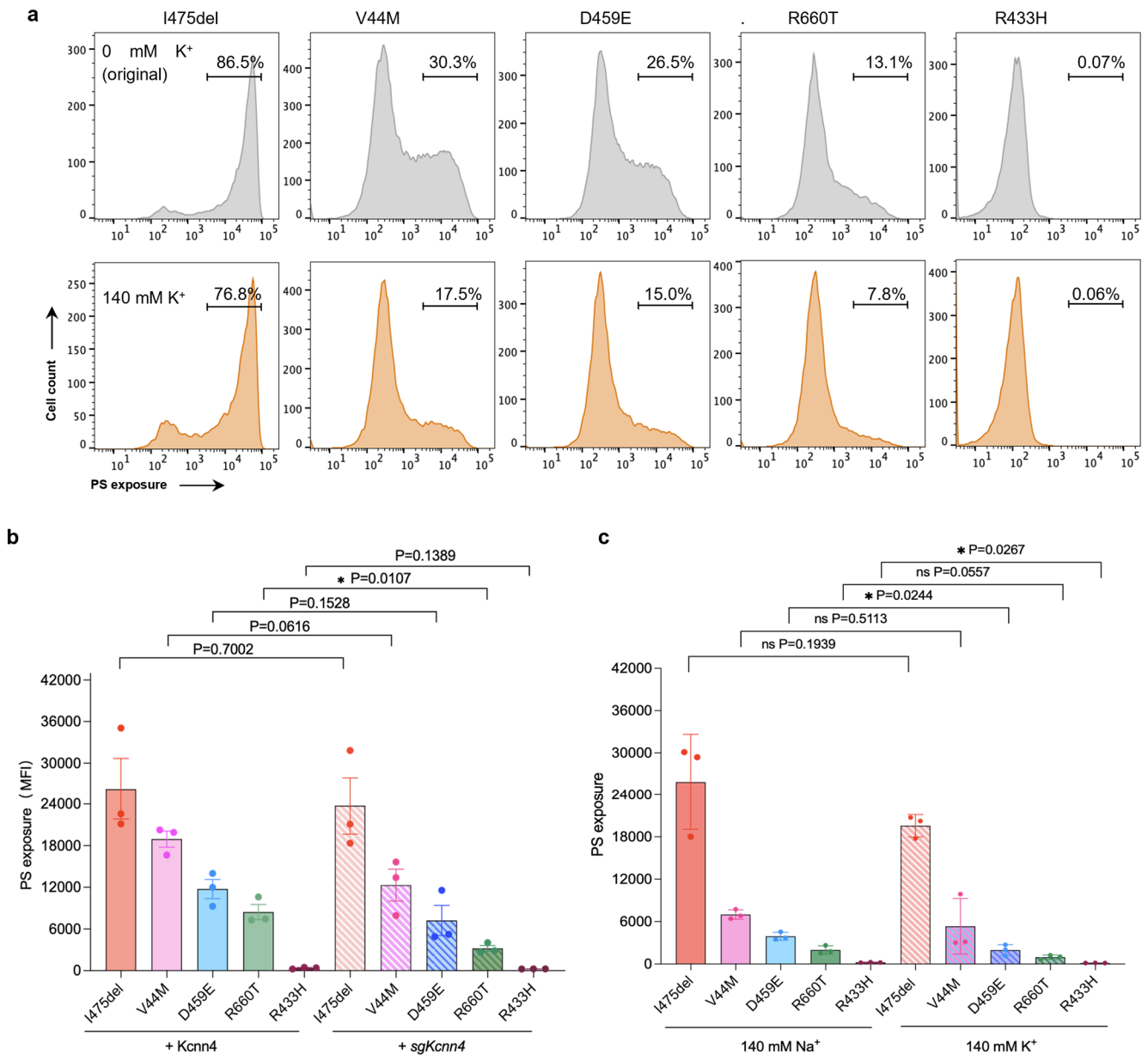

Fig. 3-13: Kcnn4 effects on Tmem63b mutants-PLS activity. a 4˚C PS exposure. Statistical analysis of PS exposure among Tmem63b mutations cells. Extracellular K^+ (140 mM) was replaced with Na^+ in the Annexin V/PI buffer without A23187 stimulation. Upper represents PS exposure in original 140 mM Na^+; bottom represents PS exposure in 140 mM K^+. PS exposure was recorded at 10 min without A23187 stimulation. **b** 4 ˚C PS exposure. PS exposure assay was performed among Tmem63b mutations cells and those with expression of Kcnn4 and *sgKcnn4.* Statistical analysis used a two-tailed Student's t-test and is presented as mean ± SEM; a P-value of less than 0.05 was considered statistically significant. * represents P value less than 0.05, *** represents P value less than 0.001, **** represents P value less than 0.0001. **c** 4˚C PS exposure. PS exposure assay was performed among Tmem63b mutations cells and those incubated with 140 mM K^+. Statistical analysis used a two-tailed Student's t-test and is presented as mean ± SEM; a P-value of less than 0.05 was considered statistically significant. * represents P value less than 0.05, *** represents P value less than 0.001, **** represents P value less than 0.0001.

3.5.2.2 The effect of Kcnn4 inhibitors on Tmem63b-PLS activity

K^+ efflux can be regulated by many K^+ channels and pumps. I wondered whether extracellular K^+ incubation may selectively affect Kcnn4 action or not. To directly demonstrate the role of Kcnn4 in the regulation of the Tmem63b-PLS pathway, two Kcnn4 inhibitors, TRAM-34 and Senicapoc, were utilized to block channel for exporting ion. The strategy was performed as follows: cells were suspended in Annexin V/PI buffer with 10 μM TRAM-34 or 0.5 μM Senicapoc for 4 min before stimulating with A23187, followed by PLS activity measurement. The results indicated that Tmem63b-expressing cells exposed PS during 40 min after A23187 stimulation; however, once incubated with TRAM-34 or secicapoc, the scrambling activity was greatly decreased (**Fig. 3-14a**), with statistical analysis confirming a significant difference between parental Tmem63b-expressing cells and those treated with inhibitors. Moreover, PS exposure assay was also performed at RT using different concentrations of Senicapoc (0 μM, 0.25 μM, 0.5 μM, 1 μM, 2.5 μM, and 5 μM). Tmem63b scrambling activity showed a dose-dependent manner, suggesting that Tmem63b-related PLS activity was regulated by Kcnn4 inhibition levels (**Fig. 3-14c**). Combining previous findings that extracellular K^+ reduced Tmem63b-PLS activity through slowing down K^+ efflux, I concluded that K^+-regulated Tmem63b-PLS activity is mediated by Kcnn4.

Furthermore, there is a question as to whether functional Kcnn4 is important in the Tmem63b-PLS pathway or not. To answer this question, I tried to introduce mutant Kcnn4 in Tmem63b-expressing cells. Studies indicate that the H358 residue plays a dual role in regulating Kcnn4 channel activity[106,107]: when unphosphorylated, H358 inhibits channel activity; while phosphorylated, the H358 leads to activation of Kcnn4. Mutant H358N is not activated by histidine kinase, implying that this mutant is dull for activation. Additionally, H358 localizes to the calmodulin binding site at the C terminus of Kcnn4, which may potentially slow down the reaction for Ca^{2+} activation. I then performed the PS exposure assay with Kcnn4 WT- and Kcnn4 H358N-expressing Tmem63b cells. As a result, the Kcnn4 H358N mutant exhibited lower PLS activity than Kcnn4 WT, probably due to the dull ability of K^+ efflux (**Fig. 3-14b**).

In addition, to detect the effect of TRAM-34 and Senicapoc on endogenous Tmem63b levels, PS exposure was conducted at RT using *Stim1*$^{-/-}$ BDKO cells, followed by incubation of inhibitors for 4 min and stimulation with A23187. As shown in **Fig. 3-14d**, treatment with inhibitors resulted in more evident suppression of scrambling activity in endogenous Tmem63b-related PLS activity, highlighting the function of Kcnn4 in Tmem63b-PLS activity.

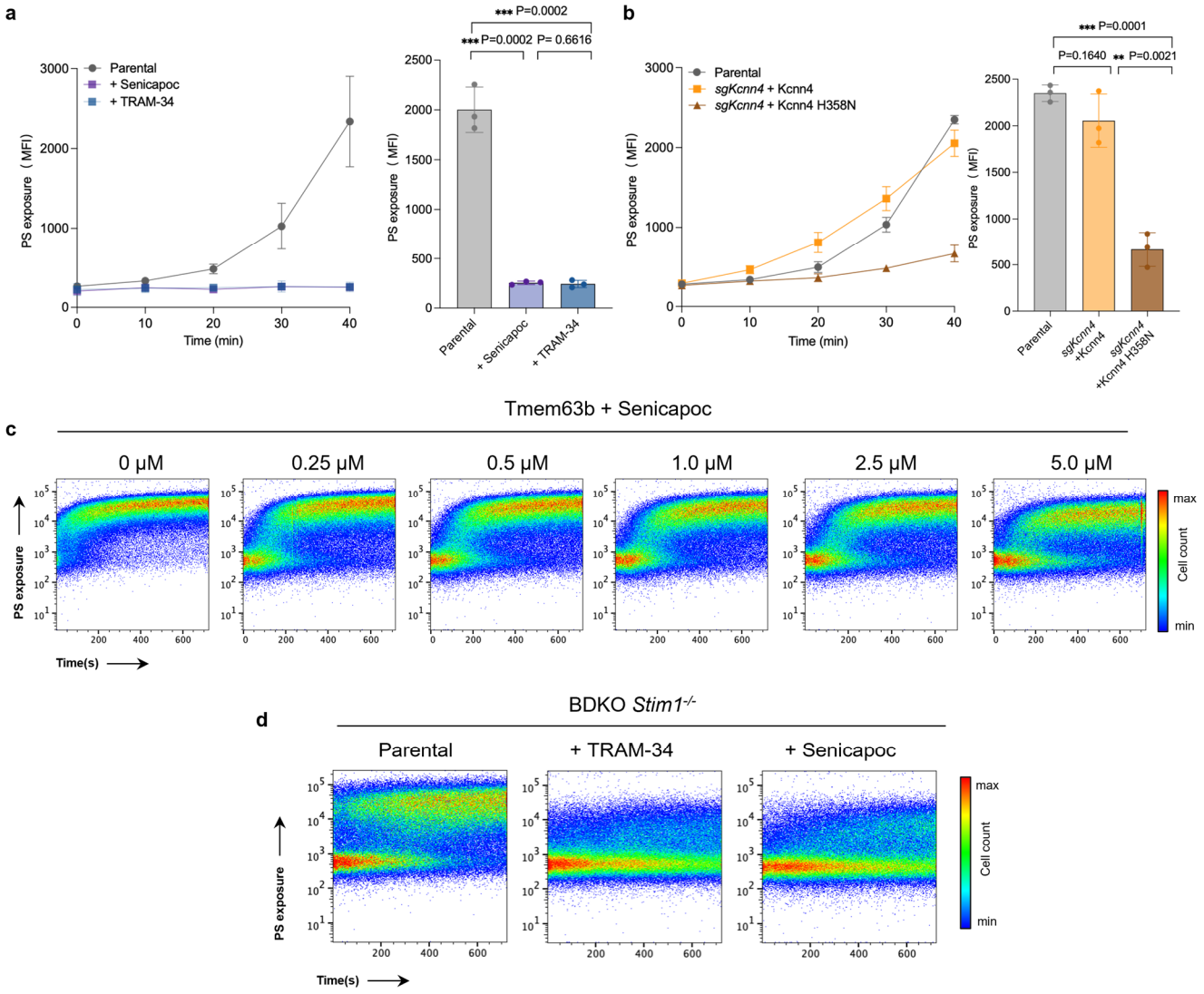

Fig. 3-14: Kcnn4 inhibitors' treatment on Tmem63b-PLS activity. a 4 ˚C PS exposure assay. Tmem63-expressing cells were stimulated by A23187, as described earlier. For Senicapoc and TRAM-34 treatment, 0.5 μM Senicapoc or 10 μM TRAM-34 was added into Annexin V/PI reaction buffer for 4 min incubation, then stimulated with A23187. Statistical analysis used two-tailed Student's t-test and is presented as mean ± SEM, P-value of less than 0.05 was considered statistically significant. * represents P value less than 0.05, *** represents P value less than 0.001, **** represents P value less than 0.0001. **b** 4 ˚C PS exposure assay. Parental Tmem63b-expressing cells and those with *sgKcnn4* + Kcnn4 WT, *sgKcnn4* + Kcnn4 H358N cells were used for PS exposure assay under A23187 treatment, and statistical analysis used a two-tailed Student's t-test (same as **a**). **c** PS exposure assay. Senicapoc from 0 μM to 5 μM was added into Annexin V/PI buffer for 4 min with Tmem63b-GFP-expressing cells before A23187 treatment. GFP positive signal was selected and PI negative region was analyzed. **d** PS exposure assay. PS exposure assay with inhibitor treatments were performed in *Stim1*$^{-/-}$ BDKO cells, recording started after 10 min A23187 stimulation.

3.5.3 Slc19a2 forms a complex with Tmem63b to exhibit scrambling activity

3.5.3.1 Tmem63 interacts with Slc19a2

Based on the known scramblases, Tmem16f and Xkr8 exist as homodimers to achieve PLS activity. The structural similarity between the Tmem16 and the Tmem63 families suggests a potential similar mechanism for PLS activity.

Next, I performed a BN-PAGE assay to verify the natural formation of Tmem63b. Tmem63b-GFP-expressing BDKO cells were solubilized with LMNG/CHS, protein concentration was determined, and 10 ug of protein was loaded onto BN-PAGE followed by a western blot. Anti-GFP was used for Tmem63b detection. Unlike Tmem16f, which forms a homodimer, only one major band corresponding to the Tmem63b monomer was mainly observed through the BN-PAGE assay, which is consistent with Cryo-EM analysis performed in other studies. However, there was a faint 'dimer-like' band above the major Tmem63b monomer band (**Fig. 3-15a**), which could indicate interaction between Tmem63b with other proteins or itself.

The potential proteins that interact with Tmem63b were then identified using the biochemical screening. Immuoprecipitation (IP) was conducted by incubating GFP-nanobody agarose beads with cell lysate from both Tmem63b-GFP-expressing cells and parental cells. Considering that Tmem63b is Ca^{2+}-dependent, Ca^{2+} was added into Tmem63b-expressing cells to maintain its activated state, while the resting state did not have Ca^{2+}added. Mass spectrometry (MS) analysis demonstrated that the components interact with Tmem63b: the most precipitated protein was Tmem63b as it was overexpressed in the cells; among the candidates, Slc19a2, identified in the revival screening result, was also enriched in the IP-MS result (**Fig. 3-15b**). Given that Slc19a2 restored Tmem63b-related PLS activity more effectively than Kcnn4, Slc19a2 may play a more direct role (**Fig. 3-11c**), possibly forming a complex that regulates Tmem63b-PLS activity.

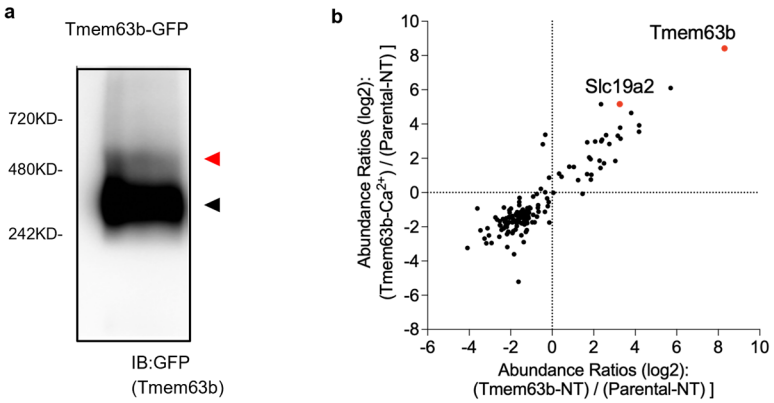

Fig. 3-15: Tmem63b mainly exists as a monomer in the cell. a BN-PAGE assay. Tmem63-GFP-expressing cells were solubilized by LMNG/CHS and applied to a BN-PAGE assay to detect complex formation, followed by western blot and detected using an anti-GFP HRP antibody. The detailed procedure was described in 'Method and Materials'. Red arrow, a minor dimer-like band; black arrow, major monomer Tmem63b. **b** IP-MS assay. Cell lysate of Tmem63b-GFP-expressing cells and BDKO parental cell lysate were generated, then applied to anti-GFP-nanobody beads incubation and mass spectrometry analysis. X axis, no Ca^{2+}-incubated Tmeme63b/parental cells; Y axis, Ca^{2+} Tmeme63b/parental cells. Red dots represent Tmem63b and Slc19a2.

3.5.3.2 Slc19a2 and Tmem63b form a complex

To identify whether Tmem63b and Slc19a2 form a complex, I introduced Slc19a2 into Tmem63b-GFP-expressing cells and performed BN-PAGE. As expected, the 'dimer-like' band was significantly increased with the expression of Slc19a2. Compared to other protein introductions, such as Kcnn4 or Csnk2b, this 'dimer-like' band exclusively aggregated in the Slc19a2-expressing case. Oppositely, the *sgSlc19a2* introduction shows less of this 'dimer-like' band (**Fig. 3-16a**). To further demonstrate that this band contains both Tmem63b and Slc19a2 protein, a gel-shift assay was performed using BDKO cells that expressed both Tmem63b-Flag-GFP and Slc19a2-HA. After preparing cell lysate and measuring protein concentration by BCA assay, 2 µl antibody was added into 30 µl 0.5 mg/ml lysate sample and incubated at 4˚C for 1 hr. Then, 10 µg protein was loaded for BN-PAGE as usual. To visualize bands containing Tmem63b, Anti-DDDDK was added, as it can specifically bind to proteins conjugated to FLAG; to demonstrate which bands contain Slc19a2, HA-1.1 antibody was added, which binds to proteins conjugated to HA-tag. As a consequence, the addition of these antibodies causes a shift in the bands due to size changes. The results showed that both the monomer and 'dimer-like' bands shifted with Anti-DDDDK, indicating these two bands contained Tmem63b (**Fig. 3-16b, left**). However, only the 'dimer-like' band shifted with the HA-1.1 antibody, suggesting this band contained Slc19a2 (**Fig. 3-16b, right**). Based on the above results, I concluded that Tmem63b forms a complex with Slc19a2 .

Tmem63b is a mechanosensitive cation channel, Slc19a2 is a thiamine transporter, yet these two different functional proteins can form a complex during scrambling activity. Whether this complex formation is critical for PLS activity needs to be clarified. Then Alphafold2 (v 2.3.2) through the AlphaFold ColabFold v1.5.5 was utilized to predict the structure of the Tmem63b/Slc19a2 complex; among the 5 predicted complex formations, one with a high pLDDT value was selected. The pLDDT value represents the accuracy of prediction, together with the 2D predicted Aligned Error (PAE), which indicates the reliability of the accuracy of the orientation of parts of the structures to one another, as shown in **Fig. 3-16c**. Although the cytoplasmic area has low confidence, the transmembrane regions exhibit high confidence in pLDDT. The lateral view of interacting sites between Tmem63b and Slc19a2 surfaces was analyzed based on the predicted structure: M711, F712, and I719 in TM 10, along with F213 and L217 in TM2 of Tmem63b,

contact F113 in TM3, F202, S199, W206, and F207 in TM6 of Slc19a2 in less than 5 Å, representing a direct interaction among these hydrophobic residues in the Tmem63b/Slc19a2 complex (**Fig. 3-16d**).

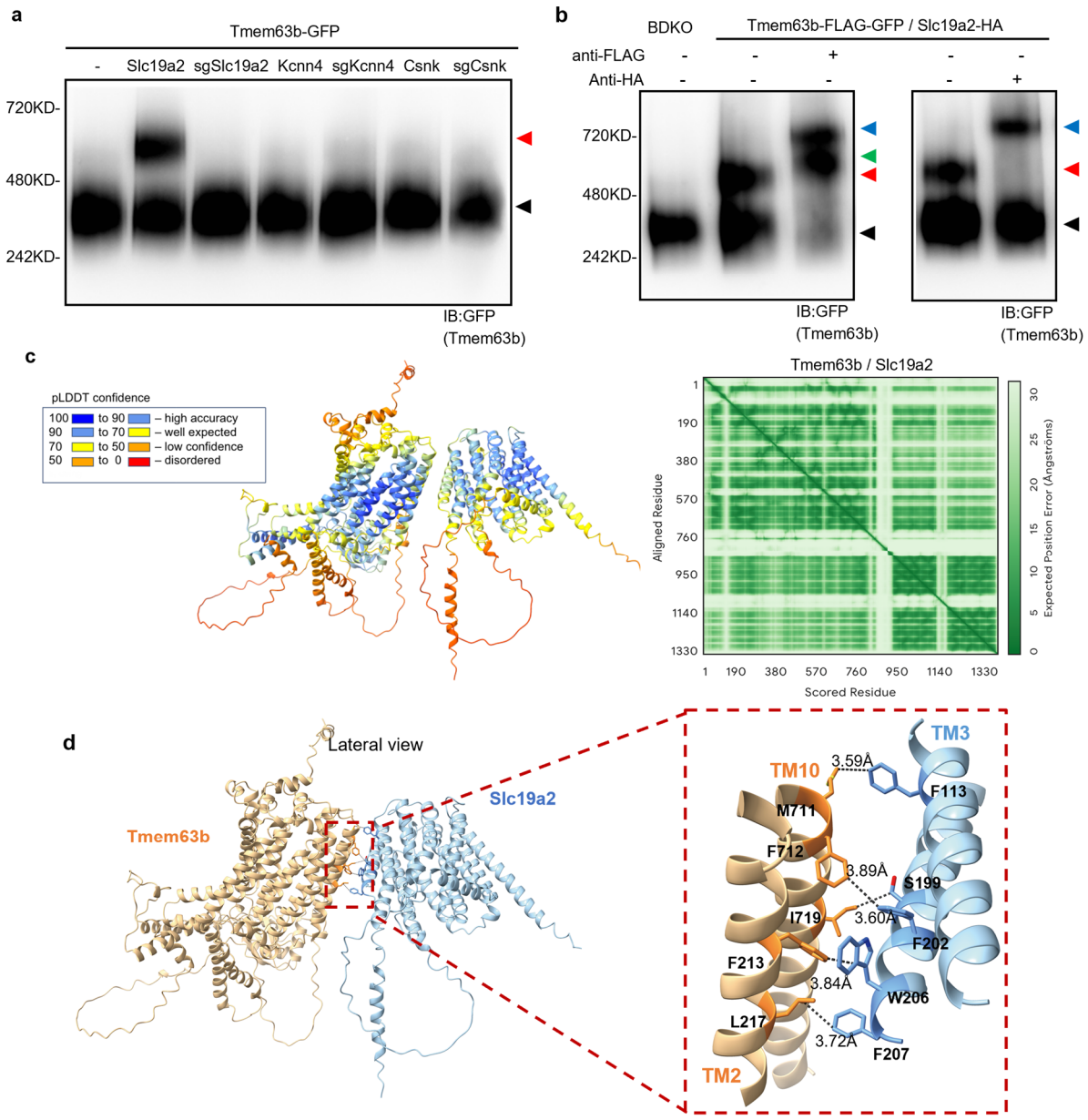

Fig. 3-16: Prediction of Tmem63b and Slc19a2 complex. a BN-PAGE assay. Tmem63-GFP-expressing cells and those with introduction of Slc19a2, *sgSlc19a2*, Kcnn4, *sgKcnn4*, Csnk2b, and *sgCsnk2b* were solubilized using LMNG/CHS and applied to a BN-PAGE assay. Anti-GFP HRP was used for Tmem63b detection. **b** Gel-shift assay. Cell lysate from Tmem63b-FLAG-GFP-expressing cells, which were introduced with Slc19a2-HA, was incubated with Anti-DDDDK or HA 1.1 antibody at 4˚C for 1h, then BN-PAGE was performed. Anti-GFP HRP was used for Tmem63b detection. Black arrow, Tmem63b monomer; red arrow, Tmem63b complex band; green, Tmem63b monomer with antibody; blue, Tmem63b complex with antibody. **c** Predicted Tmem63b/Slc19a2 complex. AlphaFold predicted structure with pLDDT score, which represents the prediction confidence, and PAE plot represents two residues reliability. **d** Lateral view of Tmem63b/Slc19a2 complex. Yellow represents Tmem63b, and blue represents Slc19a2. Surface contact sites are zoomed in and five residues are presented as amino acids; the distance between each pair is labeled.

3.5.3.3 Complex formation is essential for PLS activity

To demonstrate the necessity of the formation of Tmem63b/Slc19a2 complex for PLS activity, I substituted these five hydrophobic residues in Tmem63b with alanine to disrupt potential interactions with Slc19a2. After confirming the alanine mutations plasmid was successfully generated through sanger-sequencing, I introduced Tmem63b-Ala-GFP into BDKO cells. Compared to Tmem63b-WT-GFP-expressing cells, the alanine mutant Tmem63b did not exhibit PLS activity during 40 min under A23187 stimulation (**Fig. 3-17a**), highlighting the importance of surface residues in Tmem63b for PLS activity. To demonstrate whether these alanine mutations disrupt complex formation with Slc19a2, I introduced Slc19a2 in both Tmem63b-Ala-GFP-expressing cells and Tmem63b-WT-GFP-expressing cells. Tmem63b-WT-GFP cells with Slc19a2 expression exhibited PS exposure after A23187 treatment, while the alanine mutant of Tmem63b with Slc19a2 did not display PLS capability (**Fig. 3-17b**). To further investigate the impact of the alanine mutations on complex formation, I conducted a BN-PAGE assay using Slc19a2 introduced Tmem63b-Ala-GFP cells. As a result, the alanine mutant Tmem63b failed to form a complex with Slc19a2, unlike Tmem63b WT (**Fig. 3-17c**). This suggests that the loss of PLS activity in the alanine mutant Tmem63b results from the inability to form a complex with Slc19a2, underscoring the importance of this complex formation for eliciting PLS activity. On the other hand, confocal analysis confirmed that the alanine mutant Tmem63b maintained plasma membrane expression, indicating that the deficiency in PLS activity arises from the failure in complex formation rather than protein mislocalization (**Fig. 3-17d**).

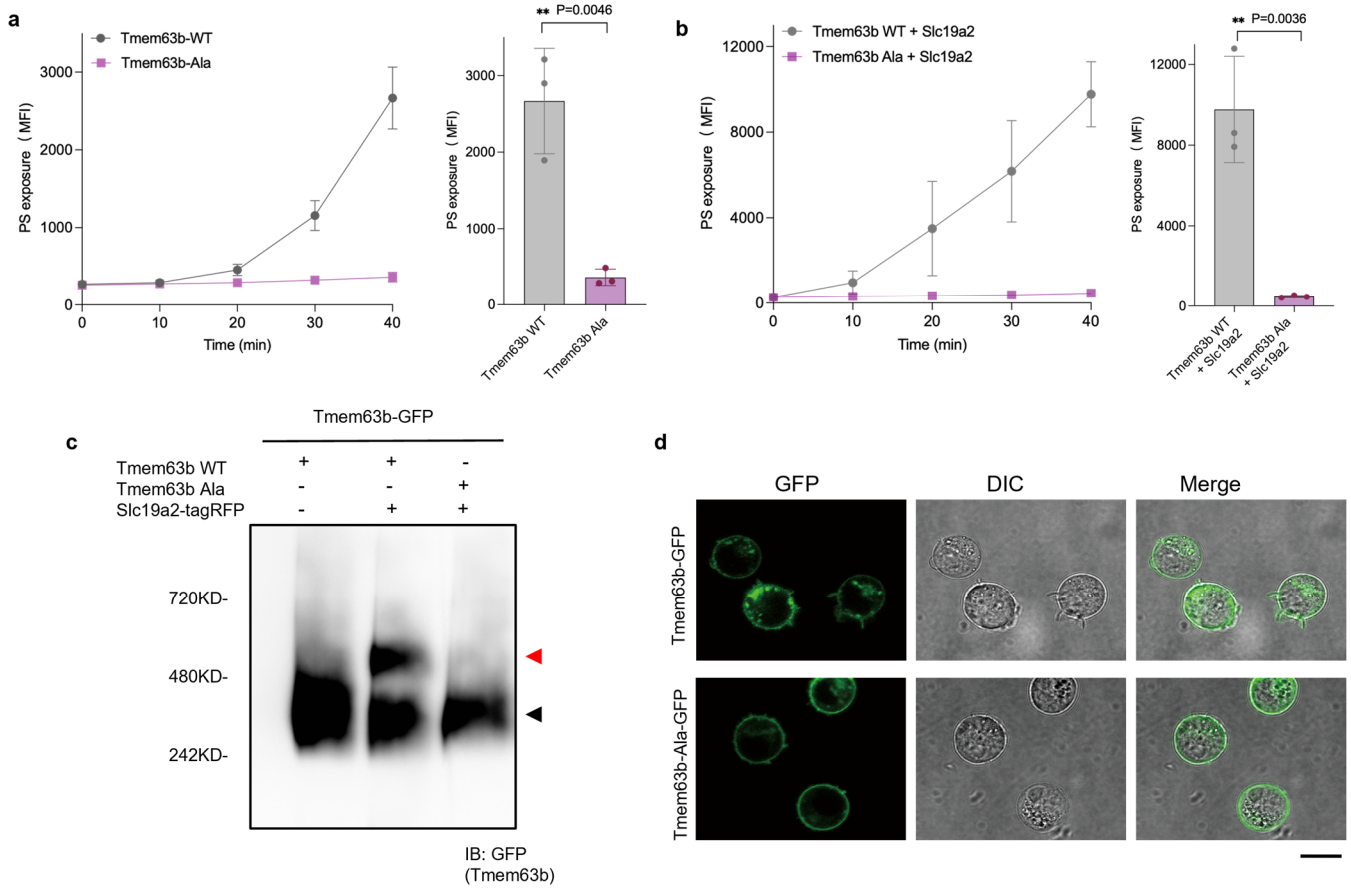

Fig. 3-17: Tmem63b/Slc19a2 complex formation is essential for PLS activity. a 4˚C PS exposure assay. PS exposure assay was performed in Tmem63b-Ala-GFP-expressing cell and Tmem63b-WT-GFP cells; the statistical analysis of PS exposure in left at 40 min was shown in a two-tailed Student's t-test and is presented as mean ± SEM, P-value of less than 0.05 was considered statistically significant. * represents P value less than 0.05, *** represents P value less than 0.001, **** represents P value less than 0.0001. **b** 4˚C PS exposure assay. PS exposure assay was performed in Slc19a2 introduced Tmem63b-Ala-GFP-expressing cells and Tmem63b-WT-GFP cells under A23187 stimulation; the statistical analysis of PS exposure in left at 40 min. **c** BN-PAGE assay. Slc19a2 was introduced into Tmem63-WT-GFP-expressing cells and Tmem63b-Ala-GFP-expressing cells; anti-GFP HRP was used to detect Tmem63b. Black arrow, Tmem63b monomer; red arrow, Tmem63b and Slc19a2 complex. **d** Confocal microscopy analysis. Tmem63b-GFP and Tmem63b-Ala-GFP were detected under Alex-488nm. Bar, 10 µm.

3.5.3.4 Functional Slc19a2 is important for Tmem63b PLS activity

To understand whether PLS activity and complex formation require functional Slc19a2 or not, I analyzed a loss-of-function mutant Slc19a2 S143F, identified in TRMA patients, which inhibits thiamine transport and causes anemia. I then introduced Slc19a2 S143F into Tmem63b-expressing BDKO cells and performed PS exposure assay and as a result, a significant reduction in PLS activity was detected compared to Slc19a2 WT (**Fig. 3-18a**). This reduction correlates with the inability to form complex, as the BN-PAGE assay revealed that only the Tmem63b forms complex with Slc19a2 WT, not with Slc19a2 S143F (**Fig. 3-18b**). Moreover, when Ca^{2+} was chelated with EGTA in solubilization buffer, the complex still

formed between Tmem63b and Slc19a2 WT but not with Slc19a2 S143F (**Fig. 3-18b**), representing complex formation probably existing in the resting state before Ca^{2+} stimulation.

Given that Tmem63b mutants are constitutively active without Ca^{2+} and display varying intensities of PLS activity (**Fig. 3-8d**), I questioned whether the level of PLS activity correlates with the amount of complex formation. Initially, I performed BN-PAGE using the Tmem63b mutant-GFP-expressing cells to confirm the complex formation under the endogenous Slc19a2 level. There was not a significant increase in complex bands among Tmem63b mutations; however, as shown in **Fig. 3-18c**, slight increases were observed in Tmem63b I475del and Tmem63b V44M mutants, which exhibited the high PLS activity among Tmem63b mutations according to **Fig. 3-8d**. When I introduced Slc19a2 into Tmem63b mutant-GFP-expressing cells, a significant increase in complex formation was observed. And the complex-to-monomer ratio decreased in accordance with PLS activity. Notably, the loss-of-function R433H mutant displayed a similar complex-to-monomer pattern as Tmem63b WT, suggesting that complex formation occurs in the resting state prior to the PLS activation. Therefore, the impaired PLS activity in the R433H mutant is likely caused by disruptions in the phospholipid scrambling ability or the conformational change in Tmem63b, rather than a loss of complex formation with Slc19a2 (**Fig. 3-18d**).

To further explore the role of Slc19a2 in Tmem63b mutants, *sgSlc19a2* was introduced into Tmem63b mutant-expressing cells. Unlike Kcnn4, Tmem63b mutants can skip the requirement of Kcnn4, however, statistical analysis indicated that Tmem63b mutants still need Slc19a2 to induce PLS activity (**Fig. 3-18f**). Additionally, Tmem63b mutants with Slc19a2 S143F-expressing cells also did not bring significant PLS activity compared to those with Slc19a2 WT (**Fig. 3-18g**). Despite that when Slc19a2 S143F was introduced into Tmem63b mutant cells they showed some complex formation in I475del, V44M, and D459E cases, the amount of the complex was significantly lower level than with Slc19a2 WT. This indicates the necessity of functional Slc19a2 in stabilizing the complex in activated Tmem63b (**Fig. 3-18e**).

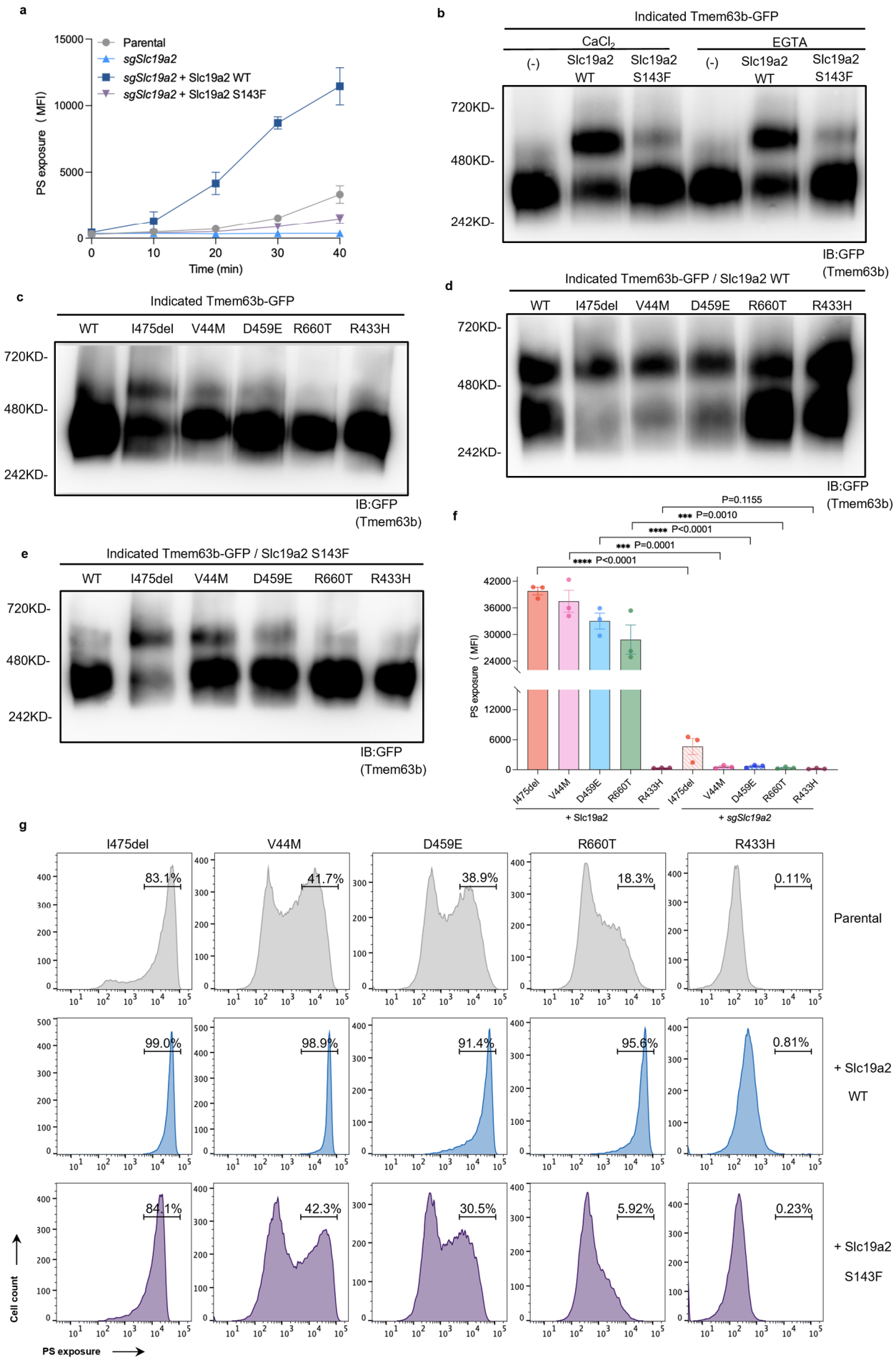
a
Parental
sgSlc19a2
sgSlc19a2 + Slc19a2 WT
sgSlc19a2 + Slc19a2 S143F
PS exposure (MFI)
Time (min)
b
Indicated Tmem63b-GFP
CaCl2
EGTA
(-)
Slc19a2 WT
Slc19a2 S143F
720KD-
480KD-
242KD-
IB:GFP (Tmem63b)
c
Indicated Tmem63b-GFP
WT
I475del
V44M
D459E
R660T
R433H
d
Indicated Tmem63b-GFP / Slc19a2 WT
e
Indicated Tmem63b-GFP / Slc19a2 S143F
f
P=0.1155
*** P=0.0010
**** P<0.0001
*** P=0.0001
**** P<0.0001
+ Slc19a2
+ sgSlc19a2
g
83.1%
41.7%
38.9%
18.3%
0.11%
99.0%
98.9%
91.4%
95.6%
0.81%
84.1%
42.3%
30.5%
5.92%
0.23%
Parental
+ Slc19a2 WT
+ Slc19a2 S143F
Cell count
PS exposure

Fig. 3-18: Slc19a2 effects on Tmem63b mutants-induced PLS activity. a 4˚C PS exposure assay. Slc19a2 WT and Slc19a2 S143F were restored into Tmem63b-expressing cells, which had *sgSlc19a2* introduced. PS exposure assay was conducted with A23187 stimulation; the statistical analysis of PS exposure in left at 40 min used a two-tailed Student's t-test and is presented as mean ± SEM. A P-value of less than 0.05 was considered statistically significant. * represents P value less than 0.05, *** represents P value less than 0.001, **** represents P value less than 0.0001. **b** BN-PAGE assay. Tmem63b-GFP-expressing cells with Slc19a2 WT or Slc19a2 S143F introduction were solubilized with or without EGTA adding. Anti-GFP HRP was used for Tmem63b detection. **c** BN-PAGE assay. BN-PAGE was performed in Tmem63b-WT-expressing and Tmem63-mutant-GFP-expressing cells. **d** BN-PAGE assay. BN-PAGE was conducted using Tmem63b-WT-expressing cells and Tmem63-mutant-GFP-expressing cells with Slc19a2 introduction. **e** 4˚C PS exposure assay. Slc19a2 WT and *sgSlc19a2* were introduced into Tmem63b-mutant-GFP-expressing cells. PS exposure assay was conducted without A23187 stimulation and recorded at 10 min; the statistical analysis of PS exposure in left was used a two-tailed Student's t-test and is presented as mean ± SEM. A P-value of less than 0.05 was considered statistically significant. * represents P value less than 0.05, *** represents P value less than 0.001, **** represents P value less than 0.0001. **f** BN-PAGE assay. Slc19a2 S143F was introduced into Tmem63b-WT-expressing and Tmem63-mutant-GFP-expressing cell, respectively. LMNG/CHS was used to solubilize cell membrane and Anti-GFP HRP was used for Tmem63b detection. **g** 4 ˚C PS exposure assay. Slc19a2 WT and Slc19a2 S143F were restored into Tmem63b-mutant-GFP-expressing cells, respectively. PS exposure assay was conducted without A23187 stimulation and recorded at 10 min; bar, PS exposure region; number, cell population in the bar.

4. Discussion

In this study, based on unbiased sgRNA library screening, two independent scrambling activity regulating factors were identified in the NGS result. Stim1/Orai1-related epSCR-PLS pathway and Tmem63b/Slc19a2-PLS pathway were demonstrated under Ca^{2+} stimulation.

Tmem63b is identified as a cation channel that functions as both a mechanosensor and osmosensor in mammals. Recent research based on structural analysis indicates the presence of a 'proteo-lipidic pore' in its plant ortholog, OSCA1.2, where lipids constitute a wall for the ion permeation pathways, distinguishing it from canonical ion channels. Given its structural similarities with the Tmem16 family, which contains both ion channels and scramblases, it is proposed that Tmem63b may possess scramblase function beyond its ion channel. In this study, Tmem63b was shown to be a Ca^{2+}-dependent phospholipid scramblase factor. Moreover, the elicitation of scrambling activity by Tmem63b necessitates the formation of a complex with Slc19a2, a thiamine transporter, and this PLS activation works alongside Kcnn4 activation.

In red blood cells, activated Kcnn4 triggers K^+ efflux, leading to cell shrinkage, which is associated with membrane tension-activated Piezo1-induced Ca^{2+} influx; both Piezo1 and Kcnn4 mutants are implicated in hereditary xerocytosis (HX) disease. It is hypothesized that when the cell membrane experiences a stress stimulus, it activates Piezo1-mediated Ca^{2+} influx, which in turn activates Kcnn4 to achieve K^+ efflux. The loss of K^+ results in cell dehydration, a phenomenon also observed in this study during PS exposure assay on Tmem63b-expressing cells. PLS activity was not elicited when extracellular K^+ over 50 mM, as cell size did not change; conversely, when extracellular K^+ was lower than 5 mM, PLS activity was detected and cells became smaller, indicative of cell shrinkage (**Fig. 4-1a**). Dehydration of the cells likely results in a decrease in osmotic balance and alterations in membrane tension, which may contribute to the activation of Tmem63b and subsequent phospholipid scrambling (PLS) activity. Given that Tmem63b functions as an osmosensor responsive to hypotonic stimuli[59], I conducted the PS exposure assay to determine whether hyposmotic conditions (200 Osmo/L and 100 Osmo/L, corresponding to 100 mM NaCl and 50 mM NaCl in AnnexinV buffer) could induce Tmem63b-PLS activity. The results demonstrated an increase in cell size and PLS activity following stimulation with the Ca^{2+} ionophore. The scrambling activity was more pronounced at 100 Osmo/L, which may be attributed to the increased membrane softness due to cell swelling, thereby facilitating the scrambling of phospholipids (**Fig. 4-1b**). However, in the absence of the Ca^{2+} ionophore, cells neither undergo dehydration nor swelling in hypertonic or hypotonic conditions, preventing PLS activity. This indicates that osmotic stress is inadequate to induce Tmem63b-mediated scrambling activity; instead, the combined effects of Ca^{2+} influx and K^+ efflux serve as the primary stimuli for activating scrambling activity.

However, as the mechanosensor, Tmem63b can be activated following mechanistic stimuli[60,62]; however, the relationship between mechanistic stimuli with Tmem63b-mediated PLS activity remains unclear. Further investigation is required to determine whether the scrambling activity of Tmem63b can be activated by membrane curvature and alterations in tension.

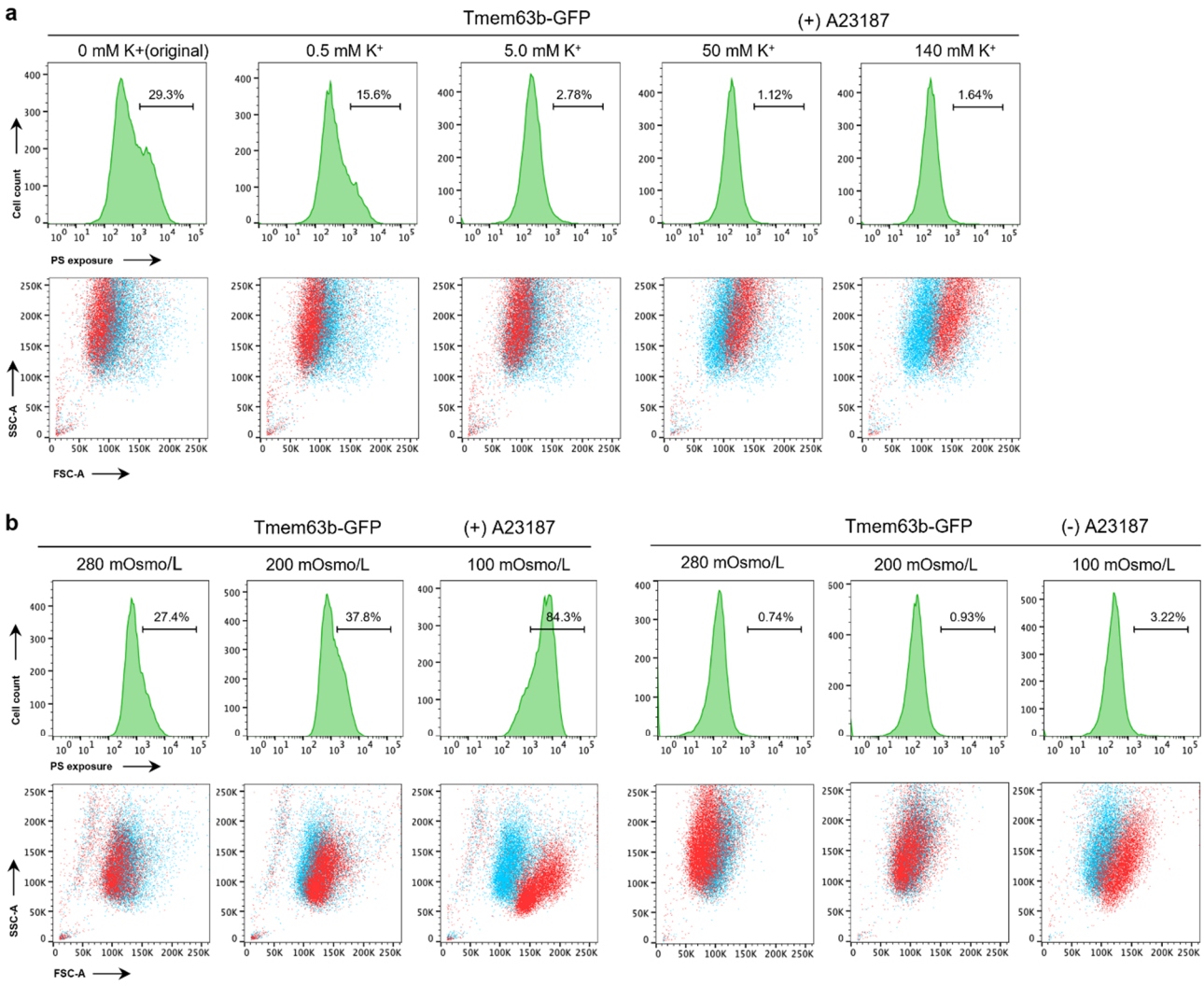

Fig. 4-1: Cell dehydration during Tmem63b-PLS activity. a Tmem63-expressing cells were incubated in various K^+ concentration (0 mM, 0.5 mM, 5 mM, 50 mM, and 140 mM) and stimulated with Ca^{2+} ionophore. PS exposure assay was performed at 4˚C, bar, PS exposure region; number, cell population in the bar. FSC-A and SSC-A at 40 min were shown to compare cell size: blue, parental cells at 0 mM K^+ at 0 min; red, samples under series K^+ incubation at 40 min. **b** Tmem63-expressing cells were incubated in different osmolarity conditions. 140 mM Na^+ represents 280 mOsmo/L, 100 mM Na^+ represents 200 mOsmo/L, and 50 mM Na^+ represents 100 mOsmo/L. PS exposure assay was performed at 4˚C with or without Ca^{2+} ionophore. Bar, PS exposure region; number, cell population in the bar. Blue, parental cells incubated at 0 min; red, cells incubated for 40 min.

Tmem63b primarily acts as an ion channel, facilitating cation influx. It remains uncertain whether Tmem63b possesses Ca^{2+} binding sites, as proposed by the Tmem16f "credit card" model, which requires Ca^{2+} for conformational changes that permit phospholipid passage. In Tmem16f, several amino acids in

TM6, 7, and 8 bind with two Ca^{2+} ions as shown in **Fig. 4-2**. Notably, two conserved amino acids—glutamate and aspartic acid—in Tmem63b imply a potential for Ca^{2+} binding. However, the role of Ca^{2+} binding in activating Tmem63b-PLS activity remains unknown. Kcnn4 serves as a Ca^{2+} linker to Tmem63b activation thus it would be intriguing to explore whether Tmem63b requires both Ca^{2+} binding and K^+ efflux for activation, and which activation is more dominant.

Furthermore, the 'stepping stone' model for Tmem16f activation highlights *Se* site and *Si* site—two lipid headgroup interaction sites that are conserved among many Tmem16 family members, but less so in those with reduced scrambling ability. In the *Se* site, two oppositely charged amino acids E604 and R478 in Tmem16f are positioned near Tmem63b mutants I475, D459, and V44, which elicit constitutive scrambling activity. This proximity suggests that these mutants may play a role in facilitating phospholipid head interactions, potentially forming a chain of lipids that penetrate into the groove. Nevertheless, further study is required to confirm whether the effect of these mutants on PLS activity is directly or indirectly related to the *Se* site. On the other hand, in the *Si* site, the loss-of-function mutant R433 in Tmem63b is located near E529 and K530 in Tmem16f (**Fig. 4-2**), which may compromise the formation of a hydrophilic pore for the lipid heads. Exploring the mutations of both *Se* and *Si* sites into hydrophobic residues or the substitution of them with Tmem63a or Tmem63c residues may clarify whether the lipid stacking interactions at these sites are associated with scrambling activity. Additionally, structural, computational, and atomistic analyses could provide insights into the distribution of lipids and charged residues surrounding the groove.

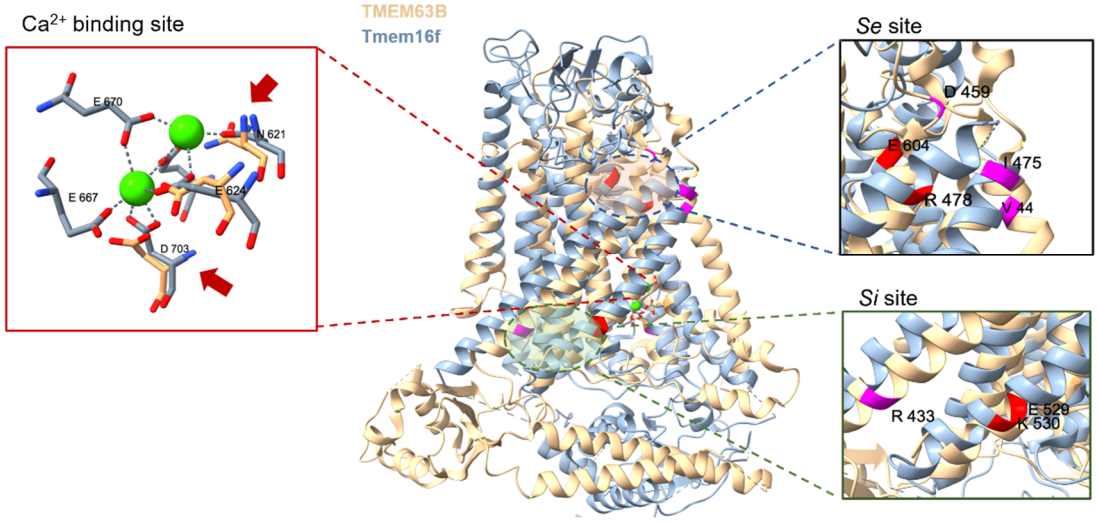

Fig. 4-2: Tmem63b structural analysis. Structure of mouse Tmem16f (yellow, PDB: 8b8q) and human TMEM63B (blue, PDB: 8ehx); mutants I475, V44, and D459 in Tmem63b are labeled in pink, which are close to the *Se* site (circled in blue and colored in red) in Tmem16f; R433 in Tmem63b is proximal to the *Si* site of Tmem16f (circled in green and colored in red); Tmem16f Ca^{2+} binding residues are presented in blue-grey, two conserved residues in Tmem63b are presented in yellow; the red arrow represents the conserved residues.

Although other known scramblases, Tmem16f and Xkr8 exist as homodimers; here I found that Tmem63b forms a heterodimer with Slc19a2. The existence of this complex in resting state suggests that complex formation likely occurs prior to PLS activity. Because the loss-of-function mutant Slc19a2 S143F affects complex formation and impairs PLS activity, Slc19a2 likely plays a crucial role in stabilizing Tmem63b conformation through this complex. The structural differences between functional Slc19a2 and Slc19a2 S143F in forming complex with Tmem63b still remains to be elucidated. On the other hand, the loss-of-function Tmem63b mutant does not exhibit PLS activity; however, it still forms a complex with Slc19a2. This observation supports the previous hypothesis that Tmem63b is responsible for phospholipid scrambling, while Slc19a2 likely plays a role in conformational stabilization. However, a swapping experiment of the "SCRD" region revealed that TM4 and TM5 of Tmem63b did not confer scrambling activity to Tmem63a and Tmem63c, suggesting that the "SCRD" region of Tmem63b may differ from that of Tmem16f, potentially accommodating a distinct activation model beyond "credit card" and "stepping stone". Furthermore, the thiamine deficient Slc19a2 could not interact with Tmem63b, putting into question whether thiamine contributes to complex formation. As thiamine is critical for cells growth and proliferation, depletion of thiamine to investigate its role in complex formation may be challenging in a cell system. Additionally, it will be interesting to explore whether other members of Tmem63 family, such as Tmem63a and Tmem63c, can also form heterodimers with Slc19a2 or Slc19a3 and induce PLS activity. Regarding the significance of Tmem63b working with Slc19a2 to mediate scrambling activity, Tmem63b differs from other homodimer mechanosensitive channels in that it exists as a monomer; and it differs from other scramblases in that it has fewer Ca^{2+} binding sites. These differences or limitations suggest that Tmem63b probably needs a partner to induce a conformational change that allows phospholipids to pass through. The binding of Slc19a2 to Tmem63b serves to prepare for subsequent action. Following Ca^{2+} influx accompanied by K^{+} efflux, the resting state-formed Tmem63b/Slc19a2 complex may be regarded as the readily mobilizable store that can be rapidly activated to achieve scrambling activity.

Tmem63b mutants from patients suffering from DEE and hematological disorders exhibit constitutive PLS activity without Ca^{2+}stimulation, with the intensity of PLS activity correlating with severity of anemia. Furthermore, TMEM63B shows specific localization in RBCs, suggesting that the Tmem63b related PLS activity is associated with the disease, particularly in anemia. The physiological function of PS exposure by Xkr8 is to release the 'eat-me' signal for phagocytes, facilitating the clearance of apoptotic cells. Here, I propose a hypothesis regarding the contribution of constitutive PLS activity of Tmem63b to anemia: When gain-of-function TMEM63B mutations are expressed in late erythrocytes, these mutant proteins will be expressed on RBCs' plasma membrane, releasing the 'eat-me' signal and recruiting macrophages to engulf the RBCs, resulting in a decreased RBCs number, which is a hallmark of anemia. Besides 'gain-

of-function' mutants of Tmem63b, one 'loss-of-function' mutant was also identified in this research. As this mutant could not elicit PS exposure neither with nor without Ca^{2+} stimulation but still remained on the plasma membrane, it is associated with the presence of abnormal RBCs rather than anemia in the patient. The mechanism of Tmem63b-PLS activity's association with hematological disorder is described as below (**Fig. 4-3**).

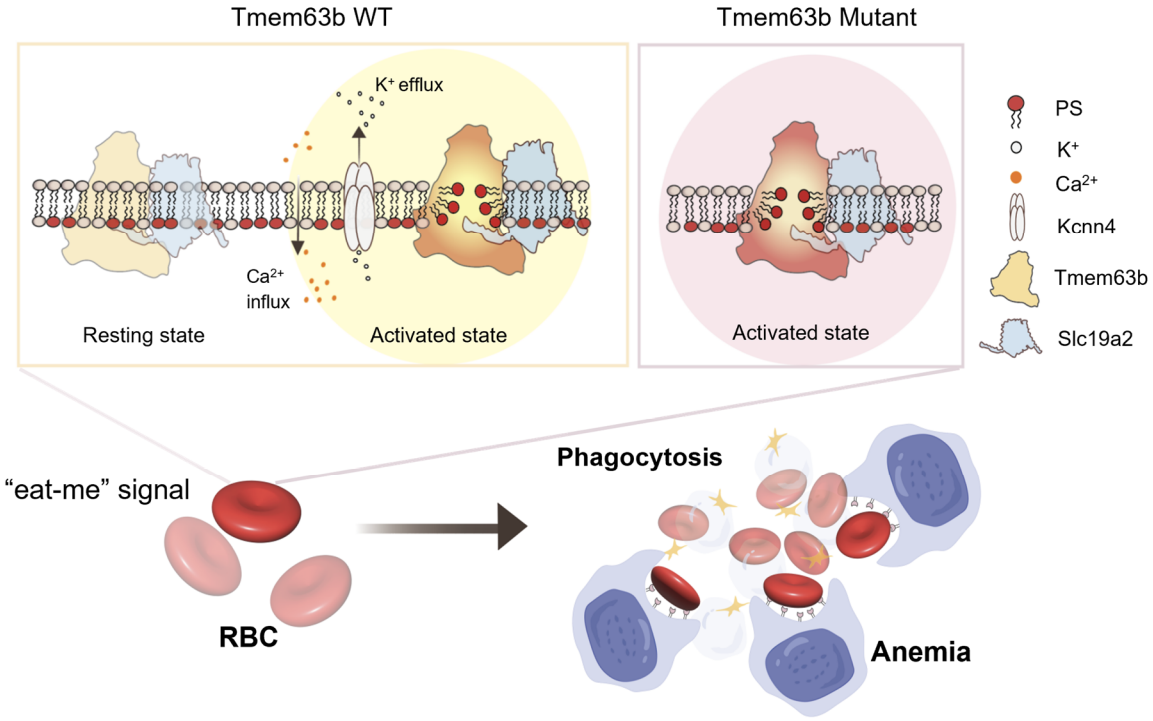

Fig. 4-3: Description for Tmem63b-PLS activity associated anemia. Tmem63 and Slc19a2 form complexes in the resting state when Ca^{2+} enters the intracellular milieu, activating Kcnn4 and facilitating K^+ efflux. Then the Tmem63b/Slc19a2 complex functions as a scramblase to expose PS. In red blood cells, PS exposure releases the 'eat-me' signal for macrophages to achieve engulfment. The mutant Tmem63b activates independently of Ca^{2+}, bypasses the Kcnn4 for K^+ efflux; it can constitutively expose PS, triggering phagocytosis and resulting in anemia.

To prove this hypothesis, in vivo experiments are required. However, this study did not perform animal experiments to support the 'gain-of-function' Tmem63b triggers phagocytosis in red blood cells. Considering homogenous Tmem63b mutations probably contribute to early mortality in mice; hence, bone marrow transplantation is a more practical approach to observe red blood cells characteristics, including their number, size, and shape. In the case of TMC, in vivo studies conducted by Ballesteros, A. *et al.* demonstrated that *Tmc*$^{-/-}$ hair cells fail to expose PS, while mutant TMC1 elicits PS exposure (**Fig. 4-4**)[48]. In mice with heterozygous TMC1 mutations, constitutive PS exposure was suggested to contribute to deafness. It is highly possible that PS exposure in inner hair cells releases an 'eat me' signal for macrophages, thereby facilitating phagocytosis. This explains the loss of hair cells reported in Tmc1 mutant mice. However, TMC1 may function as Ca^{2+}-inhibited lipid scramblase in inner hair cells.

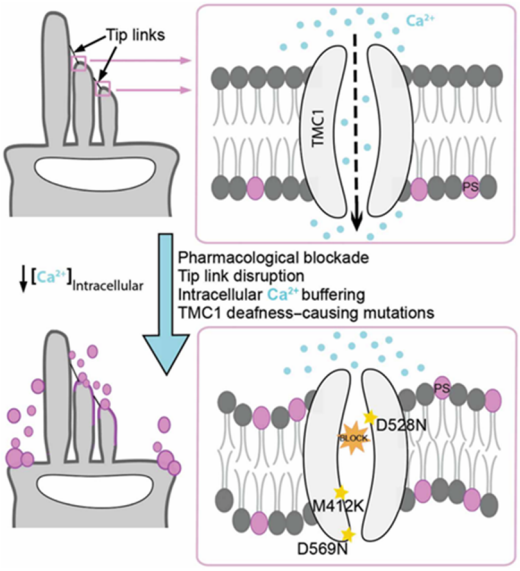

Fig. 4-4: TMC1-dependent regulation of the apical hair cell membrane homeostasis. In wild-type murine auditory hair cells, the asymmetry of the phospholipids is preserved. When the MET channel is blocked, the tip links are disrupted, or intracellular Ca^{2+} buffering is inhibited, PS is externalized and membrane blebbing occurs at the stereocilia and apical region of hair cells expressing TMC1. TMC1 deafness–causing mutations M412K and D569N cause constitutive externalization of PS that correlates with the deafness phenotype in these mutant mice, emphasizing the importance of membrane homeostasis to hearing. The picture came from Ballesteros, A. *et al*.[48]

Tmem63b serves physiological functions, acting as thirst control in neural cells, contributing to hearing in inner ear cells, and potentially functioning as a scramblase in RBCs, which may be linked to anemia. It is worth investigating whether Tmem63b has specific functions depending on its localization and whether PLS activity is coordinated with ion transduction. It would be interesting to see whether these two functions can occur simultaneously or if each function is dominant under different stimuli or in various cell types, such as neural cells, inner ear cells or red blood cells. Additionally, will Slc19a2 act as a regulator of the Tmem63b functional switch? What is the difference between Slc19a2 when it forms complex with Tmem63b and when it does not? Will it transport thiamine normally in its interaction with Tmem63b? Addressing these questions will enhance the understanding of physiological functions of both Tmem63b and Slc19a2.

In summary, this study demonstrates two distinct functional proteins: a cation channel and a thiamine transporter can form a complex that achieves a new function beyond their original roles, likely contributing to anemia. This study offers theoretical support for disease treatment and provides insight into how different proteins combine to play a new role.

5. References

1. Vance, J. E. Phospholipid Synthesis and Transport in Mammalian Cells. *Traffic* **16**, 1–18 (2015).
2. Kannan, M., Lahiri, S., Liu, L.-K., Choudhary, V. & Prinz, W. A. Phosphatidylserine synthesis at membrane contact sites promotes its transport out of the ER. *J. Lipid Res.* **58**, 553–562 (2017).
3. Cell Membranes. in *Medical Cell Biology* 27–57 (Elsevier, 2008). doi:10.1016/B978-0-12-370458-0.50007-4.
4. Murate, M. *et al.* Transbilayer lipid distribution in nano scale. *J. Cell Sci.* **128**, 1627–1638 (2015).
5. Yang, Y., Lee, M. & Fairn, G. D. Phospholipid subcellular localization and dynamics. *J. Biol. Chem.* **293**, 6230–6240 (2018).
6. Van der Mark, V., Elferink, R. & Paulusma, C. P4 ATPases: Flippases in Health and Disease. *Int. J. Mol. Sci.* **14**, 7897–7922 (2013).
7. Segawa, K., Kurata, S. & Nagata, S. The CDC50A extracellular domain is required for forming a functional complex with and chaperoning phospholipid flippases to the plasma membrane. *J. Biol. Chem.* **293**, 2172–2182 (2018).
8. van Meer, G. Dynamic Transbilayer Lipid Asymmetry. *Cold Spring Harb. Perspect. Biol.* **3**, a004671–a004671 (2011).
9. Sakuragi, T. & Nagata, S. Regulation of phospholipid distribution in the lipid bilayer by flippases and scramblases. *Nat. Rev. Mol. Cell Biol.* **24**, 576–596 (2023).
10. Segawa, K., Suzuki, J. & Nagata, S. Flippases and scramblases in the plasma membrane. *Cell Cycle* **13**, 2990–2991 (2014).
11. Nagata, S., Sakuragi, T. & Segawa, K. Flippase and scramblase for phosphatidylserine exposure. *Curr. Opin. Immunol.* **62**, 31–38 (2020).
12. Nagata, S. & Segawa, K. Sensing and clearance of apoptotic cells. *Curr. Opin. Immunol.* **68**, 1–8 (2021).
13. Nagata, S., Suzuki, J., Segawa, K. & Fujii, T. Exposure of phosphatidylserine on the cell surface. *Cell Death Differ.* **23**, 952–961 (2016).
14. Zhou, Q. *et al.* Molecular Cloning of Human Plasma Membrane Phospholipid Scramblase. *J. Biol. Chem.* **272**, 18240–18244 (1997).
15. Bevers, E. M. & Williamson, P. L. Phospholipid scramblase: An update. *FEBS Lett.* **584**, 2724–2730 (2010).
16. Aloulou, A., Rahier, R., Arhab, Y., Noiriel, A. & Abousalham, A. Phospholipases: An Overview. in *Methods in Molecular Biology* 69–105 (Springer New York, 2018). doi:10.1007/978-1-4939-8672-9_3.
17. Suzuki, J., Umeda, M., Sims, P. J. & Nagata, S. Calcium-dependent phospholipid scrambling by TMEM16F. *Nature* **468**, 834–838 (2010).
18. Fujii, T., Sakata, A., Nishimura, S., Eto, K. & Nagata, S. TMEM16F is required for phosphatidylserine exposure and microparticle release in activated mouse platelets. *Proc. Natl. Acad. Sci. U. S. A.* **112**, 12800–12805 (2015).
19. Suzuki, J. *et al.* Calcium-dependent phospholipid scramblase activity of TMEM16 protein family members. *J. Biol. Chem.* **288**, 13305–13316 (2013).
20. Brunner, J. D., Lim, N. K., Schenck, S., Duerst, A. & Dutzler, R. X-ray structure of a calcium-activated TMEM16 lipid scramblase. *Nature* **516**, 207–212 (2014).

21. Alvadia, C. *et al.* Cryo-EM structures and functional characterization of the murine lipid scramblase TMEM16F. *Elife* **8**, e44365 (2019).
22. Herrera, S. A., Grifell-Junyent, M. & Pomorski, T. G. NBD-lipid Uptake Assay for Mammalian Cell Lines. *Bio-protocol* **12**, e4330 (2022).
23. Yu, K. *et al.* Identification of a lipid scrambling domain in ANO6/TMEM16F. *Elife* **4**, e06901 (2015).
24. Bethel, N. P. & Grabe, M. Atomistic insight into lipid translocation by a TMEM16 scramblase. *Proc. Natl. Acad. Sci. U. S. A.* **113**, 14049–14054 (2016).
25. Gyobu, S., Ishihara, K., Suzuki, J., Segawa, K. & Nagata, S. Characterization of the scrambling domain of the TMEM16 family. *Proc. Natl. Acad. Sci. U. S. A.* **114**, 6274–6279 (2017).
26. Malvezzi, M. *et al.* Out-of-the-groove transport of lipids by TMEM16 and GPCR scramblases. *Proc. Natl. Acad. Sci. U. S. A.* **115**, E7033–E7042 (2018).
27. Feng, Z. *et al.* In or out of the groove? Mechanisms of lipid scrambling by TMEM16 proteins. *Cell Calcium* **121**, 102896 (2024).
28. Feng, S. *et al.* Cryo-EM Studies of TMEM16F Calcium-Activated Ion Channel Suggest Features Important for Lipid Scrambling. *Cell Rep.* **28**, 567–579.e4 (2019).
29. Suzuki, J., Imanishi, E. & Nagata, S. Exposure of phosphatidylserine by Xk-related protein family members during apoptosis. *J. Biol. Chem.* **289**, 30257–30267 (2014).
30. Kawano, M. & Nagata, S. Lupus-like autoimmune disease caused by a lack of Xkr8, a caspase-dependent phospholipid scramblase. *Proc. Natl. Acad. Sci. U. S. A.* **115**, 2132–2137 (2018).
31. Hanayama, R. *et al.* Autoimmune Disease and Impaired Uptake of Apoptotic Cells in MFG-E8-Deficient Mice. *Science* **304**, 1147–1150 (2004).
32. Suzuki, J., Imanishi, E. & Nagata, S. Xkr8 phospholipid scrambling complex in apoptotic phosphatidylserine exposure. *Proc. Natl. Acad. Sci. U. S. A.* **113**, 9509–9514 (2016).
33. Sakuragi, T. *et al.* The tertiary structure of the human Xkr8-Basigin complex that scrambles phospholipids at plasma membranes. *Nat. Struct. Mol. Biol.* **28**, 825–834 (2021).
34. Sakuragi, T., Kosako, H. & Nagata, S. Phosphorylation-mediated activation of mouse Xkr8 scramblase for phosphatidylserine exposure. *Proc. Natl. Acad. Sci. U. S. A.* **116**, 2907–2912 (2019).
35. Calenda, G. *et al.* Identification of two new members, XPLAC and XTES, of the XK family. *Gene* **370**, 6–16 (2006).
36. Sukharev, S. & Sachs, F. Molecular force transduction by ion channels: diversity and unifying principles. *J. Cell Sci.* **125**, 3075–3083 (2012).
37. Hamant, O. Widespread mechanosensing controls the structure behind the architecture in plants. *Curr. Opin. Plant Biol.* **16**, 654–660 (2013).
38. Jeong, H. *et al.* Structures of the TMC-1 complex illuminate mechanosensory transduction. *Nature* **610**, 796–803 (2022).
39. Sorum, B., Docter, T., Panico, V., Rietmeijer, R. A. & Brohawn, S. G. Tension activation of mechanosensitive two-pore domain K+ channels TRAAK, TREK-1, and TREK-2. *Nat. Commun.* **15**, 3142 (2024).
40. Franks, N. P. & Honoré, E. The TREK K2P channels and their role in general anaesthesia and neuroprotection. *Trends Pharmacol. Sci.* **25**, 601–608 (2004).
41. Coste, B. *et al.* Piezo proteins are pore-forming subunits of mechanically activated channels. *Nature* **483**, 176–181 (2012).
42. Corrigan, M. A. *et al.* TRPV4-mediates oscillatory fluid shear mechanotransduction in mesenchymal stem cells in part via the primary cilium. *Sci. Rep.* **8**, 3824 (2018).

43. Pan, B. *et al.* TMC1 Forms the Pore of Mechanosensory Transduction Channels in Vertebrate Inner Ear Hair Cells. *Neuron* **99**, 736–753.e6 (2018).
44. Jia, Y. *et al.* TMC1 and TMC2 Proteins Are Pore-Forming Subunits of Mechanosensitive Ion Channels. *Neuron* **105**, 310–321.e3 (2020).
45. Jojoa-Cruz, S. *et al.* Cryo-EM structure of the mechanically activated ion channel OSCA1.2. *Elife* **7**, e41845 (2018).
46. Liu, X., Wang, J. & Sun, L. Structure of the hyperosmolality-gated calcium-permeable channel OSCA1.2. *Nat. Commun.* **9**, 5060 (2018).
47. Ballesteros, A. & Swartz, K. J. Regulation of membrane homeostasis by TMC1 mechanoelectrical transduction channels is essential for hearing. *Sci. Adv.* **8**, eabm5550 (2022).
48. Han, Y. *et al.* Mechanical activation opens a lipid-lined pore in OSCA ion channels. *Nature* **628**, 910–918 (2024).
49. Kalienkova, V. *et al.* Stepwise activation mechanism of the scramblase nhTMEM16 revealed by cryo-EM. *Elife* **8**, e44364 (2019).
50. Lim, N. K., Lam, A. K. M. & Dutzler, R. Independent activation of ion conduction pores in the double-barreled calcium-activated chloride channel TMEM16A. *J. Gen. Physiol.* **148**, 375–392 (2016).
51. Whitlock, J. M. & Hartzell, H. C. A Pore Idea: the ion conduction pathway of TMEM16/ANO proteins is composed partly of lipid. *Pflugers Arch.* **468**, 455–473 (2016).
52. Jiang, T., Yu, K., Hartzell, H. C. & Tajkhorshid, E. Lipids and ions traverse the membrane by the same physical pathway in the nhTMEM16 scramblase. *Elife* **6**, e28671 (2017).
53. Yan, H. *et al.* Heterozygous Variants in the Mechanosensitive Ion Channel TMEM63A Result in Transient Hypomyelination during Infancy. *Am. J. Hum. Genet.* **105**, 996–1004 (2019).
54. Tábara, L. C. *et al.* TMEM63C mutations cause mitochondrial morphology defects and underlie hereditary spastic paraplegia. *Brain* **145**, 3095–3107 (2022).
55. Zhang, M., Shan, Y., Cox, C. D. & Pei, D. A mechanical-coupling mechanism in OSCA/TMEM63 channel mechanosensitivity. *Nat. Commun.* **14**, 3943 (2023).
56. Qin, Y. *et al.* Cryo-EM structure of TMEM63C suggests it functions as a monomer. *Nat. Commun.* **14**, 7265 (2023).
57. Zhao, X., Yan, X., Liu, Y., Zhang, P. & Ni, X. Co-expression of mouse TMEM63A, TMEM63B and TMEM63C confers hyperosmolarity activated ion currents in HEK293 cells. *Cell Biochem. Funct.* **34**, 238–241 (2016).
58. Du, H. *et al.* The Cation Channel TMEM63B Is an Osmosensor Required for Hearing. *Cell Rep.* **31**, 107596 (2020).
59. Li, S., Li, B., Gao, L., Wang, J. & Yan, Z. Humidity response in Drosophila olfactory sensory neurons requires the mechanosensitive channel TMEM63. *Nat. Commun.* **13**, 3814 (2022).
60. Yang, G. *et al.* TMEM63B channel is the osmosensor required for thirst drive of interoceptive neurons. *Cell Discov.* **10**, 1 (2024).
61. Li, Q. & Montell, C. Mechanism for food texture preference based on grittiness. *Curr. Biol.* **31**, 1850–1861.e6 (2021).
62. Vetro, A. *et al.* Stretch-activated ion channel TMEM63B associates with developmental and epileptic encephalopathies and progressive neurodegeneration. *Am. J. Hum. Genet.* **110**, 1356–1376 (2023).
63. Fleming, J. C. *et al.* Characterization of a Murine High-Affinity Thiamine Transporter, Slc19a2. *Mol. Genet. Metab.* **74**, 273–280 (2001).

64. Ortigoza-Escobar, J. D. *et al.* Free-thiamine is a potential biomarker of thiamine transporter-2 deficiency: a treatable cause of Leigh syndrome. *Brain* **139**, 31–38 (2015).
65. Fraccascia, P., Sniekers, M., Casteels, M. & Van Veldhoven, P. P. Presence of thiamine pyrophosphate in mammalian peroxisomes. *BMC Biochem.* **8**, 10 (2007).
66. Ganapathy, V., Smith, S. B. & Prasad, P. D. SLC19: the folate/thiamine transporter family. *Pflugers Arch. Eur. J. Physiol.* **447**, 641–646 (2004).
67. Marcé-Grau, A., Martí-Sánchez, L., Baide-Mairena, H., Ortigoza-Escobar, J. D. & Pérez-Dueñas, B. Genetic defects of thiamine transport and metabolism: A review of clinical phenotypes, genetics, and functional studies. *J. Inherit. Metab. Dis.* **42**, 581–597 (2019).
68. Zhang, S. *et al.* Identification of novel compound heterozygous variants in SLC19A2 and the genotype-phenotype associations in thiamine-responsive megaloblastic anemia. *Clin. Chim. Acta* **516**, 157–168 (2021).
69. Yu, S. P. & Choi, D. W. Ions, cell volume, and apoptosis. *Proc. Natl. Acad. Sci. U. S. A.* **97**, 9360–9362 (2000).
70. Thompson, G. J., Langlais, C., Cain, K., Conley, E. C. & Cohen, G. M. Elevated extracellular [K+] inhibits death-receptor- and chemical-mediated apoptosis prior to caspase activation and cytochrome c release. *Biochem. J.* **357**, 137–145 (2001).
71. Karki, P. *et al.* Intracellular K+ inhibits apoptosis by suppressing the Apaf-1 apoptosome formation and subsequent downstream pathways but not cytochrome c release. *Cell Death & Differ.* **14**, 2068–2075 (2007).
72. Lang, K. S. *et al.* Cation channels trigger apoptotic death of erythrocytes. *Cell Death & Differ.* **10**, 249–256 (2003).
73. Lang, P. A. *et al.* Role of Ca^{2+}-activated K^+ channels in human erythrocyte apoptosis. *Am. J. Physiol. Physiol.* **285**, C1553–C1560 (2003).
74. Begenisich, T. *et al.* Physiological Roles of the Intermediate Conductance, Ca2+-activated Potassium Channel Kcnn4. *J. Biol. Chem.* **279**, 47681–47687 (2004).
75. Andolfo, I. *et al.* Novel Gardos channel mutations linked to dehydrated hereditary stomatocytosis (xerocytosis). *Am. J. Hematol.* **90**, 921–926 (2015).
76. Rapetti-Mauss, R. *et al.* A mutation in the Gardos channel is associated with hereditary xerocytosis. *Blood* **126**, 1273–1280 (2015).
77. Zarychanski, R. *et al.* Mutations in the mechanotransduction protein PIEZO1 are associated with hereditary xerocytosis. *Blood* **120**, 1908–1915 (2012).
78. Albuisson, J. *et al.* Dehydrated hereditary stomatocytosis linked to gain-of-function mutations in mechanically activated PIEZO1 ion channels. *Nat. Commun.* **4**, 1884 (2013).
79. Glogowska, E., Lezon-Geyda, K., Maksimova, Y., Schulz, V. P. & Gallagher, P. G. Mutations in the Gardos channel (KCNN4) are associated with hereditary xerocytosis. *Blood* **126**, 1281–1284 (2015).
80. Rapetti-Mauss, R. *et al.* Red blood cell Gardos channel (KCNN4): the essential determinant of erythrocyte dehydration in hereditary xerocytosis. *Haematologica* **102**, e415–e418 (2017).
81. Cahalan, S. M. *et al.* Piezo1 links mechanical forces to red blood cell volume. *Elife* **4**, e07370 (2015).
82. Ran, L. *et al.* KCNN4 links PIEZO-dependent mechanotransduction to NLRP3 inflammasome activation. *Sci. Immunol.* **8**, eadf4699 (2023).
83. Pinton, P., Giorgi, C., Siviero, R., Zecchini, E. & Rizzuto, R. Calcium and apoptosis: ER-mitochondria Ca2+ transfer in the control of apoptosis. *Oncogene* **27**, 6407–6418 (2008).

84. Berridge, M. J., Bootman, M. D. & Roderick, H. L. Calcium signalling: dynamics, homeostasis and remodelling. *Nat. Rev. Mol. Cell Biol.* **4**, 517–529 (2003).
85. Rizzuto, R. & Pozzan, T. Microdomains of Intracellular Ca^{2+}: Molecular Determinants and Functional Consequences. *Physiol. Rev.* **86**, 369–408 (2006).
86. Clapham, D. E. Calcium Signaling. *Cell* **131**, 1047–1058 (2007).
87. Pinton, P. & Rizzuto, R. Bcl-2 and Ca2+ homeostasis in the endoplasmic reticulum. *Cell Death & Differ.* **13**, 1409–1418 (2006).
88. Ma, G. *et al.* Inside-out Ca(2+) signalling prompted by STIM1 conformational switch. *Nat. Commun.* **6**, 7826 (2015).
89. Kang, F. *et al.* E-syt1 Re-arranges STIM1 Clusters to Stabilize Ring-shaped ER-PM Contact Sites and Accelerate Ca(2+) Store Replenishment. *Sci. Rep.* **9**, 3975 (2019).
90. Lérias, J. R. *et al.* A novel microscopy-based assay identifies extended synaptotagmin-1 (ESYT1) as a positive regulator of anoctamin 1 traffic. *Biochim. Biophys. Acta - Mol. Cell Res.* **1865**, 421–431 (2018).
91. Palty, R., Raveh, A., Kaminsky, I., Meller, R. & Reuveny, E. SARAF Inactivates the Store Operated Calcium Entry Machinery to Prevent Excess Calcium Refilling. *Cell* **149**, 425–438 (2012).
92. Picard, C. *et al.* STIM1 mutation associated with a syndrome of immunodeficiency and autoimmunity. *N. Engl. J. Med.* **360**, 1971–1980 (2009).
93. Lacruz, R. S. & Feske, S. Diseases caused by mutations in ORAI1 and STIM1. *Ann. N. Y. Acad. Sci.* **1356**, 45–79 (2015).
94. Ko, Y.-J., Lee, M., Kang, K., Song, W. K. & Jun, Y. In vitro assay using engineered yeast vacuoles for neuronal SNARE-mediated membrane fusion. *Proc. Natl. Acad. Sci. U. S. A.* **111**, 7677–7682 (2014).
95. Hong, W. & Lev, S. Tethering the assembly of SNARE complexes. *Trends Cell Biol.* **24**, 35–43 (2014).
96. Furuta, N. & Amano, A. SNARE mediates autophagosome–lysosome fusion. *J. Oral Biosci.* **54**, 83–85 (2012).
97. Schneider, C. A., Rasband, W. S. & Eliceiri, K. W. NIH Image to ImageJ: 25 years of image analysis. *Nat. Methods* **9**, 671–675 (2012).
98. Martin, M. Cutadapt removes adapter sequences from high-throughput sequencing reads. *EMBnet.journal* **17**, 10 (2011).
99. Li, W. *et al.* MAGeCK enables robust identification of essential genes from genome-scale CRISPR/Cas9 knockout screens. *Genome Biol.* **15**, 554 (2014).
100. Noguchi, Y. *et al.* In vivo CRISPR screening directly targeting testicular cells. *Cell genomics* **4**, 100510 (2024).
101. Sanjana, N. E., Shalem, O. & Zhang, F. Improved vectors and genome-wide libraries for CRISPR screening. *Nat. Methods* **11**, 783–784 (2014).
102. Zhang, P. *et al.* Extracellular calcium functions as a molecular glue for transmembrane helices to activate the scramblase Xkr4. *Nat. Commun.* **14**, 5592 (2023).
103. Jardine, L. *et al.* Blood and immune development in human fetal bone marrow and Down syndrome. *Nature* **598**, 327–331 (2021).
104. Jumper, J. *et al.* Highly accurate protein structure prediction with AlphaFold. *Nature* **596**, 583–589 (2021).
105. Maruoka, M. *et al.* Caspase cleavage releases a nuclear protein fragment that stimulates phospholipid scrambling at the plasma membrane. *Mol. Cell* **81**, 1397–1410.e9 (2021).

106. Srivastava, S. *et al.* Phosphatidylinositol 3-phosphate indirectly activates KCa3.1 via 14 amino acids in the carboxy terminus of KCa3.1. *Mol. Biol. Cell* **17**, 146–154 (2006).
107. Srivastava, S. *et al.* Histidine Phosphorylation of the Potassium Channel KCa3.1 by Nucleoside Diphosphate Kinase B Is Required for Activation of KCa3.1 and CD4 T Cells. *Mol. Cell* **24**, 665–675 (2006).

6. Acknowledgements

I want to use this thesis to commemorate my father, the person I respect the most.

I would like to express my deep gratitude to my mom. She supported me through a tough time, stood by me without any hesitation and gave me the courage and confidence to pursue my career. Here I really want to say: “Thank you so much and I love you so much!”. We often take familial love for granted, but always overlook that it is the most precious emotion for human beings. I am proud of my family. Being loved is the first lesson I have learned and also is the greatest gift I have ever received. This solid backing inspires me to keep going and achieve my doctoral degree.

I appreciate my country for giving me this opportunity to go abroad and broaden my mind and horizon. I also appreciate the MEXT scholarship for supporting me to complete my studies. I am grateful to all the members in Suzuki lab. Prof. Suzuki, my supervisor, who created a favorable environment and platform for everyone to attain their goals; Maruoka sensei, he always taught us techniques with patience; Noguchi san, my senior, gave me a lot of guidance and bioinformatics help; and Prof. Kosako, our collaborator, helped us to overcome technical limitations such as mass spectrometry analysis. And Mori san, Fujimoto san, Motani sensei, Uchida san, Panpan san, Matsui san, Yamato san, Rhea san, Suh san, Ann san, Erin san, Dou san, Shaan san, Tachibana san, Gau san, Lai san, Pepe san, Ishigawa san, Yukie san, Gregory san, Daniel san, Fujita san, Ishida san, Murase san, Shimomura san, and Tadachi san. My sub-supervisors Prof. Harada, A.P. Adam, Prof. Hejna, and GSB office staff Nishimoto san. They helped me both in experiments and life in Japan.

I also thank all my friends I have met. Sometimes I felt lonely, helpless and anxiety, they always there for me. Du Qiping, Wang Siyu, and Liu Xianghui, they played important roles in my life here, we spent unforgettable time together and encouraged each other a lot.

Finally, I want to thank myself. I have noticed how much I have changed, perhaps this is what it means to “grow up”. The experience I gained over the past four years has been invaluable to me throughout my whole life. And I want to say to myself: “Congratulations! You got the ticket for the next station, keep on going girl, everything will go exactly what is supposed to be.”

This thesis is based on material in the following scholarly papers.

Authors: Niu Han, Masahiro Maruoka, Yuki Noguchi, Hidetaka Kosako, and Jun Suzuki.

Title: Phospholipid scrambling induced by an ion channel/metabolite transporter complex.

Name of journal: Nature Communications.

DOI: 10.1038/s41467-024-51939-w

Published date: 31/Aug/2024